

Final
Report

Anomalies

20610

Copy No. _____

PSE



**Aerospace
Systems Division**



**Aerospace
Systems Division**

Investigation of PSE Anomalies
Apollo 12 Mission

NO. SSSED-R 57 (a)	REV. NO.
PAGE <u>1</u> OF <u>43</u>	
DATE 28 May 1970	

This report provides the results of investigations of PSE anomalies from Apollo 12 mission. Reference 97/510-454, CCP-237, 16 February 1970.

TASK TITLE: Investigation of Apparent Loss of Gain in the
SPZ Vertical Seismometer.

Prepared by: L. Hogeboom
L. Hogeboom

Prepared by: R. Gibson
R. Gibson

Approved by: J. Lewko, Jr.
J. Lewko, Jr.

CONTENTS

<u>Paragraph</u>	<u>Title</u>	<u>Page</u>
1.0	INTRODUCTION	5
2.0	DISCUSSION	5
2.1	STATEMENT OF WORK	5
2.2	ANALYSIS	6
3.0	SUMMARY OF RESULTS	42
4.0	CONCLUSIONS AND RECOMMENDATIONS	42
5.0	REFERENCES	43

TABLES

<u>Table No.</u>	<u>Title</u>	<u>Page</u>
2.2-1	Teledyne T-13081 Test Data	8 & 9
2.2-2	Computed Data from Measured Data of T-13081	10
2.2-3	T-13044 Test Data	11 & 12
2.2-4	SPZ SN03, SN04, SN05, SN06, SN07 Sensor Period Versus "G"	13, 14, 15 16, 17
2.2-5	SPZ of SN01 Sensor-Period Versus "G"	18
2.2-6	T-13081 Earth Spring Test	20
2.2-7	T-13044 Float Test Data	21
2.2-8	SPZ T-030 Period Versus "G"	22
2.3-1	Test Specification T-13044 - Float Test for Short Period SN05 Seismometer Assembly	28
2.3-2	Determination of Spring Constant K for Short Period Seismometer Suspension Spring on SN05	31
2.3-3	Possible Tolerance Build Up When Installing 233221 Coil Assembly into Seismometer Assembly 2341609	37

ILLUSTRATIONS

<u>Figure</u>	<u>Title</u>	<u>Page</u>
2.2-9	SPZ Delta Rod Configuration	24
2.3-1	SN05 Short Period Seismometer Assembly Showing Areas of Rework	26
2.3-2	Float Test for SN05 Short Period Seismometer	29
2.3-3	Short Period SN05 Seismometer Suspension Spring	32
2.3-4	Cross Section of the Short Period Seismometer Showing Functional Elements	34
2.3-5	Short Period Seismometer Assy. Nominal Tolerances	35
2.3-6	Tolerance Build-Up of 233221 Coil Assy. when Assembled with 2341609, Seismometer Assy.	36
2.3-7	Top View - Short Period Seismometer	39
2.3-8	Bottom View - Short Period Seismometer	40
2.3-9	Delta Rod Installation	41

1.0 INTRODUCTION

This report addresses the results of the study of the Apollo 12 Short Period Vertical Seismometer anomaly namely, loss of SPZ gain at low signal levels (millimicron region). When the Apollo 12 SPZ was functioning, the signal amplitude and frequency in the range of 1-2 HZ correlates to the LPZ output signal filtered to 1-2 HZ. This anomaly became evident when the SPZ seismometer failed to detect small seismic events and did not respond as expected to S. P. calibration commands.

2.0 DISCUSSION

2.1 Statement of Work

The following statement of work is taken from the MCP originally prepared for this anomaly study.

2.1.1 Investigation of apparent loss of gain, SPZ Vertical Seismometer.

2.1.2 Review SPZ transformer coupling measurements of T-13081.

2.1.3 Examine results of previously conducted SPZ float tests and strip chart records available showing natural period and damping.

2.1.4 Perform an engineering analysis of:

- (a) Method of SPZ rework to establish the possibility of damage to the SPZ seismometer.
- (b) SPZ suspension system. Analysis to investigate the resultant mass displacement as a function of individual and combinational broken delta rods.

2.1.5 Perform an engineering evaluation test using the SN01 PSS. This test will be done during the performance of in-process test T-13069 by interrupting this test and inserting two special engineering tests.

2.1.5.1 Generate an engineering (special test) plan to:

- (a) Transmit SP cal commands to sensor at all gain settings using ETS.
- (b) Transmit LPZ and motor turn on command record output of SPZ seismometer and electronics at all gain settings using ETS.
- (c) These tests will be done with sensor uncaged.

- (d) Data resulting from this test will be compared to Apollo 12 records.

2.2 Analysis

The following section establishes the basis for the expected gain of the SPZ seismometer which is in the SN05 PSS of the ALSEP Flight 1 system.

$$\text{Volts/meter} = \frac{G (\text{DRX}) A}{\text{CDR @ 1 sec}}$$

G = 176.1 from final float test data after rework 02-15-69.

DRX = 5636 from T. P. 2338815 Acceptance Test Procedure of 02-28-69.

A = Amplifier gain @ 0 db.

From T. P. 2338815, A = 8900 @ -10 db, and noting that Digital to Analog converter of test set has gain of 2, then -

$$\frac{8900}{2} \times 3.16 = 14,062 \text{ gain @ 0 db.}$$

CDR @ 1 sec = 4683 as recalculated using data from float test of 02-15-69.

$$\text{Volts/meter} = \frac{(3.1416) (1.761) (5.636) (1.4062) 10^9}{(4.683) 10^3}$$

$$= (9.363) 10^6 \text{ V/meter @ 1 sec}$$

or 9.363 V/ μ @ 1 sec.

and Minimum Detectable Signal of .53 nanometer at 1 sec. *

* As noted in a science report by Gary Latham, this sensitivity is not realized on Apollo 12.

Science Report by Gary Latham - Page 3-7 - Short-Period Seismometer

"The threshold ground motion acceleration required to produce an observable signal cannot be determined accurately; however, the smallest signals observed correspond to a surface acceleration of $8 \times 10^{-4} \text{ cm/sec}^2$ (peak-to-peak surface motion amplitude of 2 nanometers at a frequency of 10 hertz). Lunar surface accelerations less than this approximate threshold are apparently not detected by the SPZ seismometer."

2.2.1 Summary of Results as Regards Short Period Seismometer Float Test Investigation

A summary of all T-13081, earth spring test data is shown on Table 2.2-1 (2 sheets). The earth spring test consists of measuring signal coil current required to restore a 15 gram weight at three different positions, center, .050 above and .050 below center. The natural period of the seismometer with the earth spring is also measured at these positions. The calibration coil "G" is computed by measuring current required to equal movement of known weight lift.

Table 2.2-2 shows a recalculation of "G" (motor constant) and a computed "K" (spring constant) using measured data from T-13081 data.

Table 2.2-3, a summary of T-13044 float test data vs. position, was used to calculate a "G" factor using the relation:

$$G = .8333 \times m \times 9.807/I$$

where m = total mass weight in kilograms

I = current required to float mass in amperes

9.807 - acceleration of gravity in meters/sec²

.8333 - 5/6 of total mass floated by current in signal coil

G = Newtons/ampere

Table 2.2-4 (5 sheets) shows a summary plot of all period and "G" measurements for each unit. It is noted that seismometers showing little or no period variations at earth spring test also show the largest float test range, that is, the mass may be floated at the lower positions. It is also noted that in general there is a decrease in "G" after rework, rework being tension bolt replacement. This change is attributed to a decrease in flux density due to bolt change.

From the Period vs. "G" plots it is noted that the period vs. center position at float test before and after rework shows the least change where the units also show the least period deviation at earth spring test.

The SN01 PSE has been reworked to flight configuration and the results of the T-13081 and T-13044 tests are shown on Table 2.2-5.

S/N Date	Weight Added	Position to Center	Period Seconds	Volts @ 2.01K	15 Gram Current	Calculated "G"
03	0	+.045	1.12	1.6407	816	183.82
10-09-67	+2 gm	.000	1.14	1.6474	819	179.47
125-10	+4 gm	-.045	1.12	1.6443	818	181.04
04	0	+.055	1.23	1.6798	8.363	176
10-13-67	+2 gm	-.010	1.14	1.6785	8.301	177.2
125-11	+4 gm	-.060	1.08	1.6749	8.333	176.7
05	0	+.060	1.14	1.6009	.79647	185
03-04-68	+2 gm	+.005	1.26	1.5987	.7954	185
125-12	+4 gm	-.050	1.18	1.6077	.79985	184
06	0	+.063	1.16	1.6462	.81815	179.8
05-13-68	+2 gm	-.003	1.49	1.6385	.81432	180.64
125-5	+4 gm	-.073	1.17	1.6574	.823	178.58
07	0	+.050	1.15	1.6439	.8166	180.14
05-27-68	+2 gm	+.005	1.17	1.6325	.811	181.34
125-6	+4 gm	-.045	1.18	1.6333	.8114	181.30

Teledyne T-13081 Test Data

Earth Spring Data:

10-09-67 and 10-12-67
03-04-68
05-13-68 and 05-27-68

F = 554.05 gm
F = 55.04 gm
F = 544.05 gm

K = 12.07 gm/cm
K = 12.07 gm/cm
K = 12.07 gm/cm

S/N	03	04	05	06	07
Damp Ratio	1.025	1.064	1.079	1.13124	1.04
Critical Damp	.0078	.0209	.02446	.0391	.01248
Damp @ 1 Sec	.00889	.02382	.02982	.058259	.0146
Signal Coil Ω	1842.7	1850.3	1870.5	1823.3	1882.1
Mean G	181.44	176.6	184.7	179.67	180.95
CDR /sec	4865	4670	5135	5044	4715
DRX /sec	5107	4820	5670	5382	4856
Calib Coil Ω	24.28	24.13	24.68	24.04	25.84
Weight	2 grm	2 grm	2 grm	3 grm	3 grm
Deflection Ratio	.998	1.000	1.005	1.000	1.000
Voltage @ 2.01 K	17.673	17.873	17.323	27.947	27.05
"G"	2.24	2.21	2.285	2.11663	2.188
Calib. Res. Ω	6600	6500	6730	62.8 K	63.44 K

Teledyne T-13081 Test Data

Table 2.2 - 1 (Sheet 2 of 2)

S/N	Position to Center	Period Seconds	Total Weight	15 Gram Current	Computed "G"	Total "K"	Delta "K"
03	+.045	1.12	543	.8162	180.2	17.43	5.36
	.000	1.14	545	.8196	179.5	16.88	4.81
	-.045	1.12	547	.8180	179.8	17.55	5.48
04	+.055	1.23	542.2	.8357	176.0	14.42	2.35
	-.010	1.14	544.2	.8350	176.2	16.85	4.78
	-.060	1.08	546.2	.8332	176.5	18.85	6.78
05	+.060	1.14	543.1	.7964	184.7	16.81	4.74
	+.005	1.26	545.1	.7953	185.0	13.79	1.72
	-.050	1.18	547.1	.7998	183.9	15.79	3.72
06	+.062	1.16	540.8	.8190	179.6	16.17	4.10
	-.008	1.49	542.8	.8151	180.5	9.84	-2.13
	-.073	1.17	544.8	.8245	178.4	16.01	3.94
07	+.050	1.15	553	.8178	179.9	16.83	4.76
	+.005	1.17	555	.8121	181.1	16.31	4.24
	-.045	1.18	557	.8125	181.0	16.10	4.03

Computed data from measured data of T-13081

Delta "K" is from total K minus Earth Spring K of 12.07

G = Newtons/ampere

K = grams/cm

Table 2.2 - 2

S/N		----- ABOVE -----			- CENTER -		----- BELOW -----			
Date		.075	.050	.025	.000	.010	.020	.030	.040	.05
03	Period	.78	.85	.96	1.18	1.32	1.52	1.85	1.90	
10-18-67	Volts	52.23	51.99	51.79	51.65	51.61	51.58	51.568	51.563	
	"G"	170.8	171.6	172.3	172.7	172.8	172.9	173.0	173.0	
04	Period	.79	.90	1.05	1.37	1.47	1.70			
10-16-67	Volts	51.45	51.25	51.12	51.09	51.04	51.03			
	"G"	173.1	173.8	174.3	174.4	174.5	174.6			
05	Period	.83	.95	1.28	1.80					
3-5-68	Volts	50.31	50.11	49.98	49.96					
	"G"	177.4	178.1	178.5	178.6					
06	Period	.87	1.02	1.54						
5-14-68	Volts	49.86	49.68	49.63	49.61					
	"G"	178.2	178.8	179.0						
07	Period	.67	.72	.82	.97	1.05	1.12	1.21	1.37	1.50
5-28-68	Volts	51.20	50.88	50.63	50.45	50.39	50.36	50.35	50.30	50.28
	"G"	177.4	178.5	179.4	180.1	180.3	180.4	180.4	180.6	180.7

T-13044 Test Data

Table 2.2 - 3 (Sheet 1 of 2)

Test Procedure Data							Record Review Data	
S/N	Date	Proc. No.	Temp.	Travel Inches	Mass Grams	Float Voltage	Period Seconds	Damp. Ratio
03	5-8-69	WO/OS 2338815C	Room	0.241	544.4	53.38	1.160	.0035
	7-7-69		50°C			53.43	0.980	.0060
04	2-16-69	2338810	50°C	0.243	542.5	51.77	0.78*	.004
	6-6-69	WO/OS	Room			52.86	1.110	.0031
	11-14-69	233815C	50°C			53.66	0.805	.0030
05	2-15-69	WO/OS	Room	0.240	543.1	50.68	0.900	.0028
	2-21-69	2338815	Room			50.49	0.905	.0028
	2-25-69	2338815	50°C			50.65	0.955	.0045
06	3-18-69	2338810	50°C	0.241	541.5	50.30	0.850	.0036
	4-16-69	WO/OS	Room			51.00	1.310	.0049
	5-20-69	2338815B	50°C			51.25	0.990	.0057
07	1-24-69	2338810	50°C	0.240	553.7	51.20	0.755	.0029
	2-26-69	WO/OS	Room			51.02	0.935	.0023
	3-21-69	2338815	50°C			51.02	0.715	.0025

WO/OS - Work Order Operations Sheet (Rework)

* - Record not Available use T. P. Data

S/N 07 is on Apollo 11 (EASEP)

S/N 05 is on Apollo 12

S/N 06 is on Apollo 13

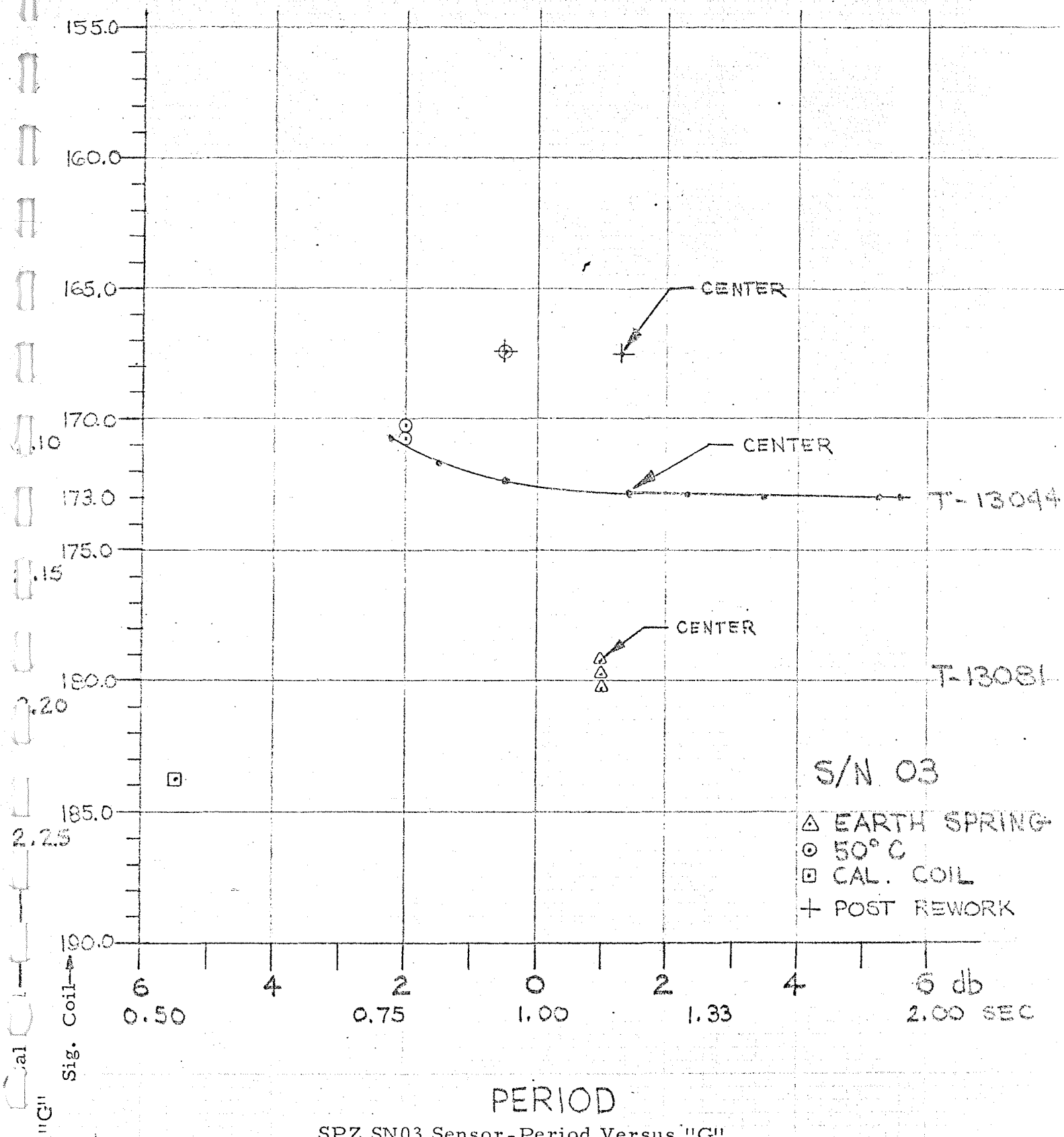
Note: (1) For 2338810 & 8815 Float Voltage is Measured Across 1.99 K Resistor

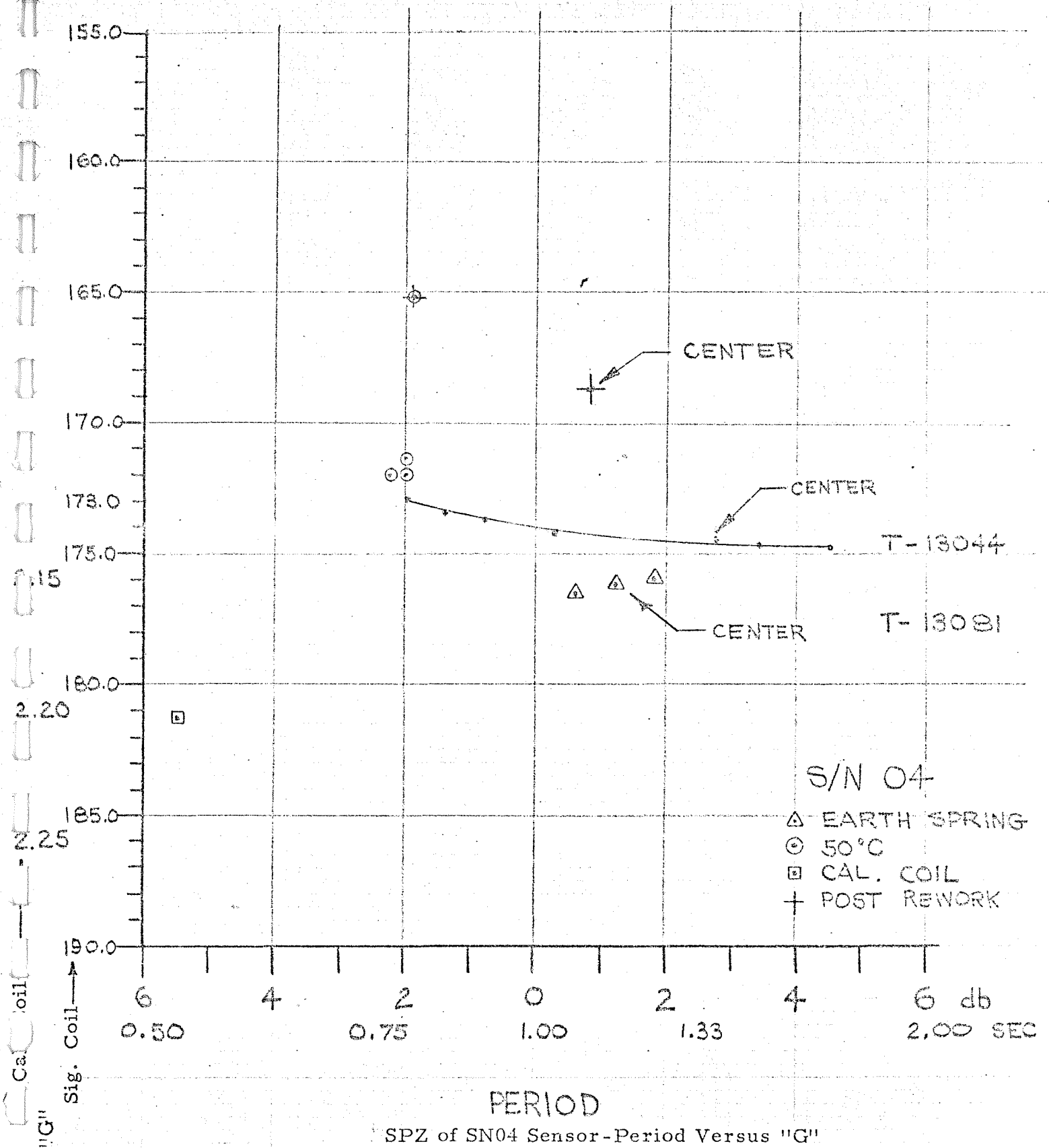
(2) For WO/OS Float Voltage is Measured Across 2.01 K Resistor

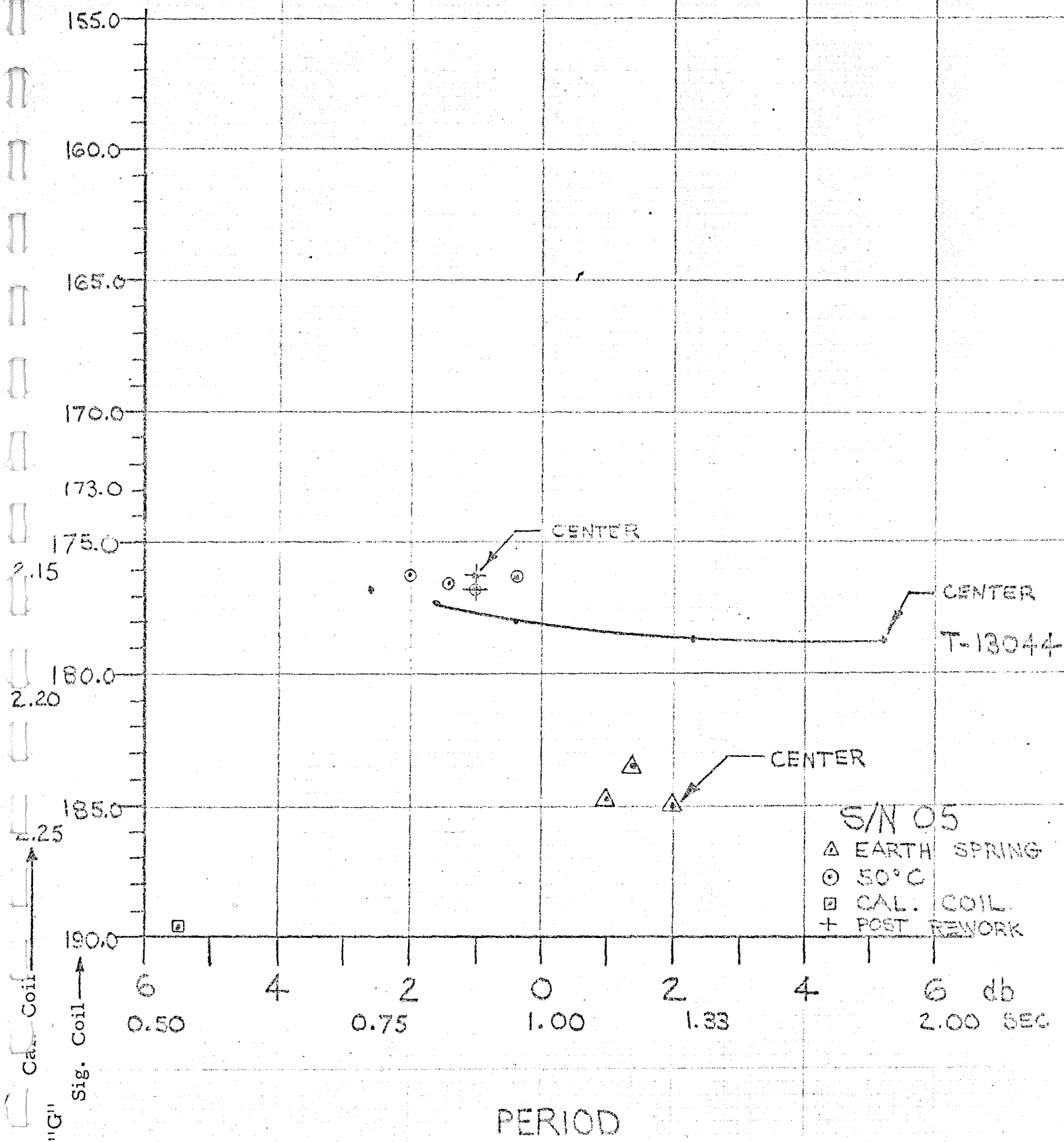
(3) For WO/OS Float Test, mass is at mechanical center position

TABLE 2.2-3 (Sheet 2 of 2)

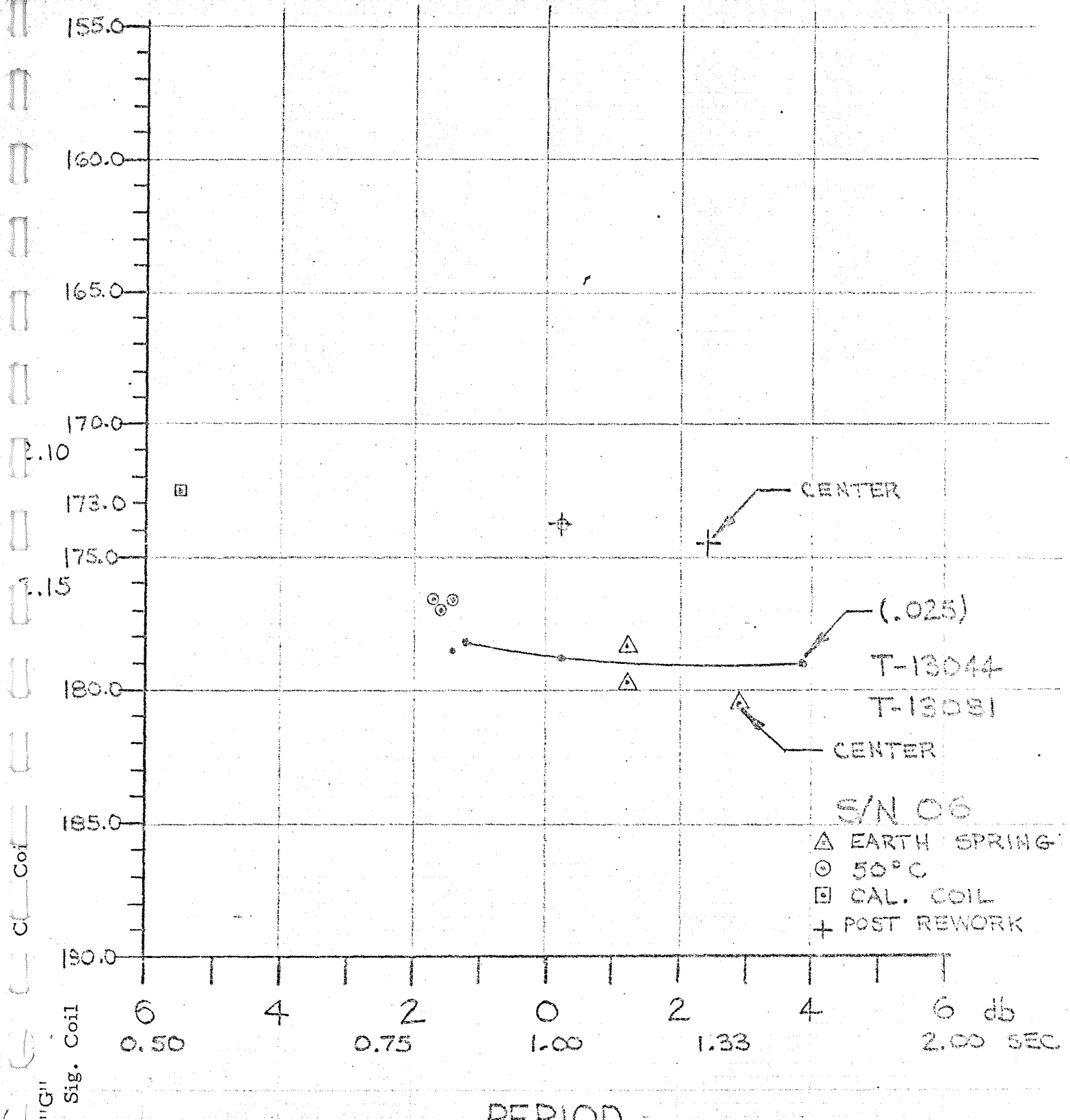
BENDIX S. P. FLOAT TEST DATA



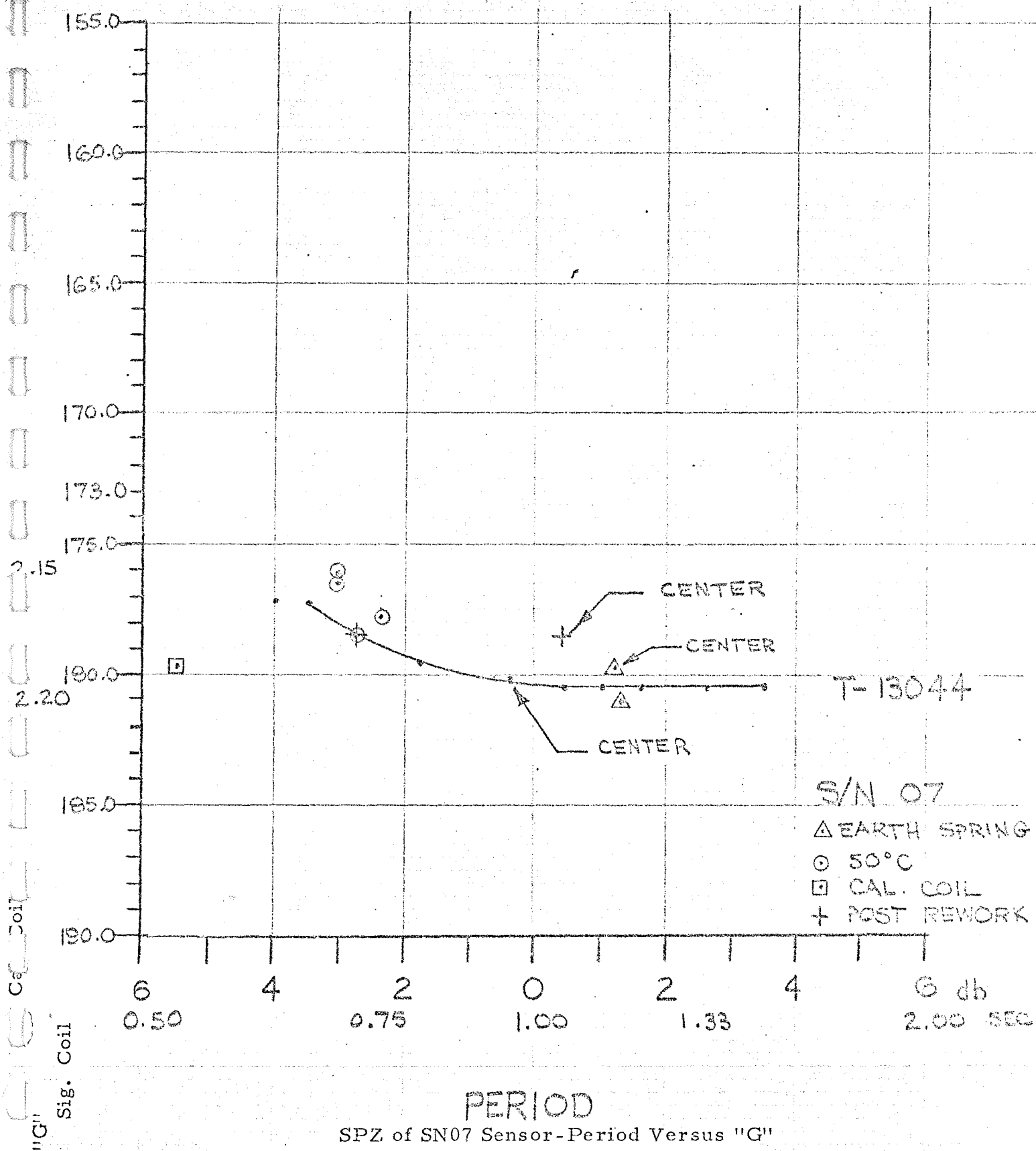




PERIOD
SPZ of SN05 Sensor-Period Versus "G"



SPZ of SN06 Sensor-Period Versus "G"



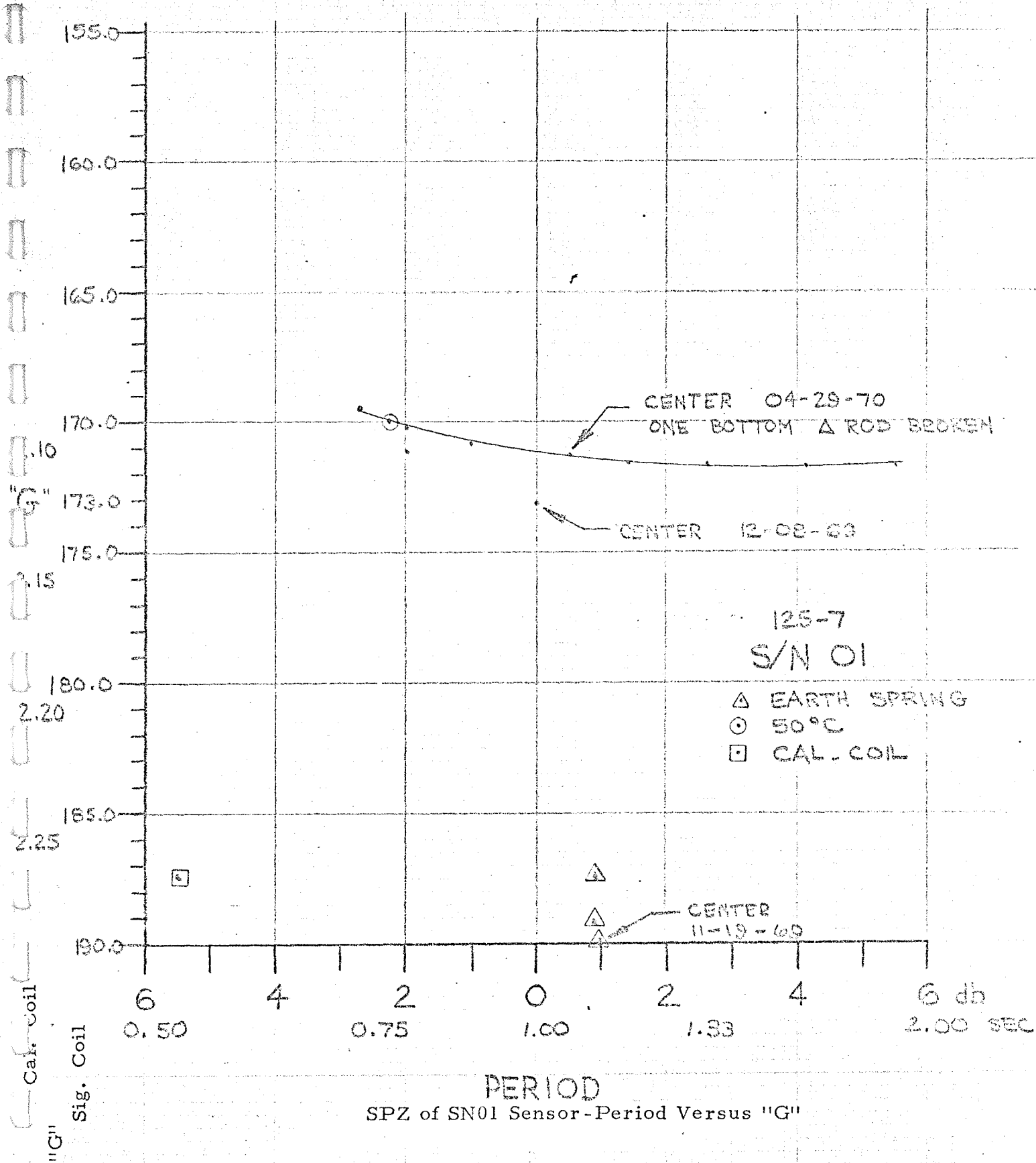


Table 2.2-5

In the process of updating the Level B Spare Short Period Seismometer it was required to perform a T-13044 and T-13081 test to determine the characteristics of the unit before rework. The results of these tests are shown on Table 2.2-6, 7 and 8. It is noted that there is a large deviation in period at T-13081 Earth Spring test and no float below center at T-13044 and an irregular measurement of "G" at .075 above center.

After replacing tension bolt the T-13081 and T-13044 tests were repeated, these results are also recorded on Tables 2.2-6, 7, and 8. The "G" has changed to an out of tolerance condition and when "G" of calibration coils is rechecked it is verified that the flux density of the magnet has decreased. The results of period vs. position has not changed over what was originally recorded at T-13081 but the T-13044 data shows no float at .025 above center.

The delta rods were photographed before and after the rework cycle to show variations as a result of rework. Three delta rods were readjusted (see Figure 2.2-9) A, D and E and the T-13044 test repeated. The mass is now capable of floating at .030 below center. T-13081 earth spring test was repeated and now shows a decreased variation of period with position as shown on Table 2.2-6.

S/N Date	Weight Addition	Position to Center	Period Seconds	Voltage	15 Gram Current	"G"
T030 05-01-70	0	+.041	.73	1.728	.8644	170.1
	+2 gm	.000	1.005	1.731	.8659	169.8
	+4 gm	-.052	1.110	1.730	.8654	169.9
Replaced Bolt						
05-08-70	0	+.036	.73	1.977	.9880	148.8
	+2 gm	.000	1.008	1.975	.9870	148.9
	+4 gm	-.066	1.120	1.996	.9975	147.3
Adjusted Delta Rod						
05-21-70	0	+.025	.970	1.998	.9988	147.28
	+2 gm	-.004	.845	2.005	1.0022	146.78
	+4 gm	-.030	.840	1.990	.9948	147.86

T-13081 Earth Spring Test

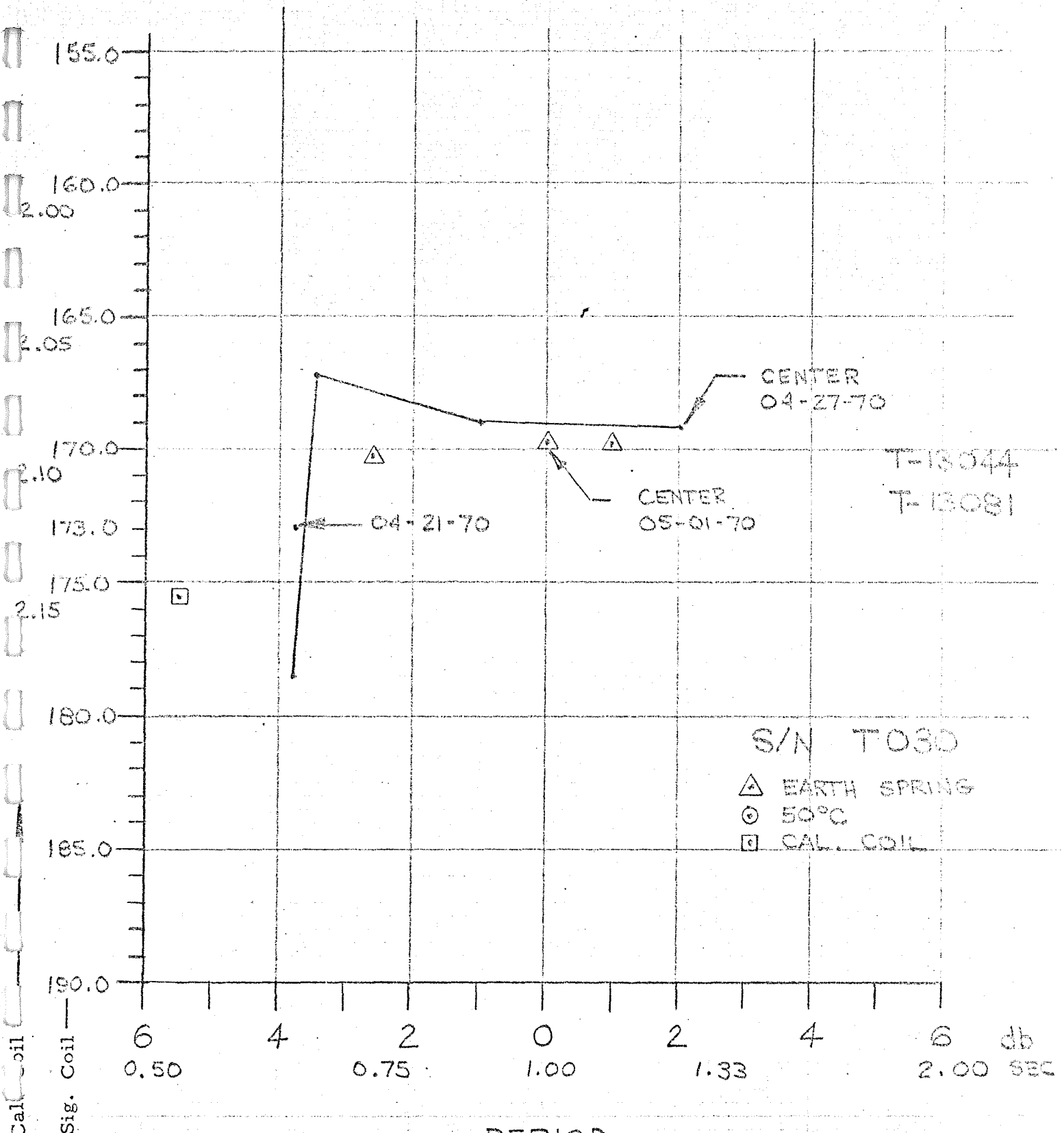
Table 2.2 - 6

Mass 553.2 gm ----- ABOVE ----- - CENTER - ----- BELOW -----
 .075 .050 .025 .000 .010 .020 .030 .040 .050

4-24-70	Period Volts "G"	.645 50.95 178.4	.665 54.05 168.2	.890 53.74 169.1	1.26 53.71 169.2				
Replaced Bolt									
5-13-70	Period Volts "G"	7.55 61.80 147.1	7.40 61.80 147.1						
Adjusted Delta Rods									
5-18-70	Period Volts "G"	.875 62.12 146.3	.925 61.89 146.9	.960 61.70 147.3	.995 61.57 147.6	1.055 61.49 147.8	1.190 61.44 147.9	1.400 61.43 148.0	
5-20-70	Period Volts "G"	.89 62.01 146.6	.95 61.84 147.0	.99 61.66 147.4	1.00 61.49 147.8	1.03 61.42 148.0	1.135 61.36 148.1	1.375 61.31 148.2	

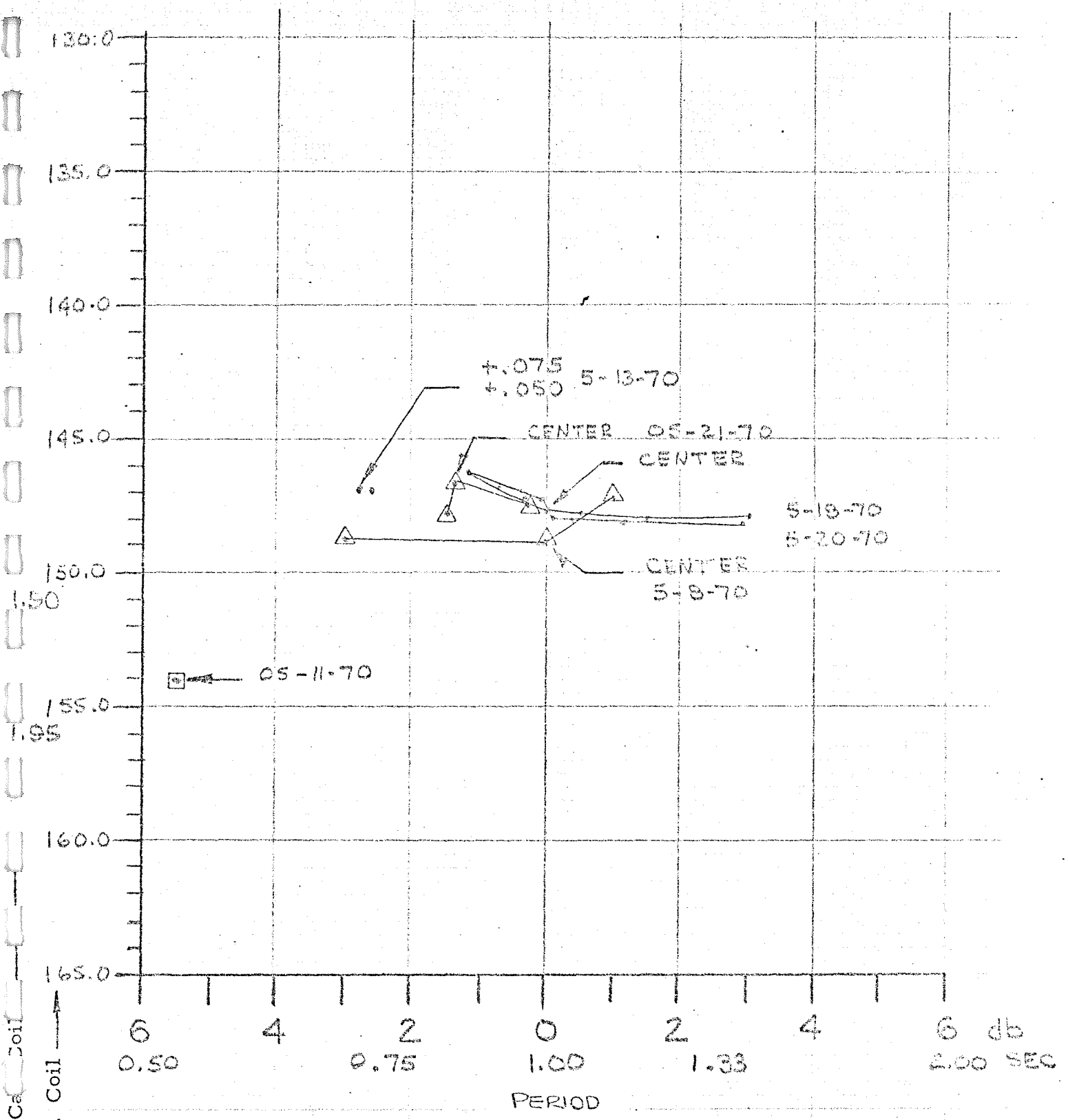
T-13044 Float Test Data

Table 2.2 - 7



PERIOD
SPZ T T-030 Period Versus "G"

TABLE 2.2-8 (SHEET 1 OF 2)



SPZ T-030 Period Versus "G"

TABLE 2.2-8 (SHEET 2 OF 2)

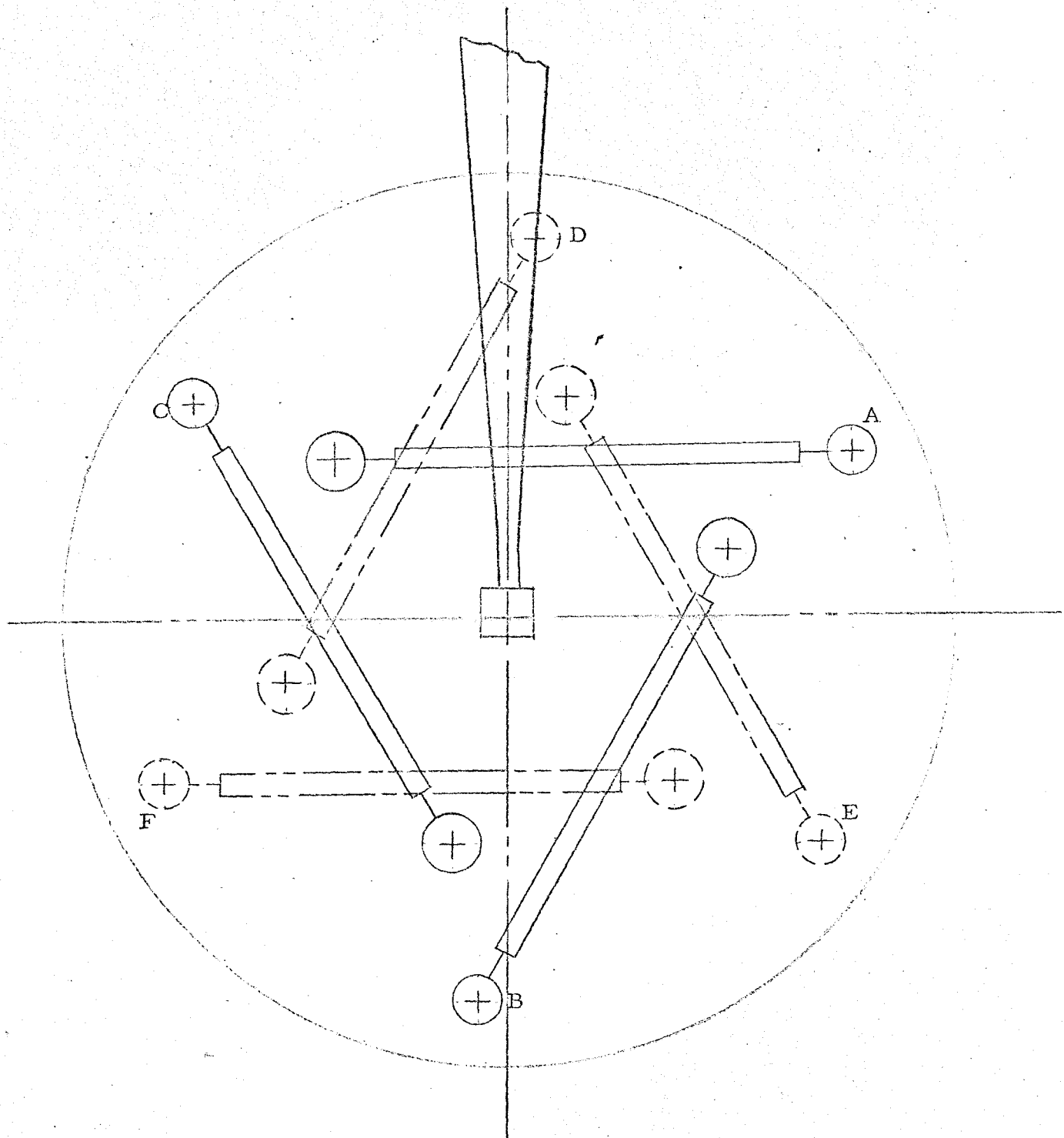


Figure 2.2-9

The following section of this report describes the results of an analysis of SPZ rework and the SPZ suspension system.

2.3.1 Method of SPZ rework to establish the possibility of damage to the SPZ seismometer.

2.3.1.1 The following rework was performed by Bendix on the SN05 Short Period Seismometer (Ref. Figure 2.3-1).

- (a) The 210234-3 suspension wire was replaced twice.
- (b) The Teledyne 233161 tension bolt assembly was replaced with the Bendix 2338790 tension bolt assembly.
- (c) Two 233151 bottom delta rods were replaced.

These areas of rework will be discussed in the following paragraphs from the standpoint of determining if the functional performance of the SN05 SPZ seismometer could have been affected by this rework.

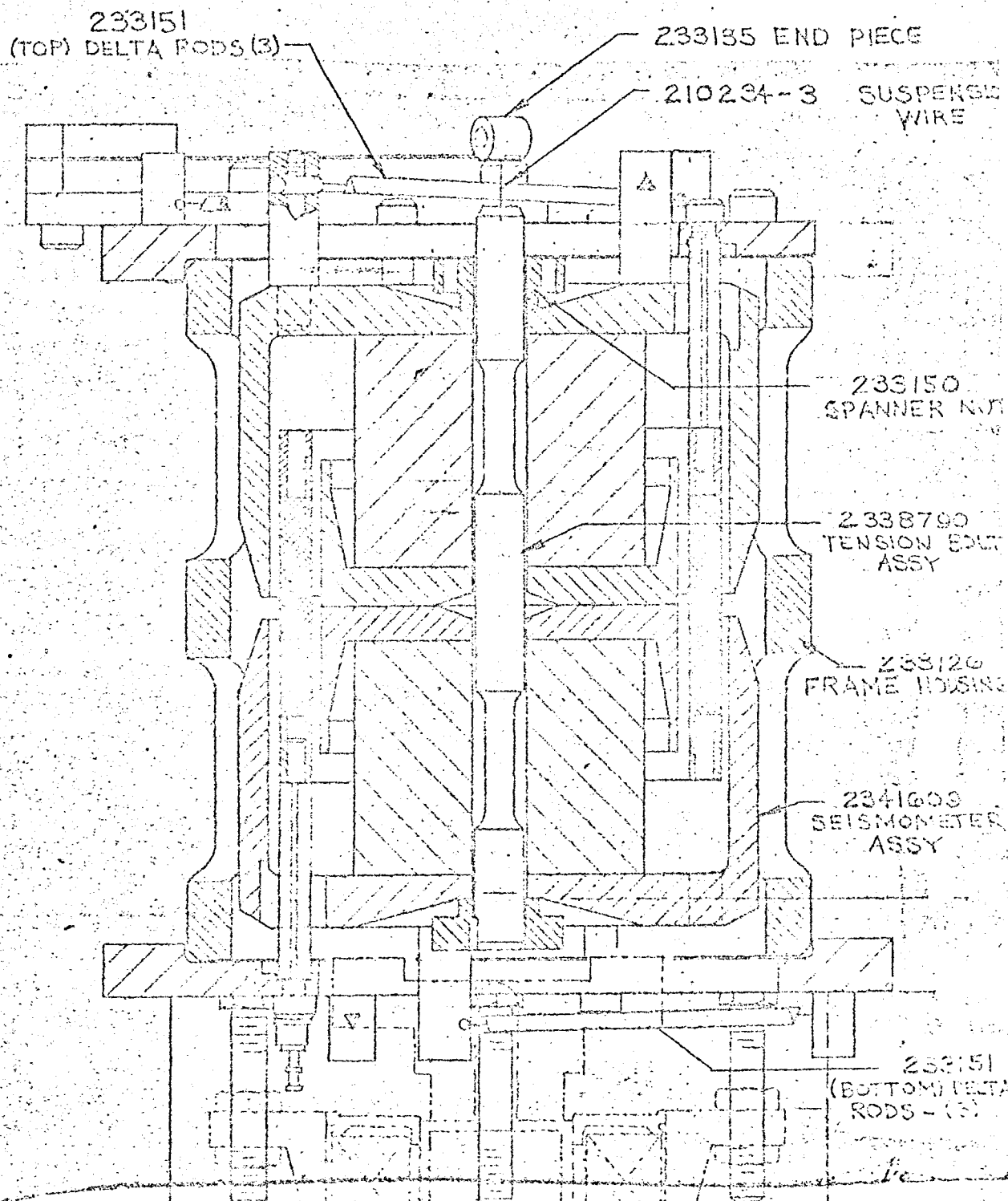
2.3.1.2 Replacement of the 210234-3 Suspension Wire and the Teledyne 233161 Tension Bolt Assembly.

On January 10, 1969 DR-2688 was written against the SN05 Short Period Seismometer stating that the 210234-3 suspension wire was bent in two places and should be replaced. Refer to Figure 2.3-1.

While replacing this suspension wire it was observed that the 233151 spanner nut was loose and the Teledyne 233149 tension bolt had fractured. An investigation of this fracture was made and is documented in memo SSED-100. As a result of the investigation a new Bendix tension bolt was designed and incorporated into the SN05 Short Period Seismometer (Reference BxA 2338790) replacing the 233161 Teledyne Tension Bolt Assembly.

The replacement of the tension bolt assembly was accomplished by mechanically caging the 2341609 seismometer assembly to the 233126 frame housing with (8) eight set screws. By caging the seismometer assembly in this way the tension bolt assembly was replaced without removing or changing the adjustment of the six 233151 Delta Rods assemblies. After the tension bolt assembly was installed a new suspension wire was attached to the suspension spring.

In performing the rework as described above the suspension system of the seismometer was not changed and thus the functional operation of SN05 seismometer should not have been effected.



SN 5 SHORT PERIOD SEISMOMETER ASSEMBLY
SHOWING AREAS OF NEW WORK

FIGURE 2.3-1

2.3.1.3 Replacement of two 233151 Bottom Delta Rods and the 210234-3 Suspension Wire

The SN05 seismometer was vibrated on February 19, 1969 and during the post vibration inspection the following failures were observed. Refer to DR-4106.

- (a) The 210234-3 suspension wire was broken
- (b) Two of the bottom 233151 delta rods were broken (not identified as to which ones)

The SN05 seismometer assembly was reworked to DR 4107 which stated that the diameter of the suspension wire was to be increased from .005 to .006 inches and that the two broken delta rods were to be replaced. After this rework the SN05 seismometer satisfactorily passed the vibration test.

However, as a result of the rework the natural frequency and spring constant of the SN05 seismometer suspension system was changed. It should be noted that these changes can be expected every time delta rods are changed and/or adjusted. The method of determining this change will be discussed in the following paragraphs.

2.3.1.4 Determination of Short Period Natural Period and Spring Constant

The nominal natural period of the Short Period Seismometer is 1.0 second and the mass of the 2341609 magnet assembly was designed to be 500 grams.

From the Float Test Data shown in Table 2.3-1 the natural period curve in Figure 2.3-2 can be plotted for the SN05 seismometer. This curve shows that the natural frequency of the SN05 seismometer when pulsed in the center position was 1.8 seconds. After rework at Bendix, the natural period at the center position was checked and found to be 0.9 seconds which is much closer to the specified period of 1 second than the Teledyne test results of 1.8 seconds. The actual weight of the SN05 magnet assembly was 543.1 grams. From this data, the spring constant for the SN05 seismometer suspension system can be found using the following formula.

$$\frac{2\pi}{T} = \sqrt{\frac{K}{M}}$$

Where

T = Natural Period
K = Spring Constraint
M = Mass = W/g
W = Weight pounds

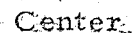
TABLE 2.3-1

Test Specification T-13044Float Test for Short Period SN-05 Seismometer Assembly

Internal Mass, M, = 543.1 grams

Total Travel .240 inches

Mass Position With Respect to Center Inches	Voltage Drop Across 2.01 K Resistor VDC	Signal Coil Current ma	Period Seconds
.075" above	50.310	25.03	.83
.050" above	50.110	24.931	.955
.025" above	49.984	24.87	1.28
Center	49.964	24.86	1.8
.010" below			
.020" below			



Float Test for SN05

Rearranging

$$K = \left(\frac{2\pi}{T} \right)^2 M \quad \text{M For Complete Suspension System}$$

(Suspension Spring Plus Delta Rods)

Solving for case when natural period is .9 second

$$K = \left(\frac{2\pi}{.9 \text{ sec}} \right)^2 (.543 \text{ kg}) \frac{2.2 \text{ lb/kg}}{386 \text{ in sec}^2}$$

$$K = \frac{4 \times 9.9}{81} \times .543 \text{ kg} \times \frac{2.2 \text{ lb/kg}}{386 \text{ in sec}^2}$$

$$K = .154 \text{ lbs/in.}$$

SN-05 Short Period Seismometer

System Spring Rate	.1540 lb/in
<u>Suspension Spring Rate</u>	<u>.0667 lb/in</u>
Combined Delta Rod Spring Rate	.0873 lb/in

Assuming equally loaded delta rod we obtain Spring Rate for each delta rod:

$$\frac{.0876}{6} = .0146 \text{ lbs/in.}$$

This spring constant of .1540 pounds per inch is the sum of the contributions from the 233132 suspension spring and the six 233151 delta rods.

The 233132 suspension spring is made of 0.0093 inch thick Ni Span-C material. It has a triangular shape, thus making it a constant stress spring along its length. The spring constant K can be determined by plotting the data in Table 2.3-2 from test specification T-13059 as shown in Figure 2.3-3. The curve in Figure 2.3-3 shows that the spring constant of the suspension spring for the SN05 seismometer is K = .0667 lb/in.

The combined delta rods have a spring constant equal to the difference between the seismometer system spring rate calculated above of .154 and the suspension spring rate of .0667 pounds/inch. This is shown below:

System Spring Rate	.1540 lb/in
<u>Suspension Spring Rate</u>	<u>.0667 lb/in</u>
Combined Delta Rod Spring Rate	.0873 lb/in

The nominal design value for the spring rate of the combined delta rods is presented in the Final Technical Report (No. 640-07-68-00571 dated 15 August 1968, page 5-17) as .06 pounds per inch.

Weight Grams	Deflection Inches	Period Average Seconds	Spring Constant K gms/cm	Spring Constant K - Pounds/inch	Temp. °F
91.5	.039 above	.552	11.96	.0680	76°F
93.93	.035 below	.542	12.77	.0715	76°F
88.96	.125 above	.556	11.58	.0648	76°F
91.5	.039 above	.552	11.96	.0680	-50°C
91.5	.041 above	.553	11.96	.0680	+100°C

$$K = \frac{M \text{ (gm)}}{T^2 \text{ 24.8 cm}}$$

where

$$M = \frac{W \text{ (gms)}}{g \text{ (lunar)}}$$

T = average period

K = spring rate*

*Spring rate to be 11.3 ± 1.1 gms/cm
gms/cm $\times 5.600 \times 10^{-3} = \text{lb/in.}$

TABLE 2.3-2

DETERMINATION OF SPRING CONSTANT K FOR SHORT PERIOD
SEISMOMETER SUSPENSION SPRING ON SN-05

Reference: Test Specification T-13059, dated 5-26-67

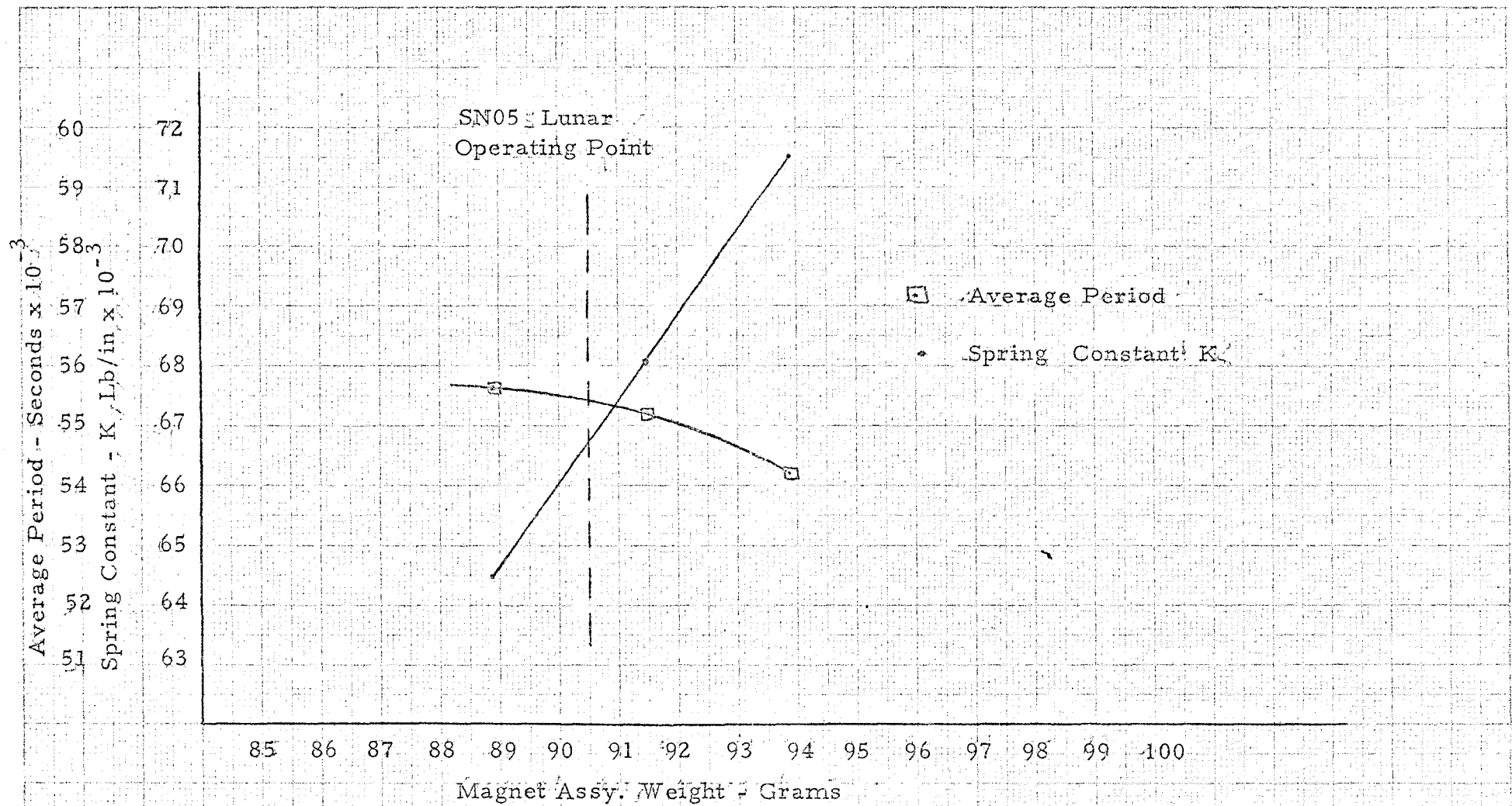


Figure 2.3-3
Short Period SN05 Seismometer Suspension Spring
Spring Constant K & Average Period Vs Magnet Assy. Weight

2.3.2 SPZ Suspension System Tolerances

A dimensional analysis was made of the Short Period Seismometer parts to determine what effect a tolerance build up would have on the functional operation of the instrument.

2.3.2.1 Short Period Suspension System Description

A cross section of the Short Period Seismometer is shown in Figure 2.3-4. The seismic mass consist of the 2341609 seismometer magnet assembly which weighs approximately 1.2 pounds. This magnet mass assembly is supported by the 233132 suspension spring and retained in position in the 233126 frame housing by six 233151 delta rod assemblies. Three on top and three on the bottom of the magnet mass assembly. The seismometer is designed to sense only vertical motion. In operation the readout is obtained through the 233141-2 coil assembly which is fixed to the 233127 top end plate and the 233128 bottom end plate and attached to the 233126 frame housing. Motion of the lunar soil moves the frame and coil assembly relative to the magnet assembly generating a voltage readout which is proportional to velocity. Of particular interest in this investigation was to determine if as a result of tolerance build-up and possible broken delta rods, that the magnet assembly could touch the coil assembly during excitation and thus effect its performance.

2.3.2.2 Dimensional and Tolerance Analysis of Coil Magnet Assembly

A drawing check was made to determine the dimensions of the Short Period Seismometer. The critical dimensions have been identified and shown with their tolerances on Figure 2.3-5.

The tolerance build-up between the 233221 coil assembly and the 233127 and 233128 end plates during the 2341609 seismometer assembly is shown in Figure 2.3-6 and tabulated in Table 2.3-3 below.

As shown in Table 2.3-2 there is a possibility that the 233221 coil assembly can be compressed by .017 inches when installed between the top and bottom end plates. This compression could "bow" the coil assembly reducing the nominal .030 clearance between magnet assembly and coil as shown in Figure 2.3-5. This compression could also crack the 233224 coil terminal boards at the mounting post terminal board interface and contribute to a potential failure.

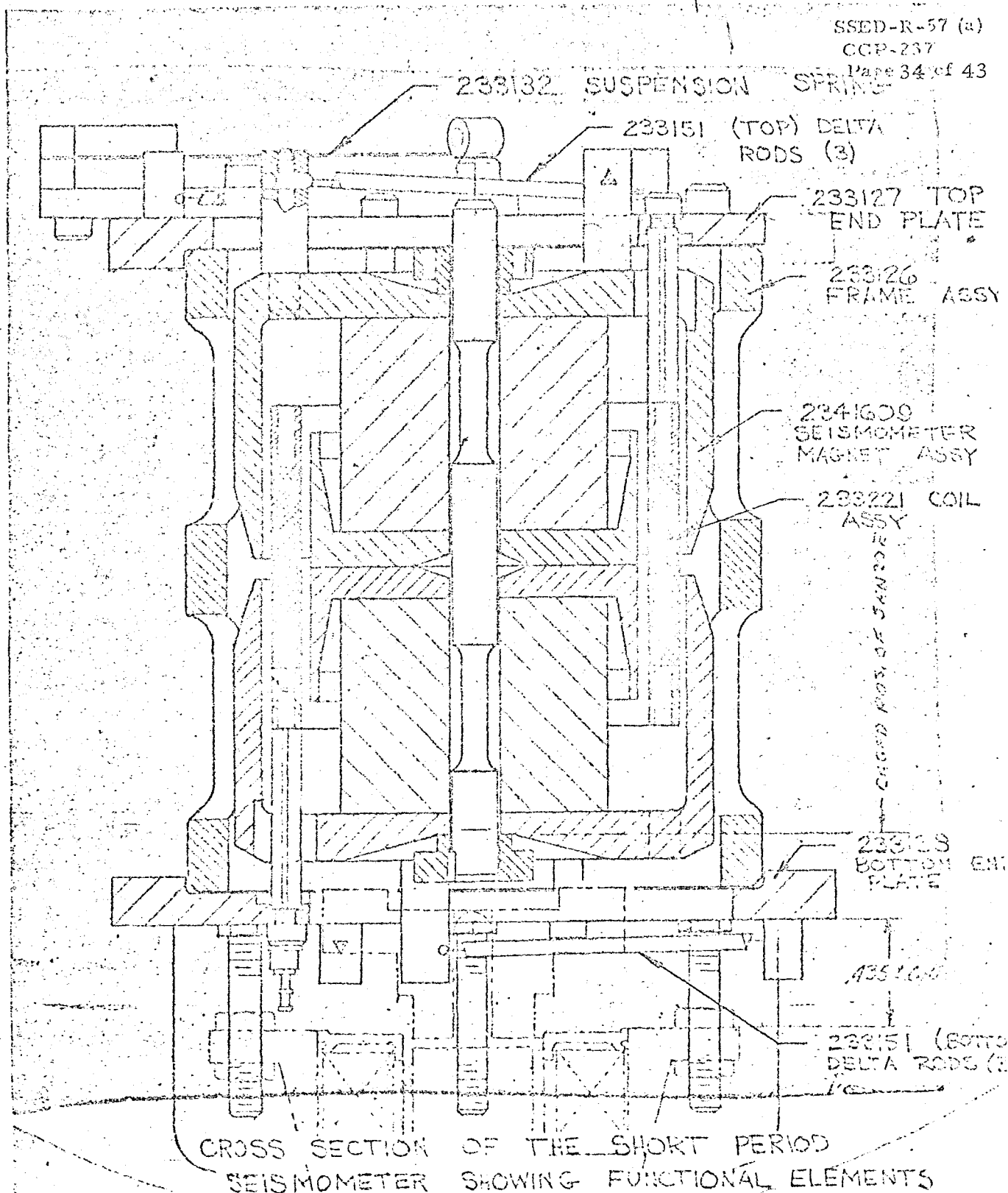


FIGURE 2.3-4

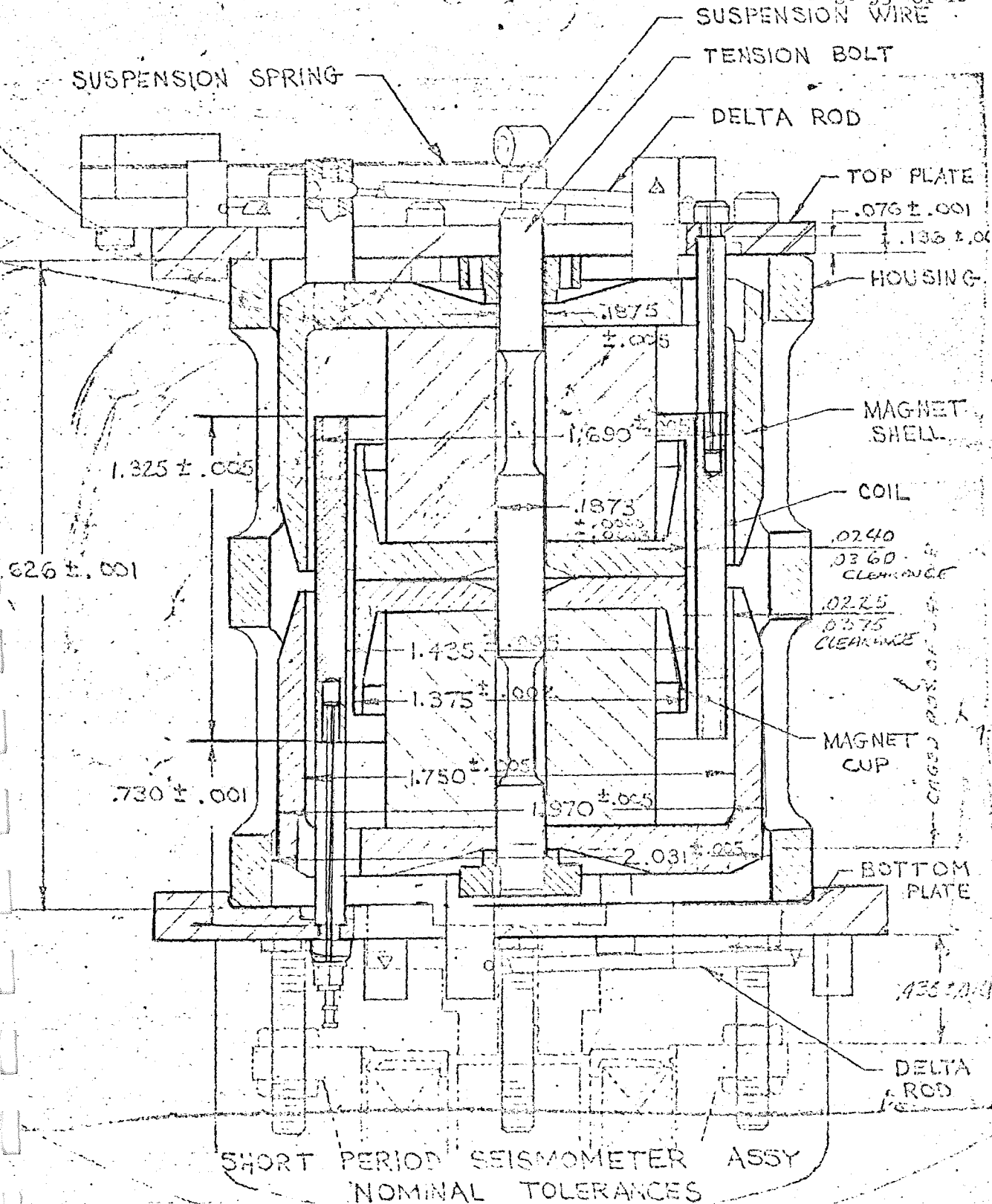
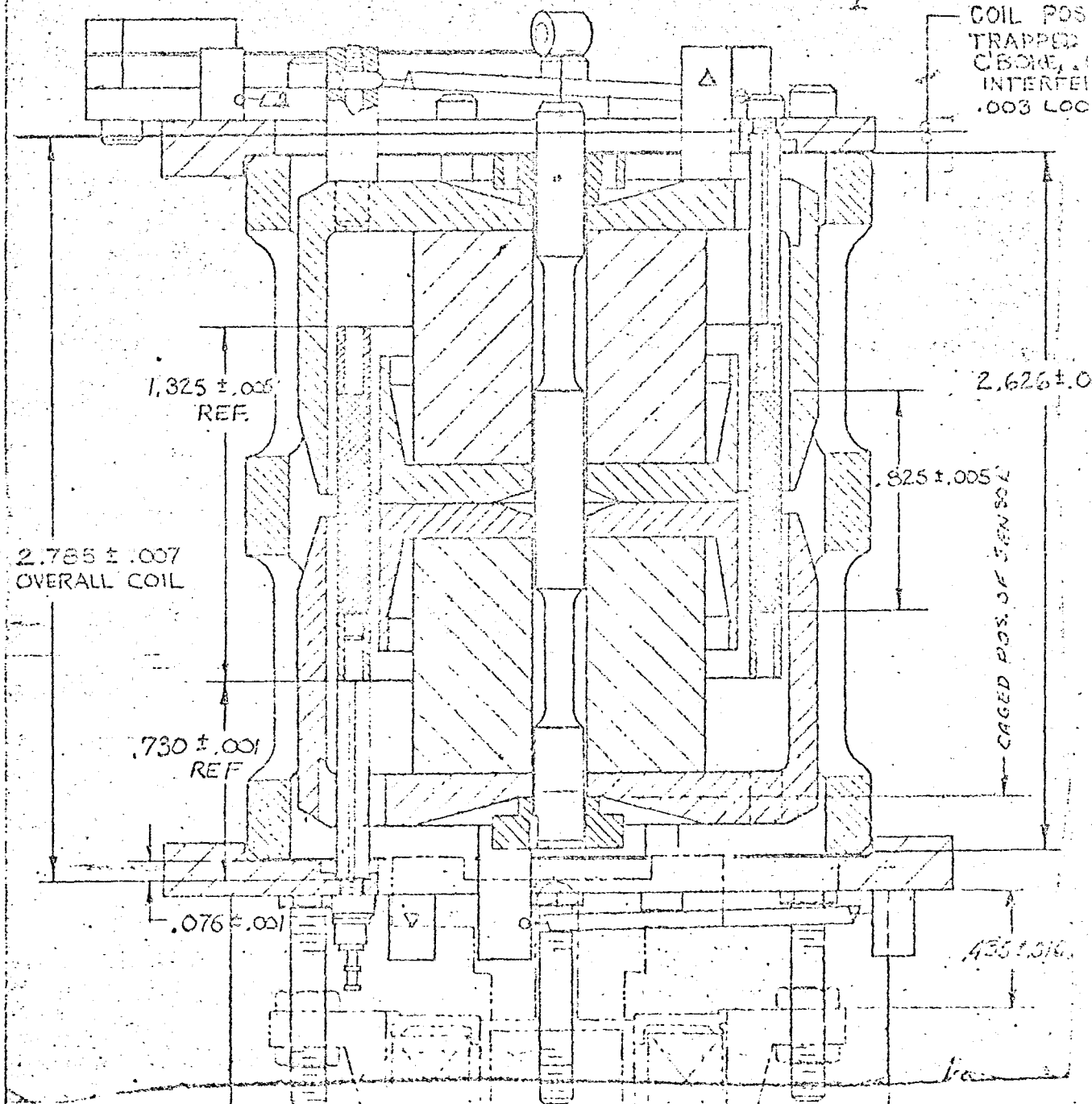


FIGURE 2.3-5



TOLERANCE BUILD-UP OF 233221 COIL ASSY
WHEN ASSEMBLED WITH 2341609 SEISMOMETER ASSY

FIGURE 2.3-6

TABLE 2.3-3

Possible Tolerance Build Up
When Installing 233221 Coil
Assembly into Seismometer Assembly 2341609

1. Minimum DISTANCE between coil support rods through housing and end plates

2.625 - Housing Min Dimension
.075 - Lower Plate Min C'Bore
.075 - Upper Plate Min C'Bore
2.775 TOTAL

2. Maximum DISTANCE between coil support rods through housing and end plates

2.627 - Housing Max Dimension
.077 - Lower Plate Max C'Bore
.077 - Upper Plate Max C'Bore
2.781 TOTAL

3. From Coil Assembly overall height of Coil Assembly, - 2.785 \pm .007

Max Dimension = 2.792 inches
Min Dimension = 2.778 inches

4. Interference Fit = 2.792 - Coil Max
2.775 - Housing Min
0.017 inches

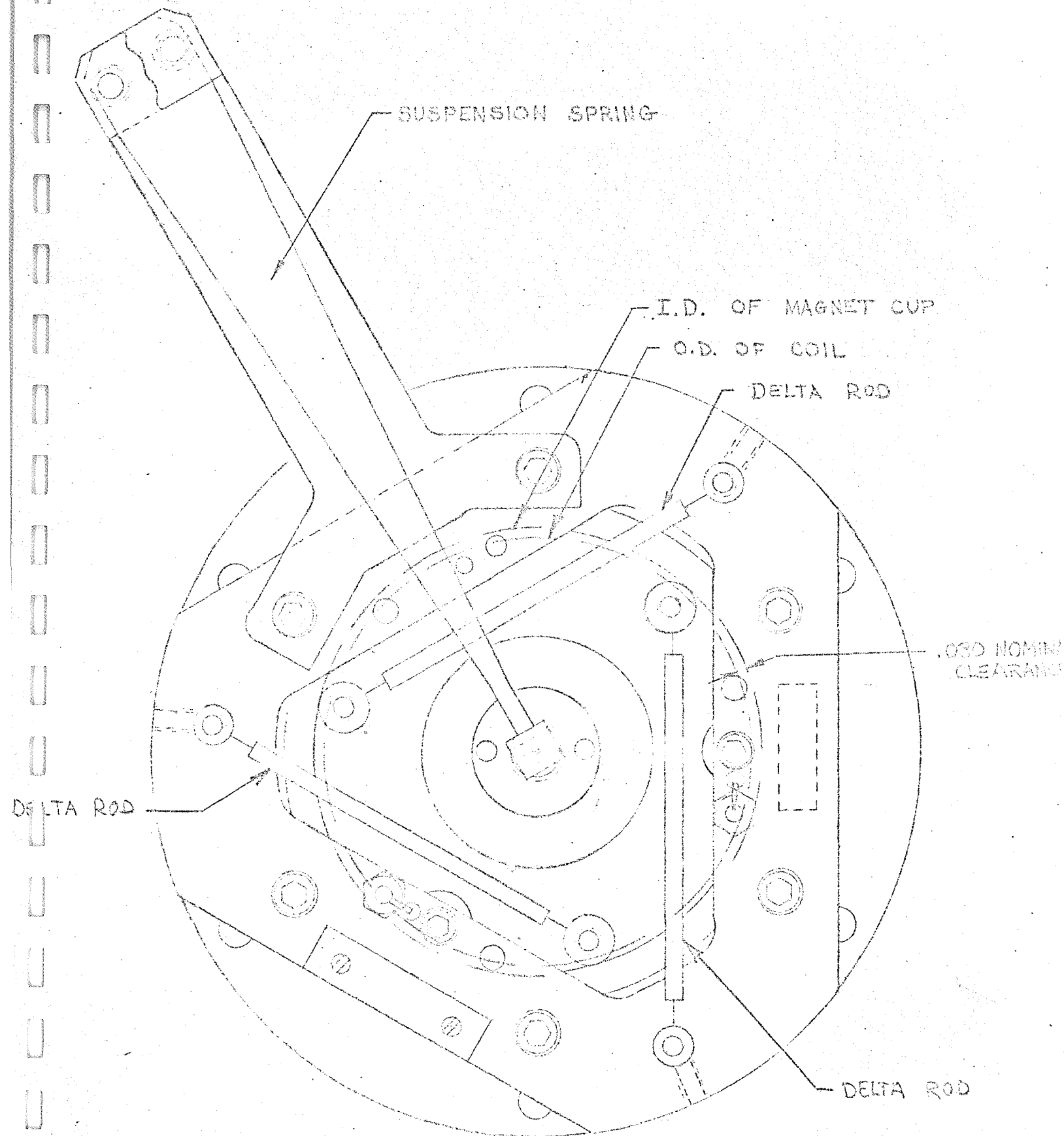
5. Loose Fit = 2.781 - Housing Max
2.778 - Coil Min
0.003 inches

2.3.2.3 Dimensional and Tolerance Analysis of Delta Rod Installation

Six delta rods, three on top and three on bottom, reference Figures 2.3-7 and 2.3-8, are used to restrain lateral movement of the seismic mass in the short period seismometer during normal operation. Delta rod assembly 233151, is dimensioned as to allow a tolerance build-up to occur in assembly causing the condition illustrated in Figure 2.3-9. As can be seen in this figure, the delta rod retaining set screws engage the delta rod end pieces in the transition area between the circular cross section and the "swaged" square cross section. The tolerance build up during delta rod assembly allows the overall distance "free from swage" to vary from 1.663/1.761. However, in order for the set screws to engage the circular cross-section at all times, this dimension must be at least 1.794 inches. It should be further noted that under the present conditions of dimensioning, it is not possible to have both set screws engaging the end pieces in the circular cross section area at the same time. This means that when the set screws are tightened it is possible to have the following unsatisfactory conditions occur.

- (a) The tightening of the delta rod retaining set screw on the transition area could apply a force to put the delta rod in compression.
- (b) The tightening of the set screw could introduce a torsional movement in the end piece, thus placing the .005 diameter wire in torsion.

Considering the above facts it is unfortunate that a multiposition float test was not run on the SNO5 Seismometer after rework. The analysis and recent laboratory tests have brought out that the present short period seismometer assembly procedures do not control the tension loads in the delta rods during installation and as a result there is no way of determining whether the combined spring force is equally divided between the six delta rods. This condition affects the damping characteristics of the system and restrains the seismometer mass, so that it will not function properly when it is displaced below the center position. The over stressing of one or more delta rods in the system also puts the seismometer into a potential failure mode, which could result in broken delta rods during launch vibration and, thus, later affect the functional operation of the seismometer on the lunar surface.



TOP VIEW - SHORT PERIOD SEISMOMETER
FIGURE 2.3-7

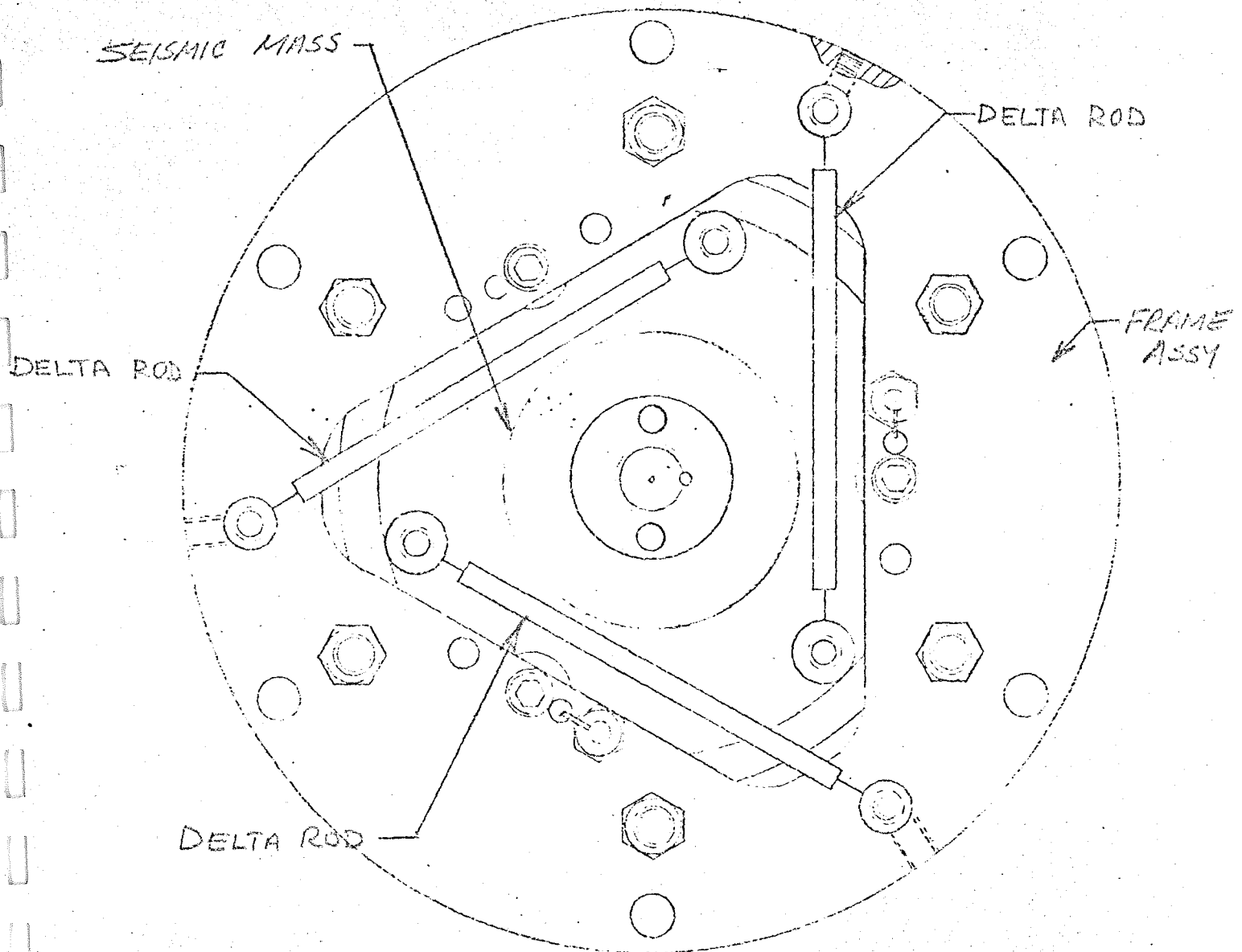
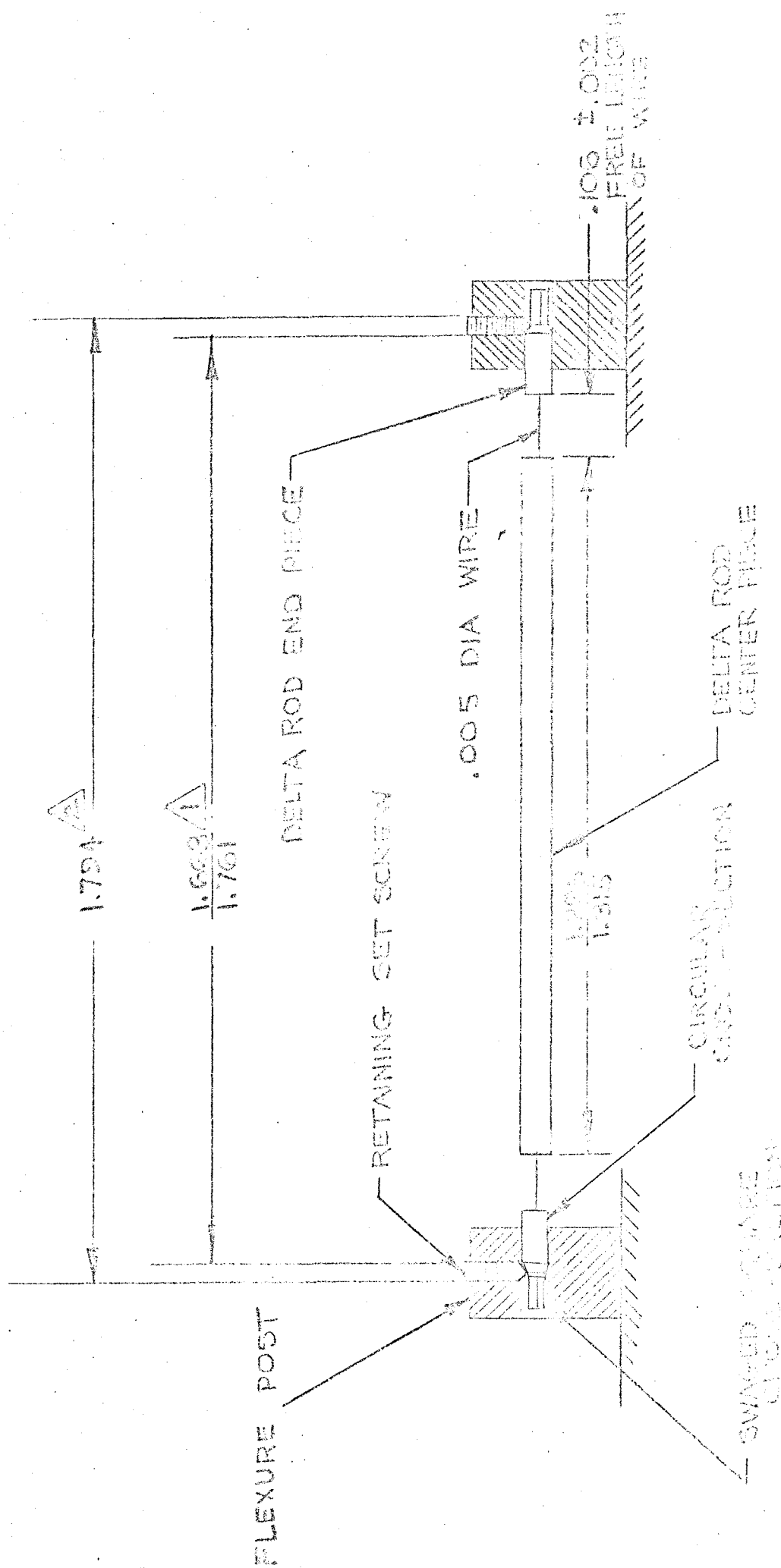


Figure 2.3-8 Bottom View - Short Period Seismometer



NOTES:

⚠ PRESENT DESIGN GIVES THIS DISTANCE FREE FROM SWAGE

⚠ THIS IS MINIMUM DIMENSION THAT MUST BE FREE FROM SWAGE

Figure 2.3-9

Delta Rod Installation

3.0 SUMMARY OF RESULTS

The investigation and study of the SN05 Short Period Seismometer anomalies has revealed the following facts:

1. There is inadequate test data available after the Bendix rework to SN05 to predict the total operation of the Short Period Seismometer.
2. Recent laboratory tests reveal that delta rod misalignment and inadequately controlled installation parameters could be causing the "stiff" operation of the SN05 Short Period Sensor on the lunar surface. There is also a strong indication that the "delta" portion of the rod is too long, which results in an excessive stiffness in each of the delta rods.
3. Investigations have not found any data to support the conclusion that there are one or more broken delta rods on the SN05 Short Period Seismometer.

4.0 CONCLUSIONS AND RECOMMENDATIONS

It is apparent from the recent laboratory tests that the delta rod adjustment is critical to the proper operation of the seismometer and proper adjustment is shown in T-13081 earth spring test by a period deviation of less than $\pm 5\%$ at the positions of center, .050 above and .050 below. Proper seismometer operation is also shown at T-13044 lunar configuration float test when it is possible to float the mass from .075 above to .050 below center. A full range float test should be possible if the delta rods are properly adjusted and the "G" measurement at earth spring test shows less than $\pm 1\%$ deviation.

The analysis also indicates that a further study of the delta rod construction and detailed assembly procedures should be made to insure the repeatability of the assembly and performance of the short period seismometers.

It is recommended that if one or more of the three delta rods on the top or bottom of a seismometer is damaged or broken that the complete set of three is replaced. This will ensure that an overstressed delta rod does not remain in the system and introduce a potential failure mode.

It is also recommended that a change be made to the T-13081 test procedure to limit the tolerance allowed between period measurements as well as a change to T-13044 procedure to require a full range float test.

It is further recommended that sensors SN03 and SN04 be subjected to a complete T-13044 float test procedure as a minimum, pending further investigation of delta rod problems.

5.0 REFERENCES

1. Reports

- 1.1 Final Technical Report for ALSEP Passive Seismic Experiment Subsystem Program - Report N 640-07-68-0057, dated 15 August 1968, prepared by Space Physics Division Staff, Earth Sciences, Teledyne Company, 171 North Santa Anita Avenue, Pasadena, California 91107. (Page 5-17).
- 1.2 SSED-100, Investigation of Tension Bolt Failure, SM05 PSS. R. Johnson
- 1.3 Interim Report, Investigation of PSE Anomalies, Apollo 12 Mission, 21 April 1970

2. Drawings

- 2.1 2.0234-3 Suspension Wire
- 2.2 233161 Tension Bolt Assembly
- 2.3 2338790 Tension Bolt Assembly
- 2.4 233151 Delta Rod Assembly
- 2.5 233149 Tension Bolt
- 2.6 233151 Spanner Nut
- 2.7 2341609 Seismometer Assembly
- 2.8 233126 Frame Housing
- 2.9 233141-2 Coil Assembly
- 2.10 233127 Top End Plate
- 2.11 233128 Bottom End Plate

3. Test Reports

- 3.1 T-13081 S. P. Seismometer and Preamp SN05
- 3.2 T-13044 Float Test SN05 Seismometer
- 3.3 T-13059 Suspension Spring Test SN05 Seismometer 5-26-67
- 3.4 TP2338815 ATP SN05

4. Discrepancy Report

- 4.1 DR-4106 Broken Suspension Wire
- 4.2 DR-4107 Increasing Diameter of Suspension Wire Frame .005 to .006.



**Aerospace
Systems Division**

Investigation of PSE Anomalies
Apollo 12 Mission

NO.	REV. NO.
SSED- R-57 (b)	
PAGE <u>1</u>	OF <u>21</u>
DATE 28 May 1970	

This report provides the results of investigations of PSE anomalies from Apollo 12 mission. Reference 97/510-454, CCP-237, 16 February 1970.

TASK TITLE: Analyze Pulse Output of the SPZ and LP Channels

Prepared by:

J. Fox
J. Fox

Prepared by:

R. Johnson
R. Johnson

Approved by:

J. Lewko, Jr.
J. Lewko, Jr.

CONTENTS

<u>Paragraph</u>	<u>Title</u>	<u>Page</u>
1.0	INTRODUCTION	5
2.0	DISCUSSION	5
2.1	STATEMENT OF WORK	5
2.2	ANALYSIS	5
3.0	SUMMARY OF RESULTS	10
4.0	CONCLUSIONS AND RECOMMENDATIONS	12
5.0	REFERENCES	12

TABLES

<u>Table No.</u>	<u>Title</u>	<u>Page</u>
1	Inter-Channel Coupling vs. Channel Gain Date: 12/2/69	7
2	PSE Sensor Temperature Gradients Prior to SP Pulse Anomaly Activity Intervals	9

ILLUSTRATIONS

<u>Figure No.</u>	<u>Title</u>	<u>Page</u>
1	Recorded Short Period Pulse Anomaly Characteristics	13
2	SP Pulse Anomaly Duration and Amplitude vs. Hours Past Sunrise (Lunations 1 through 6)	14
3	PSE Sensor Temperature (DL-07) and SP Pulse Anomaly PRF Amplitude vs. Time, Luration 1	15
4	PSE Sensor Temperature (DL-07) and SP Pulse Anomaly PRF Amplitude vs. Time, Luration 2	16
5	PSE Sensor Temperature (DL-07) and SP Pulse Anomaly PRF Amplitude vs. Time, Luration 3	17
6	PSE Sensor Temperature (DL-07) and SP Pulse Anomaly PRF Amplitude vs. Time, Luration 4	18
7	PSE Sensor Temperature (DL-07) and SP Pulse Anomaly PRF Amplitude vs Time, Luration 5	19
8	Simplified Schematic, Short Period CSE Electronics (Reference Drawing 234521)	20
9	Simplified Schematic, Long Period CSE Electronics (Reference Drawing 234616)	21

1.0 INTRODUCTION

This task has been performed to identify the probable source and cause resulting in the occurrence of square wave type pulses observed on the output of the SPZ and LP seismometer channels of the ALSEP-1 PSE. In the Interim Report (Reference 1), it was concluded that the pulse train anomalies originate in the short period seismometer high gain preamp in the PSE unit and are subsequently coupled into the long period seismometer channels within the CSE unit.

2.0 DISCUSSION

2.1 Statement of Work

The specific tasks to be performed for this study were identified in MCP task statement 2.0 of Reference 2 as follows:

Task 1 - Analyze characteristics of pulses on the output of the SPZ and LP channels.

Task 2 - Evaluate pulse occurrence with intent of isolating the source to be within the PSE sensor or CSE unit.

Task 3 - Determine if there is any correlation between pulse train anomalies and PSE sensor or CSE temperature.

Task 4 - Review characteristics of system to identify most likely source of any interference causing the observed pulse anomalies.

2.2 Analysis

2.2.1 Task 1 - Pulse Characteristics

A plot of a typical SP channel pulse segment as reconstructed from ALSEP-1 recorded data is shown in Figure 1. The decay characteristic of the pulse wave shape is assumed to be largely due to the data conversion, processing and filtering functions.

The largest peak value observed on any of the SP pulses with the attenuator set to 0 db is 3 LSB, corresponding to 15 mv at the highest gain setting. In Reference 3, an acceptable noise level at the SP channel output is defined (Section 8.8.2.12) to be 3 LSB with the attenuator set to -10 db. Hence, the amplitude of the observed SP pulse anomalies is less than the acceptable SP channel noise level.

Referring again to Figure 1, periods T_1 and T_2 may vary by 20% over a one minute interval, and over a 6:1 range for a several hour interval. The smallest value of T_1 or T_2 observed on any recording is on the order of 2 sec, but typically, the highest pulse repetition frequency (PRF) sustained for any appreciable interval is on the order of 10 pulses per minute (i.e., $T_1 = T_2 = 3$ sec).

Typical SP pulse train activity observed on the 3rd through 6th lunar days can be characterized as follows:

- o Pulse activity intervals are on the order of 20 to 30 hours
- o Normally start with a PRF of 50 to 100 pulses per hour with a linear increase in PRF to on the order to 500 to 600 pulses per hour at the interval mid-region.
- o Subsequent linear decrease in PRF to a low value prior to pulse activity termination.

From inspection of several LP and SP recordings presented in Reference 4, it can be shown that the SP pulses also appear on all LP channels with approximately equal amplitudes, when all channel attenuators are set to 0 db.

2.2.2 Task 2 - Isolation of Pulse Occurrence Source

Since the pulse train anomaly occurs on all channels with nominal gain settings, it is of interest to determine whether (1) the pulses occur independently on each channel or (2) the pulses originate on one channel and couple into the other channels.

From inspection of the recorded data available for all channels during the period 12-2-69 to 12-3-69, it can be shown that the pulses originate in the SP channel and are coupled into the LP channels at some point in the CSE unit, after the SP attenuation stage, and before the LP post amp stages.

The effect of inter-channel coupling from the SP to the LP channels is shown in the recorded data of Table 1. When the SP attenuation is successively increased in intervals 2, 3, and 4, the pulse amplitude is also proportionately reduced on each channel. An additional result is one of SP pulse levels less than the LSB amplitude (5 mv) still inducing readable pulse levels in the LP channels. Alternately, in intervals 6, 7 and 8 the LPZ post amp input attenuation is increased resulting in a reduction of only the LPZ pulse amplitude.

The following conclusions can be drawn from the data presented in Table 1:

- (a) The pulses originate in the SP sensor unit rather than in the CSE.
- (b) The SP pulses are coupled into the LP channels at some point following the SP attenuator, the most likely coupling point being the output of the SP post amp in the CSE. This point is labeled "A" in Figure 8.

Interval Number	GMT Time Interval		Channel Gain, db			Recorded P-P Pulse Amplitude			Result
						per Channel, mv			
	From	To	LP X, Y	LP Z	SP Z	LP X, Y	LP Z	SP Z	
1	1600	1605	0	0	0	20	20	20	Nominal gain settings
2	1605	1607	0	0	-10	15	15	5	Lower SP gain reduce pulse amplitude all channels
3	1607	1611	0	0	-20	10	10	5	Same as above
4	1611	1615	0	0	-30	5	5	5	Same as above
5	1615	1655	0	0	0	20	20	20	Nominal gain settings
6	1655	1700	0	-10	0	20	10	20	Lower LPZ gain re- duces pulse only on LPZ
7	1700	1703	0	-20	0	20	5	20	Same as above
8	1703	1707	0	-30	0	20	5	20	Same as above

Table 1 Inter-Channel Coupling vs. Channel Gain
Date: 12-2-69

- (c) Coupling into the LP channels apparently occurs at some point prior to the LP attenuator and post amplifier stages since (1) reducing LP gain also reduces pulse amplitude only on that channel and (2) LP channel amplification of small amplitude SP pulses is indicated. A likely candidate for the coupling point is each of the LP attenuator and post amp input signal lines in the CSE unit as indicated by points "B" and "C" in Figure 9.

- (d) A possible inter-channel coupling mechanism is presented by the ± 2.5 vdc reference lines which originate on the SPZ PWB in the CSE. These lines are physically adjacent to the SPZ post amp output point and are also printed physically adjacent to each of the LP attenuator and post amp input points "B" and "C" in Figure 9 (see PWB assembly drawings 234520 and 234615-1, -2).

2.2.3 Task 3 - Correlation of SP Pulse Anomalies with PSE Sensor or CSE Temperature

A preliminary conclusion was noted in the Interim Report (Reference 1), that the SP pulse anomaly did not appear to be correlated with PSE sensor temperature. This conclusion was based upon complete data intervals for the first and second lunations and incomplete data for the third and fourth lunations.

Since the Interim Report, complete SP pulse activity data has been compiled up to 6 days past sunrise on the fifth lunation (22 March 1970), and partial monitoring results are also available over the entire fifth and sixth lunations. The following conclusion may be drawn from the extensive compilation of SP pulse activity data: the pulse activity periods can be correlated with PSE sensor temperature gradients, but not with any restricted range of temperature magnitude.

The known periods of SP pulse anomaly activity are indicated in Figure 2 for lunations 1 through 6 in bar graph form denoting magnitudes of PRF for each train over the interval. Solid line plots denote detailed data measurements, and dashed line plots indicate approximate amplitude and/or duration wherever exact data measurements are not yet complete. As noted in Figure 2, pulse activity appeared during the first lunation between lunar noon and sunset, and also during the first lunar night at 570 and 672 hours past sunrise. During the second lunation, pulse activity appeared at sunrise, between noon and sunset and again during the second lunar night. During the third through sixth lunations, no SP pulse activity has been detected during the lunar night (except for 10 hours past theoretical sunset on Lunation 4).

The bar graph plots of PRF amplitude from Figure 2 have been transferred to separate plots of PSE sensor temperature (DL-07)* for each of the lunations, 1 through 5, in Figures 3 through 7, respectively. A computer plot has not yet been generated for Lunation 6. In Figures 4 and 5 small "no data" intervals are noted. In Figure 7, the end of the data from currently available range tape recordings are noted. On each of the Figures 3 through 7, the sensor temperature gradient value preceding SP pulse activity is noted wherever the value is known.

*DL-07 is the ALSEP telemetry word designation for Passive Seismic Instrument Temperature.

In Figures 3 and 4, for Lunations 1 and 2, respectively, the sensor temperature was off scale at the low end of the temperature range during each lunar night. Accordingly, the sensor temperature gradients for SP pulse activity during these periods is not known but is assumed to be non-zero (i.e., sensor temperature not constant during first two lunar nights).

Starting with the third lunar night, the LPZ leveling motor was maintained in the "on condition" during the lunar night causing the PSE sensor temperature to remain approximately constant starting about 24 hours past sunset each lunar night. As can be noted on Figures 2, 5, 6 and 7, no SP pulse activity has been detected during the lunar night intervals of constant PSE sensor temperature.

Furthermore, for those SP pulse activity periods where sensor temperature data is available, the sensor temperature gradient absolute value always exceeds 1.0°F per 24 hours, just prior to initiation of SP pulse activity. A listing of the gradient values for each SP pulse activity initiation is given in Table 2 below.

<u>Lunation No.</u>	<u>SP Pulse Start Time</u>	<u>PSE Sensor Temperature Gradient (°F/24 hrs)</u>
1	12-01-69 0900 GMT	-4.10
	12-12 1200	unknown, off scale low, lunar night
	12-16 2100	unknown, off scale low, lunar night
2	12-18 1200	unknown, off scale low, sunrise
	12-27 1140	+1.70
	1-05-70 1520	-5.25
3	1-23 1648	+6.50
	1-25 0550	+3.07
4	2-16 0920	-1.05
	2-23 1440	+2.88
	3-2 2200	-1.01
5	3-18 0000	-1.05
	3-25 1600	+2.70

Table 2 PSE Sensor Temperature Gradients Prior to
SP Pulse Anomaly Activity Intervals

Considering all of the combined information in Figures 2 through 7 plus Table 2 it can be noted that a definite pattern of SP pulse activity is developing with characteristics as follows (assuming sensor temperature control cycle remains the same):

- o SP pulse activity intervals occur approximately 18 hours past sunrise, with a sensor temperature gradient approximately $-1.05^{\circ}\text{F}/24$ hours. Also, occasional activity appears near sunset with the same gradient.
- o SP pulse activity intervals occur approximately 190 hours past sunrise (sun angle = 100°) with sensor temperature gradients about $2.9^{\circ}\text{F}/24$ hours.
- o The lunar afternoon pulse activity intervals are always longer than the lunar morning activity intervals apparently corresponding to the higher initiating gradient levels.

Due to the close correlation between SP pulse activity and PSE sensor temperature gradient, the correlation between SP pulse activity and CSE temperature has not been studied.

2.2.4 Task 4 - Identify Likely Interference Source

The most likely source of interference causing the observed SP pulse anomalies, is the effect of time dependent thermal gradients on the circuit element parameters in the SP high gain preamp, located in the PSE sensor unit. The preamp output is connected via the ribbon cable to the SP attenuator stage input in the CSE. Since increasing the degree of attenuation decreases the pulse amplitude on the SP channel output, in all probability, the pulses originate prior to the CSE input stage, i.e., in the SP preamp itself. This theory appears to be further confirmed by the close correlation between SP pulse activity and PSE sensor temperature gradient.

3.0 SUMMARY OF RESULTS

3.1 Pulse Characteristics

The constant pulse waveshape amplitude, and short term constant pulse widths, with slowly varying pulse repetition frequency indicate that the SP pulse anomalies are electrically generated rather than mechanical in nature. For any given pulse train, the peak PRF and activity duration are approximately proportional to the PSE sensor temperature gradient magnitude immediately preceding the SP pulse activity.

3.2 Pulse Source and Inter-Channel Coupling

The source of the square-wave pulse anomalies observed on the SP and LP channel outputs appears to be the SP preamp located in the PSE unit. Since no telemetry test points exist at the SP preamp output, this claim cannot be conclusively verified. However, the sensitivity of pulse activity to PSE temperature gradient magnitude supports this conclusion.

Inter-channel coupling of the SP pulses into all of the LP channels occurs within the CSE unit as supported by the data of Table 1. The available data indicates that the SP channel pulses are amplified when coupled into the LP channels which in turn suggests that the SP pulses are introduced into the LP channels on the LP attenuator and post amp input lines (AR1, schematic 234616 and assembly 234615-1, -2). Since the SP and LP pulse amplitudes are reduced when the SP attenuation is increased, it is concluded that the likely coupling point from the SP to the LP channels is at the SP attenuator stage output (AR2, schematic 234521 and assembly 234520). The likely candidates for the coupling mechanism are the ± 2.5 vdc reference lines which are printed physically adjacent to the SP AR2 output point and all of the LP attenuator and AR1 input lines.

3.3 Pulse Cause and Correlation with PSE Sensor Temperature

The data of Figures 3 through 7 and Table 2 shows that a necessary (but not sufficient) condition for SP pulse activity is the existence of a PSE sensor temperature gradient with an absolute value exceeding 1.0°F per 24 hours. Since the exact thermal gradients measured with respect to any given dimension within the PSE unit are unknown, it is theorized that the sufficient condition for SP pulse activity could only be defined by measurements of thermal gradients across certain elements of the "W" board assembly in the PSE unit. This board contains the SP preamp in addition to the heater control circuit.

It is concluded that the direct cause of SP pulse activity is the variation of the quiescent operating point in one or more SP preamp transistor stages. The Q point variation is due to time dependent thermal gradients within the PSE unit in close proximity to the "W" board assembly. The variation in Q point could be due to thermally induced changes in (1) the transistor parameters or (2) the reference voltage levels or (3) a combination of (1) and (2).

3.4 Predicted SP Pulse Activity

Under the assumption that the PSE thermal control cycle remains the same for lunations following the third through sixth, the following initiation times of SP pulse activity can be predicted from the data of Figure 2.

<u>Lunation</u>	<u>Predicted SP Pulse Activity Initiation Time</u>	
	<u>Date</u>	<u>Time, GMT</u>
7	5-16-70	0030
	5-23	0600
8	6-14	1130
	6-21	1700
9	7-13	2200
	7-21	0400

4.0 CONCLUSIONS AND RECOMMENDATIONS

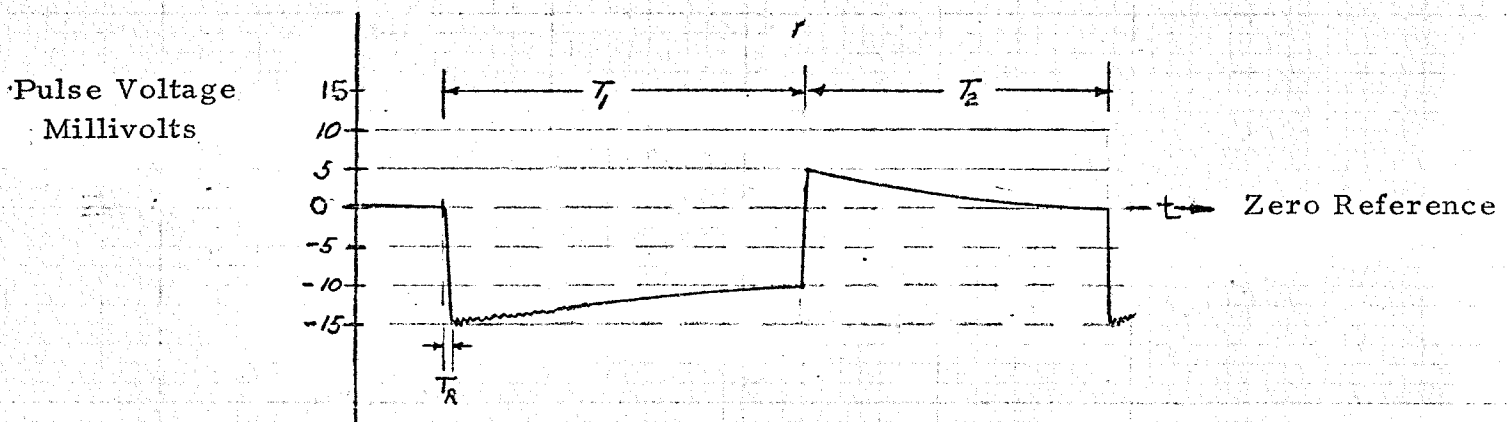
It is concluded that SP (and LP) pulse anomalies are directly caused by excessive thermal gradients within the PSE unit. If the improved PSE thermal control design ensures that PSE sensor temperature gradients are constrained to less than 1.0°F per 24 hours, then no further engineering action is recommended to resolve the SP pulse anomaly problem.

If the PSE thermal gradient constraint cannot be ensured, and it is determined that the SP and LP pulse anomaly amplitudes represent a sufficient degree of degradation to the SP and LP scientific data, then it is recommended that test measurements be performed upon the combined PSE and CSE units under simulated lunar environmental conditions. The test objectives would be to determine the exact source of the SP pulse train and the exact coupling mechanism into the LP channels. These tests would require implementation of signal analyzer equipment to detect the (assumed) periodic pulse train immersed 10 db below the nominal SP output random noise level when the attenuator stage is set to 0 db. The results of such tests could then be utilized as inputs to a redesign study of the SP preamp circuit and/or assembly in the PSE unit.

Based on the conclusions of this study, no design changes are recommended for either the SP or LP channels circuits in the CSE unit.

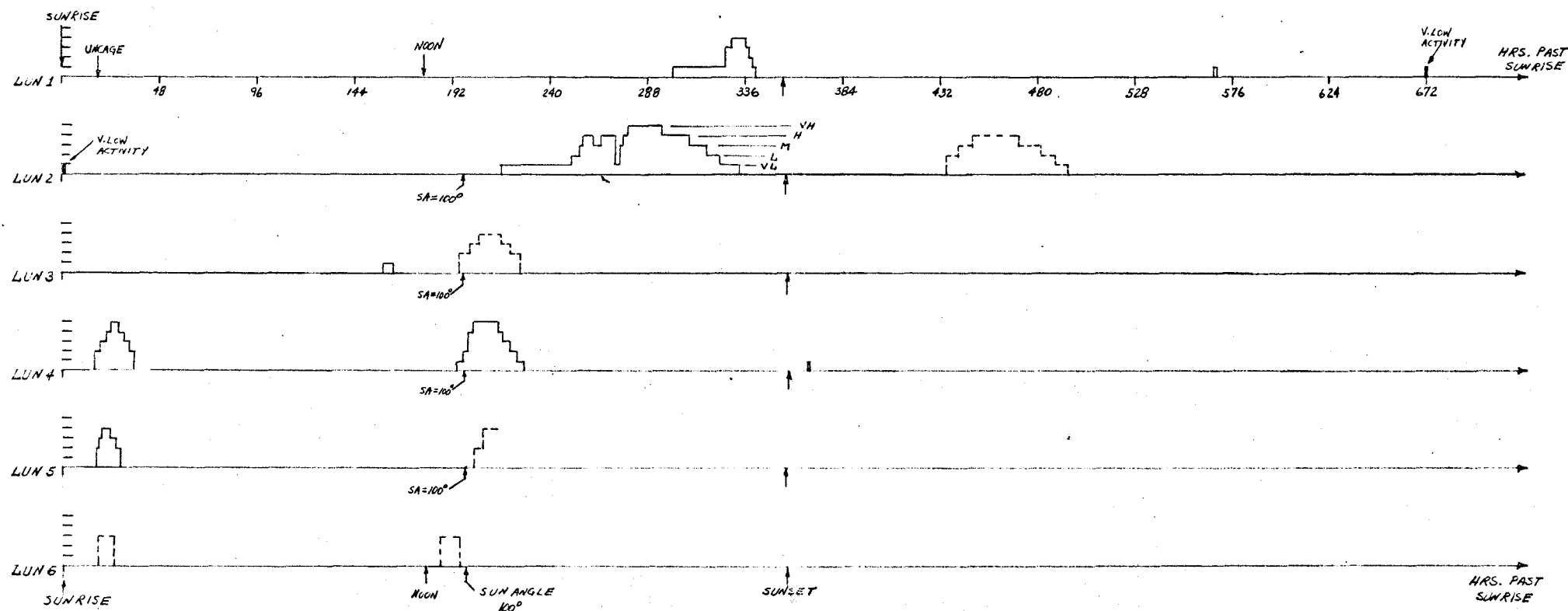
5.0 REFERENCES

1. Interim Report, Investigation of PSE Anomalies, Apollo 12 Mission, SSED-R-57 (b), 4/21/70.
2. Apollo 12 PSS Anomalies, SSED-P-1057 (a), J. Lewko, 1/8/70
3. PSE Acceptance Test Procedure, TP 2338848A, 2/3/70
4. Identification of Apollo 12 PSS Problems, Anomalies and Preliminary Action Plan, SSED-346, J. Lewko/D. Breseke, 12/10/69.



Recorded Short Period Pulse Anomaly Characteristics

Figure 1



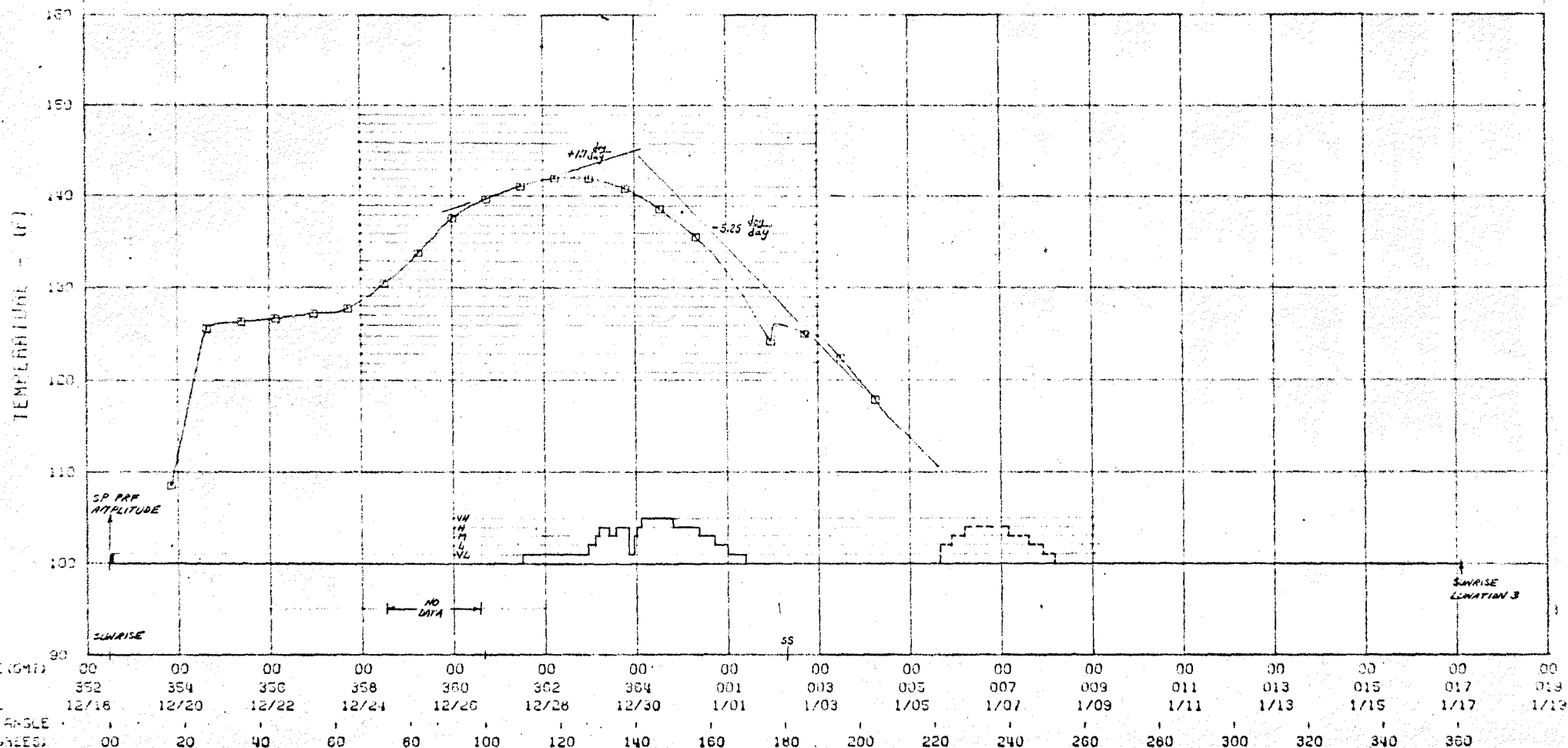
Legend

VH	Over 480 pulses per hour
H	300 to 480 pulses per hour
M	180 to 300 pulses per hour
L	60 to 180 pulses per hour
VL	below 60 pulses per hour

Figure 2. SP Pulse Anomaly Duration and Amplitude vs Hours Past Sunrise (Lunations 1 through 6)

SUNRISE DAY 352 (DECEMBER 18, 1969) AT 1118 GMT
SUNRISE DAY 017 (JANUARY 17, 1970) AT 0200 GMT

DL-07 PASSIVE SEISMIC INSTRUMENT TEMPERATURE

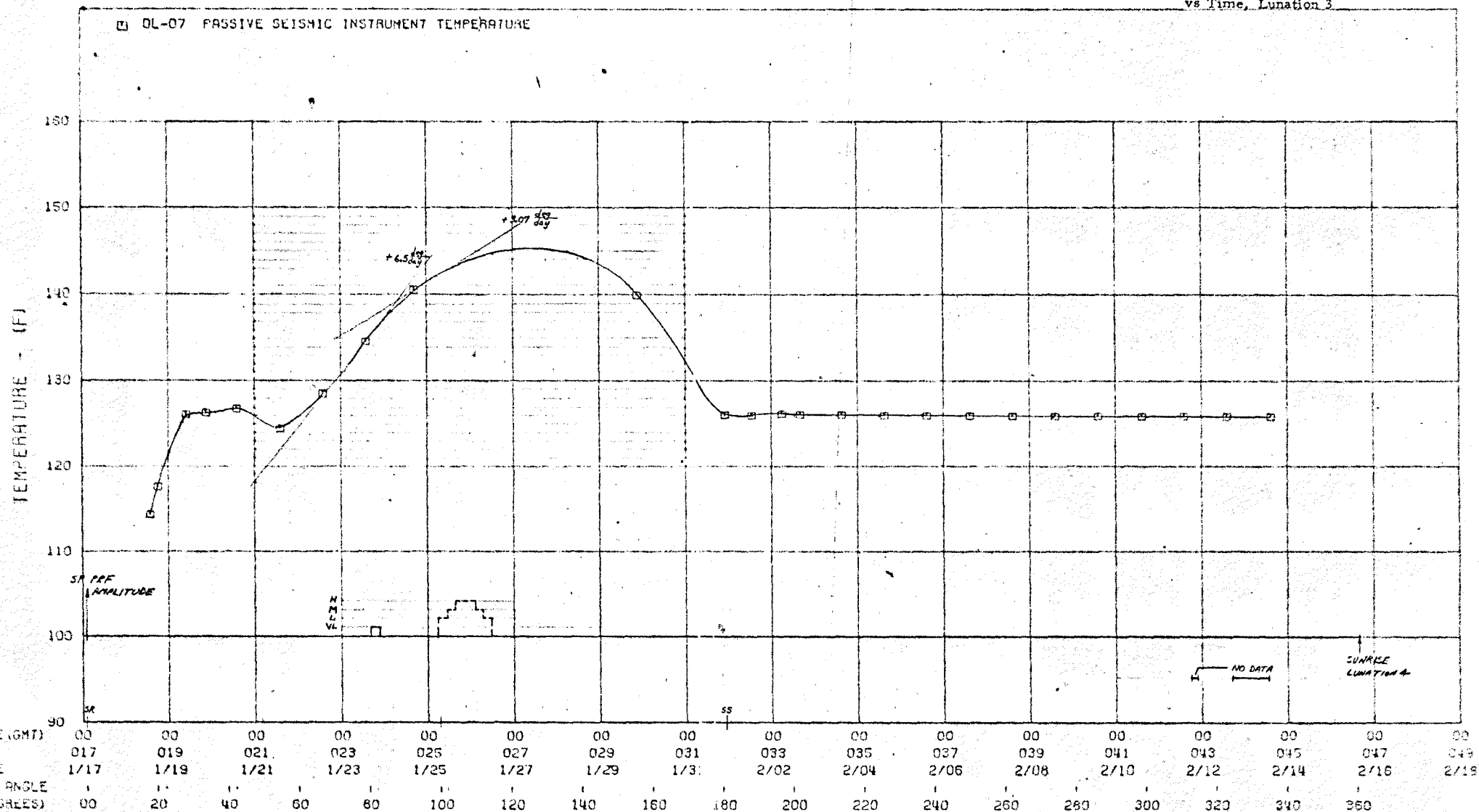


BENDIX AEROSPACE SYSTEMS DIVISION - THERMOPHYSICS GROUP
 APOLLO LUNAR SURFACE EXPERIMENTS PACKAGE (FLIGHT 1 - APOLLO 12) - THIRD ALSEP LUNATION
 SUNRISE DAY 017 (JANUARY 17, 1970) AT 0200 GMT
 SUNRISE DAY 046 (FEBRUARY 15, 1970) AT 1600 GMT

SSED-R-57 (b)

Page 17 of 21

Figure 5. PSE Sensor Temperature (DL-07)
 and SP Pulse Anomaly PRF Amplitude
 vs Time, Lunation 3



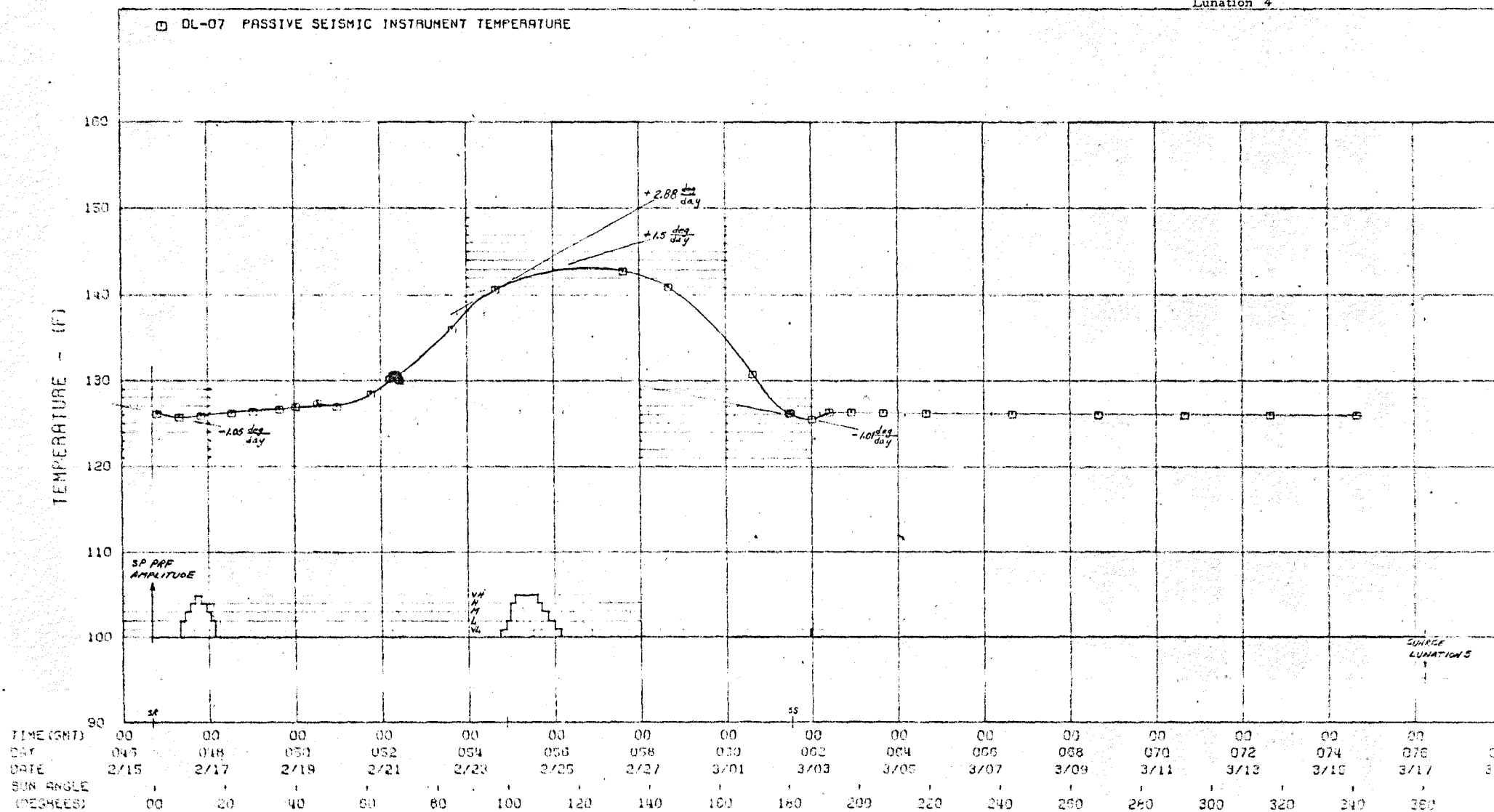
BENDIX AEROSPACE SYSTEMS DIVISION - THERMOPHYSICS GROUP
 APOLLO LUNAR SURFACE EXPERIMENTS PACKAGE (FLIGHT 1 - APOLLO 12) - 4 TH ALSEP LUNATION

SSSD-R-57 (b)

Page 18 of 21

SUNRISE DAY 046 (FEBRUARY 15, 1970) AT 1600 GMT
 SUNRISE DAY 076 (MARCH 17, 1970) AT 0600 GMT

Figure 6. PSE Sensor Temperature (DL-07) and SP Anomaly PRF Amplitude vs Time, Lunation 4



BENDIX AEROSPACE SYSTEMS DIVISION - THERMOPHYSICS GROUP
 APOLLO LUNAR SURFACE EXPERIMENTS PACKAGE (FLIGHT 1 - APOLLO 12) - FIFTH ALSEP LUNATION

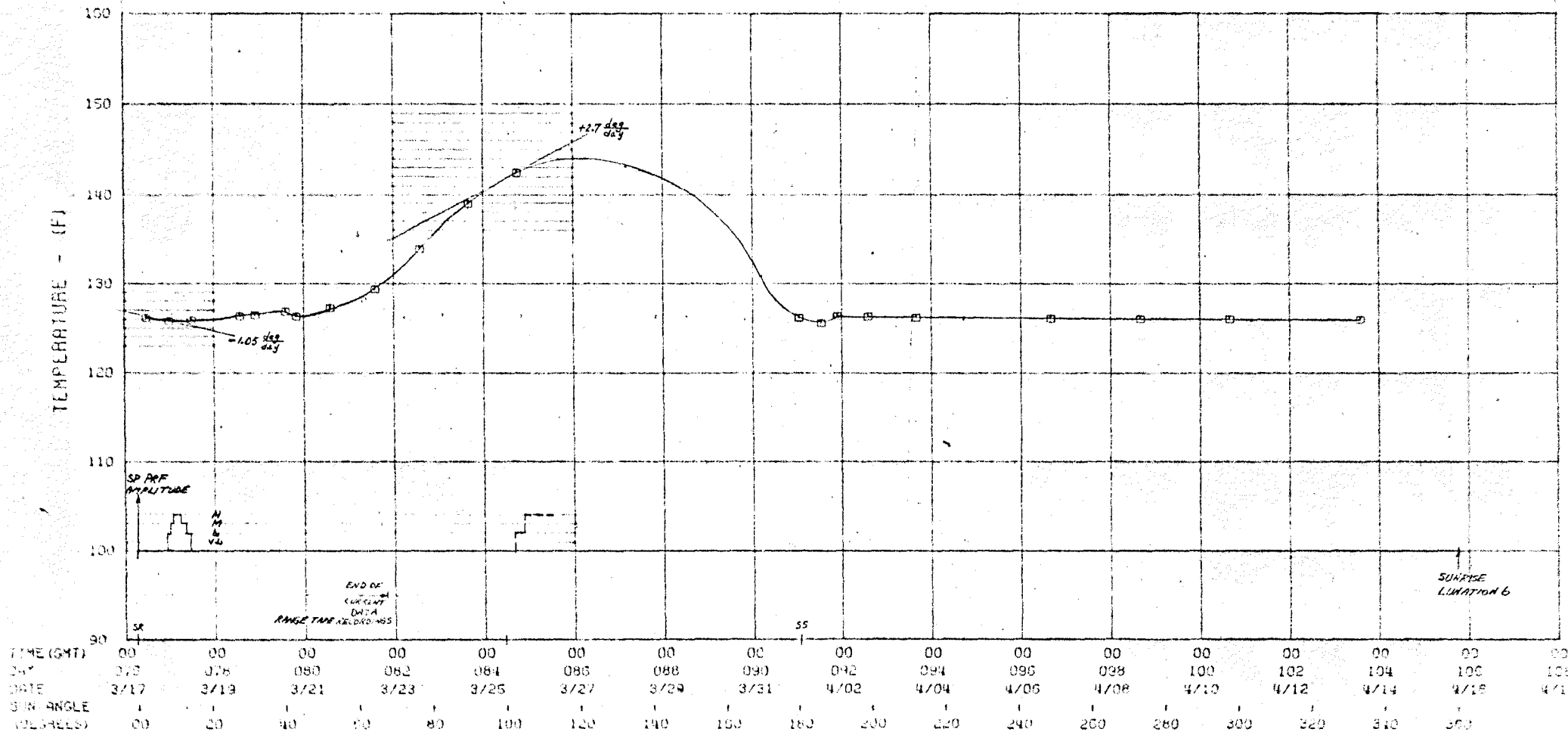
SUNRISE DAY 076 (MARCH 17, 1970) AT 0600 GMT
 SUNRISE DAY 105 (APRIL 15, 1970) AT 1900 GMT

SSED-R-57 (b)

Page 19 of 21

Figure 7. PSE Sensor Temperature (DL-07) and SP Pulse Anomaly PRF Amplitude vs Time, Lunation 5

(1) DL-07 PASSIVE SEISMIC INSTRUMENT TEMPERATURE



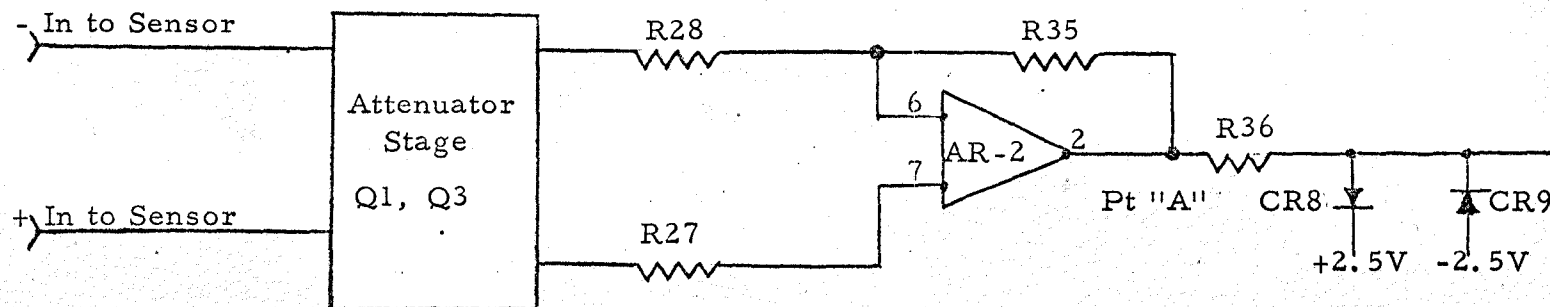


Figure 8 Simplified Schematic, Short Period CSE Electronics
(Reference Drawing 234521)

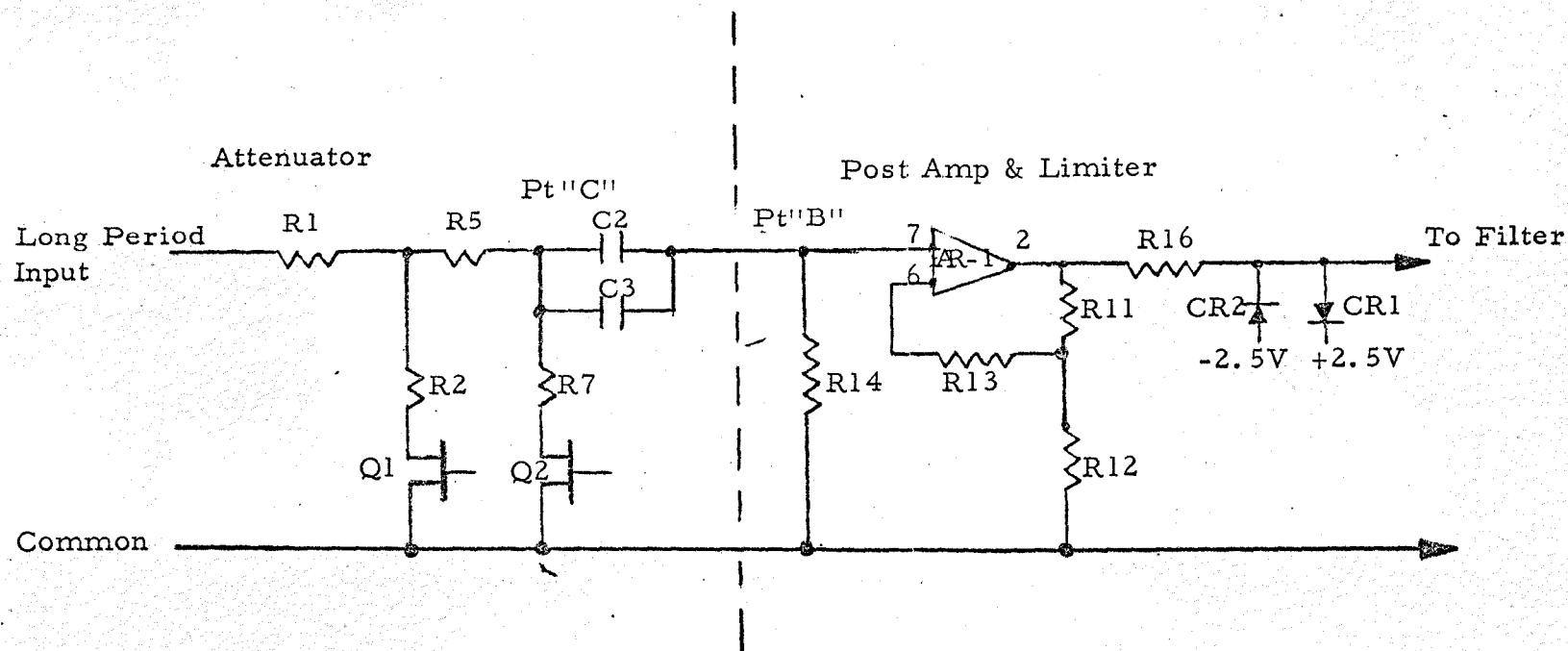


Figure 9 Simplified Schematic, Long Period CSE Electronics
(Reference Drawing 234616)



**Aerospace
Systems Division**

Investigation of PSE Anomalies

Apollo 12 Mission

SSSED-
R-57 (c)

PAGE 1 OF 21

DATE 28 May 1970

This report provides the results of investigations of PSE anomalies from Apollo 12 mission. Reference 97/510-454, CCP-237, 16 February 1970.

TASK TITLE: Investigate the Cause of Unstable LPZ Period.

Prepared by:

M. Asnani
M. Asnani

R. S. Johnson
R. Johnson

Approved by:

J. Lewko, Jr.
J. Lewko, Jr.

CONTENTS

<u>Paragraph</u>	<u>Title</u>	<u>Page</u>
1.0	INTRODUCTION	5
2.0	DISCUSSION	5
2.1	STATEMENT OF WORK	5
2.2	ANALYSIS	6
3.0	CONCLUSIONS	8
4.0	RECOMMENDATIONS	9
5.0	REFERENCES	9

ILLUSTRATIONS

<u>Figure</u>	<u>Title</u>	<u>Page</u>
1	Block Diagram - Long Period Vertical Float Test	10
2	Flexure Shapes - LPZ Boom	11
3	Flexure Bend v/s Earth Period	12
4	Flexure Bend v/s Earth Period	13
5	Flexure Bend v/s Earth Period	14
6	Flexure Bend v/s Earth Period	15
7	Flexures - Table 1, Item a	16
8	Flexures - Table 1, Item b	17
9	Block Diagram - Long Period Vertical Period Measurements	18
10	Experiment Set-Up - I	19
11	Experiment Set-Up - II	20
12	SN05 LPZ Flexures, Post Vibration ADP Record	21

TABLES

<u>TABLE</u>	<u>TITLE</u>	<u>Page</u>
1	Flexure Bend Configuration	7

1.0 INTRODUCTION

The long period vertical (LPZ) seismometer exhibited an excessively long period, to the point of instability with the filter in, whereas horizontal periods (X and Y) appeared to be normal. Due to instrument sensitivity the possibility exists that minor and/or major changes in the sensor could have caused the problem. This report summarizes the areas that were investigated which could have contributed to the problem. The areas are categorized as follows:

- a) Z-boom Litz wires
- b) Variation in the upper support or lower hinge of LPZ boom assembly.
- c) Platform tilt, only 0.0123 radians of platform tilt is required to change the period from one of 15 seconds to 45 seconds. An additional 0.001 radians changes the period from one of 45 seconds to 90 seconds.
- d) Flexure condition, and relationship of filter-in to period.

2.0 DISCUSSION

2.1 STATEMENT OF WORK

The following Statement of Work is taken from the MCP originally prepared for this Anomaly Study.

Investigate cause for unstable LPZ period.

Perform a mechanical analysis of movement of LPZ parts that could account for a change (lengthening) of period of the seismometer.

Conduct engineering tests on an engineering model seismometer.

NOTE: (1) Engineering model seismometer must be made operable prior to conducting such tests.

(2) As an option, SN02 may be made available for engineering tests.

2.2 ANALYSIS

The indicated problem areas were investigated with the following results:

2.2.1 A test was conducted in which readings of the LPZ period were obtained in the filter-in condition with the Litz wires in their normal position. When two wires at each end were bunched together, no period change occurred.

2.2.2 It seems very unlikely that slippage of the spring suspension point has occurred, since once started it would be expected to continue as the motor drives the boom assembly up or down. Furthermore, the time to center the boom assembly is still within the normal expected time scale.

2.2.3 Tilting the platform would lengthen the period, but if the platform were brought back to level, the period would return to the original operating range, providing the system remains stable. Such is not the case with the system being investigated in this study.

2.2.4 If the flexures are bent, the period will increase substantially. It can be demonstrated that if the flexures are bent in a particular shape, the period can be increased and still achieve stable conditions. An experiment was performed under the following conditions:

2.2.4.1 Flexures straight, the angle¹ between AE and CD zero.

Results:

A stable condition, while the LPZ boom natural period varied between 5.7 to 6.2 seconds for various sets of flexures, for the filter-in condition.

2.2.4.2 One straight flexure, instead of the normal two, with the angle remaining zero.

Results:

The boom remained in the bottom position and could not be centered.

2.2.4.3 The flexures were bent, shape according to shape (a), as shown in Table 1, and installed in the LPZ. The angle remained zero.

1. Refer to Figure 2 for definition of angle.

Results:

In the filter-in condition, an excessively long period was experienced and the system became unstable. The height, h , was 0.100 in.

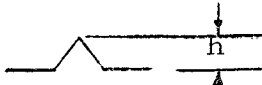
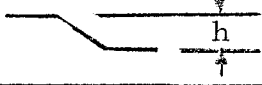
2.2.4.4 Conditions similar to 2.2.4.3 were created with the exception of h , which was reduced to 0.008 in.

Results:

The period still remained excessively long and the conditions unstable.

2.2.4.5 The flexure was changed from shape (a) to shape (b) and tests run for various h values (0-0.060). Tests were conducted on four sets of flexures. The results are plotted in graphs (Ref. Figures 3, 4, 5 and 6) which show the variation of natural period with the amount of bend in the flexure.

Table 1 - Flexure Bend Configuration

Item	Shape
a	
b	

The results show that 2 out of 4 sets of flexures, with various amounts of bend, yielded long periods of 18 seconds which is equivalent to 44.1 secs. on the lunar surface. This simulates the lunar conditions of 45 seconds stable period. By studying the graphs, a pattern emerges. The period increases with increase in bend of the flexure up to a maximum bend value. The maximum bend value varies with each set of flexures. If the bend is further increased, the period decreases. Another point to note from the graphs is that every set of flexures has different characteristics. This can be attributed to the fact that the flexures are fabricated from a 300 series stainless steel. The 300 series stainless steels are not heat treatable but achieve their strength through work hardening. The minimum required mechanical properties can be obtained with little difficulty. However, a considerable range can exist between minimum and maximum values. This situation makes it difficult to guarantee consecutive sets of hinges with reproducible characteristics.

What is the fig. showing?

Went 10-4-61

3.0 CONCLUSIONS:

An important event was demonstrated in laboratory tests. If the flexures are straight and are installed in the Z-sensor straight, keeping the angle between AB and CD zero, the flexures will remain straight, even if the system is caged at 343 psig and uncaged a few times. But if a set of flexures are installed in the Z-sensor straight, and the angle between AB and CD is not zero, the result is tilted flexures. If the system is then caged to 343 psig and uncaged several times, a permanent set will be created in the flexures. Actual flexures used for the above mentioned tests are shown in Figures 7 and 8. The LPZ assembly used for the above experiments was taken from Engineering Model #2. The electronic circuitry for this experiment is shown in Figure 9 and the experiment set-up in Figures 10 and 11.

The point which must now be resolved is the relationship between the preceding experimental work and the particular anomaly associated with SN05. At this time it is appropriate to refer to Figure 12 which represents a photograph taken of the SN05 sensor after vibration. Recalling earlier discussions, if the flexures are straight and are installed in the LPZ straight, keeping the angle between AB and CD zero (ref. Figure 2) and the system is caged and uncaged a few times, the flexures will remain straight. The flexures also appear to remain straight after vibration. However, if the flexures are straight and are installed in a tilted configuration in the assembly, any subsequent vibration and/or caging and uncaging causes the flexures to bend.

One possible hypothesis is to assume the flexures were tilted when the SN05 LPZ was assembled. The following sequence of events then took place. The assembly was caged and uncaged a few times, which could have created a permanent set in the flexures. The sensor was then vibrated, followed by 1-1/2 cycles of caging and uncaging during the performance of Test Procedure 2338815 after the last period check. By examining Figure 12 which is a photograph of SN05 post vibration conditions, the flexures appear to be bent. The mounting angle measures 2-1/2 degrees. Since the flexures were not removed from SN05 after vibration, these bent flexures remained in SN05. Subsequently, the sensor reached the lunar surface in this condition. As was explained before, bent flexures can lengthen the period to some extent and further damage can render the system unstable.

4.0 RECOMMENDATIONS

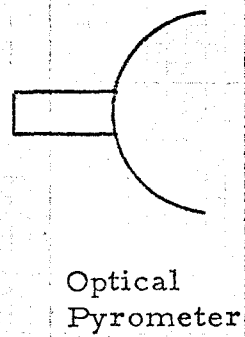
As a result of this study and laboratory tests, the following recommendations are made to assure that LPZ flexure geometry is correct.

1. A caution note will be put into the WOOS for the assembly of the LPZ. This note will require that in the process of assembly, extreme care should be taken to see that the flexures are flat and the angle formed by the flexure in the flexure clamps AB and CD (Ref. Fig. 2) is zero degrees. After installation of the flexures within the LPZ boom assembly is completed, there shall be no angle between the flexure and either flexure clamp AB or CD as shown in Figure 2.
2. Engineering will examine this suspension point after assembly with a critical review of the caution notes.
3. Hardware changes are not recommended as a result of completion of this study.

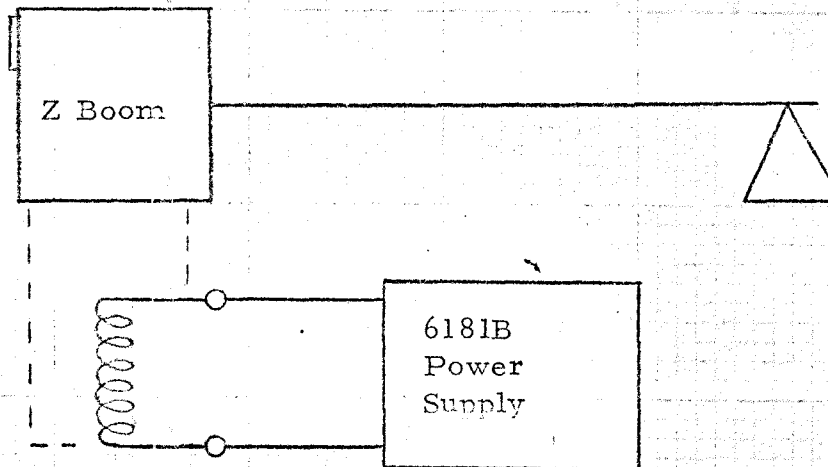
5.0 REFERENCES

- (1) Interim Report, SSED-R-57 (c) dated 21 April 1970

*what about
these dead built*



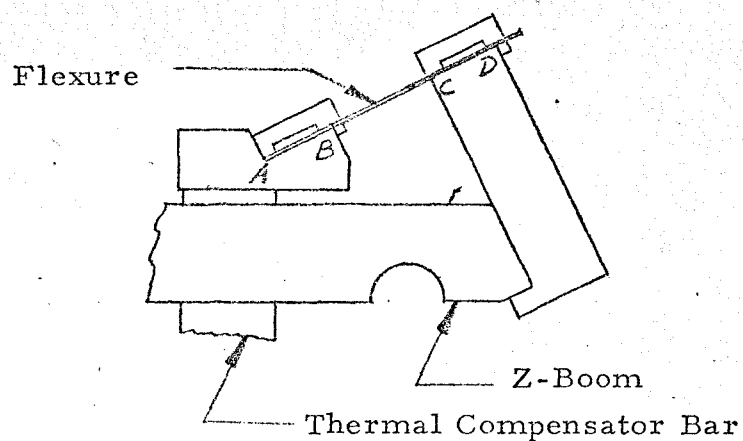
Mirror



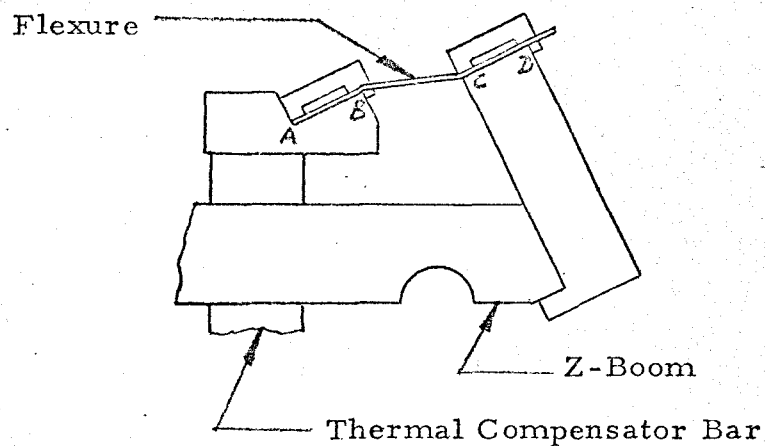
Block Diagram
Long Period Vertical
Float Test

Figure 1

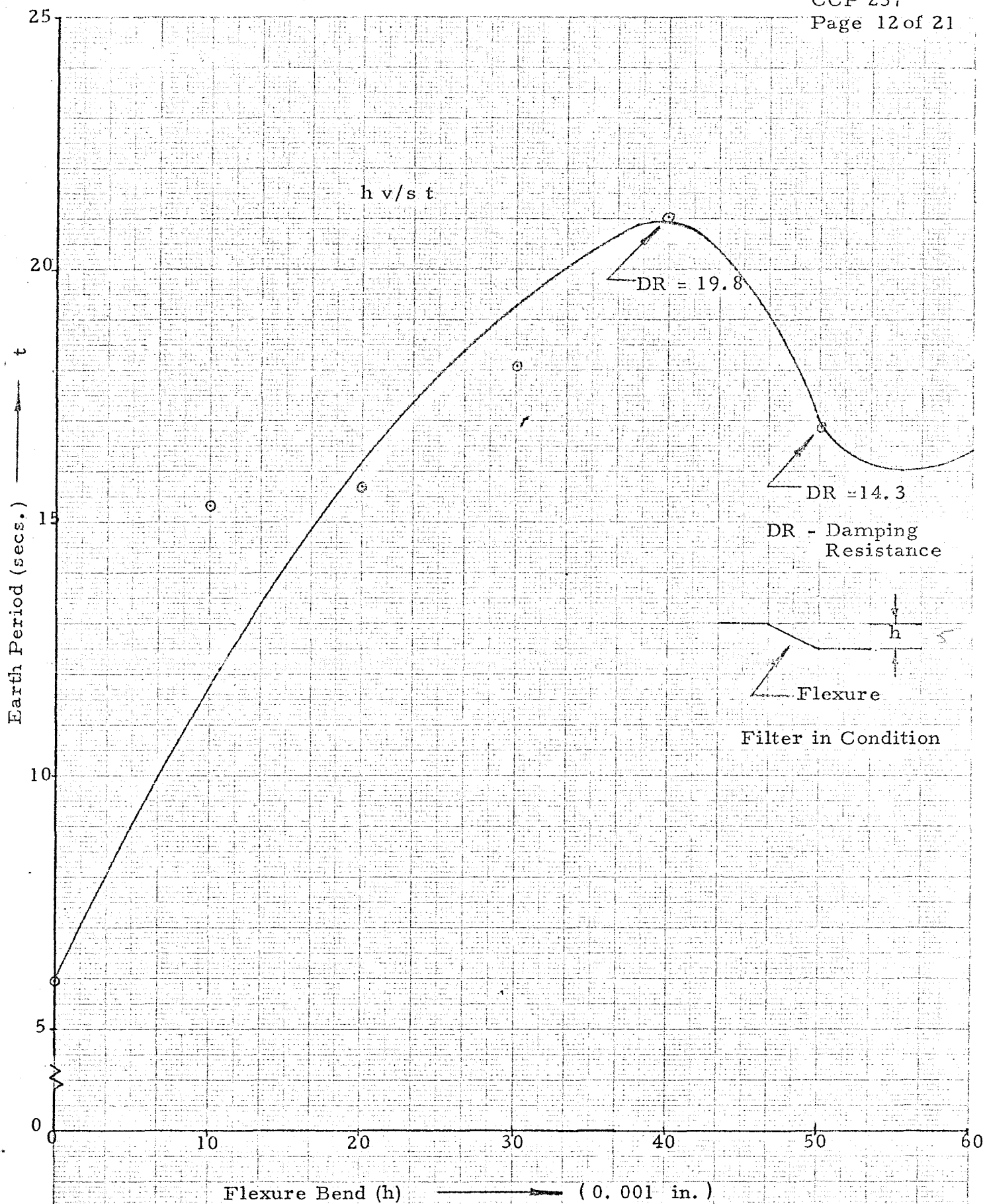
Figure 2
Flexure Shapes - LPZ Boom



1. Angle between AB & CD - Zero.
2. Flexures straight.



1. Angle between AB & CD - 180 degrees
2. Flexures Tilted or Bent.



Flexure Bend (h) (0.001 in.)

Figure 3 - Flexure Bend V/S. Earth Period

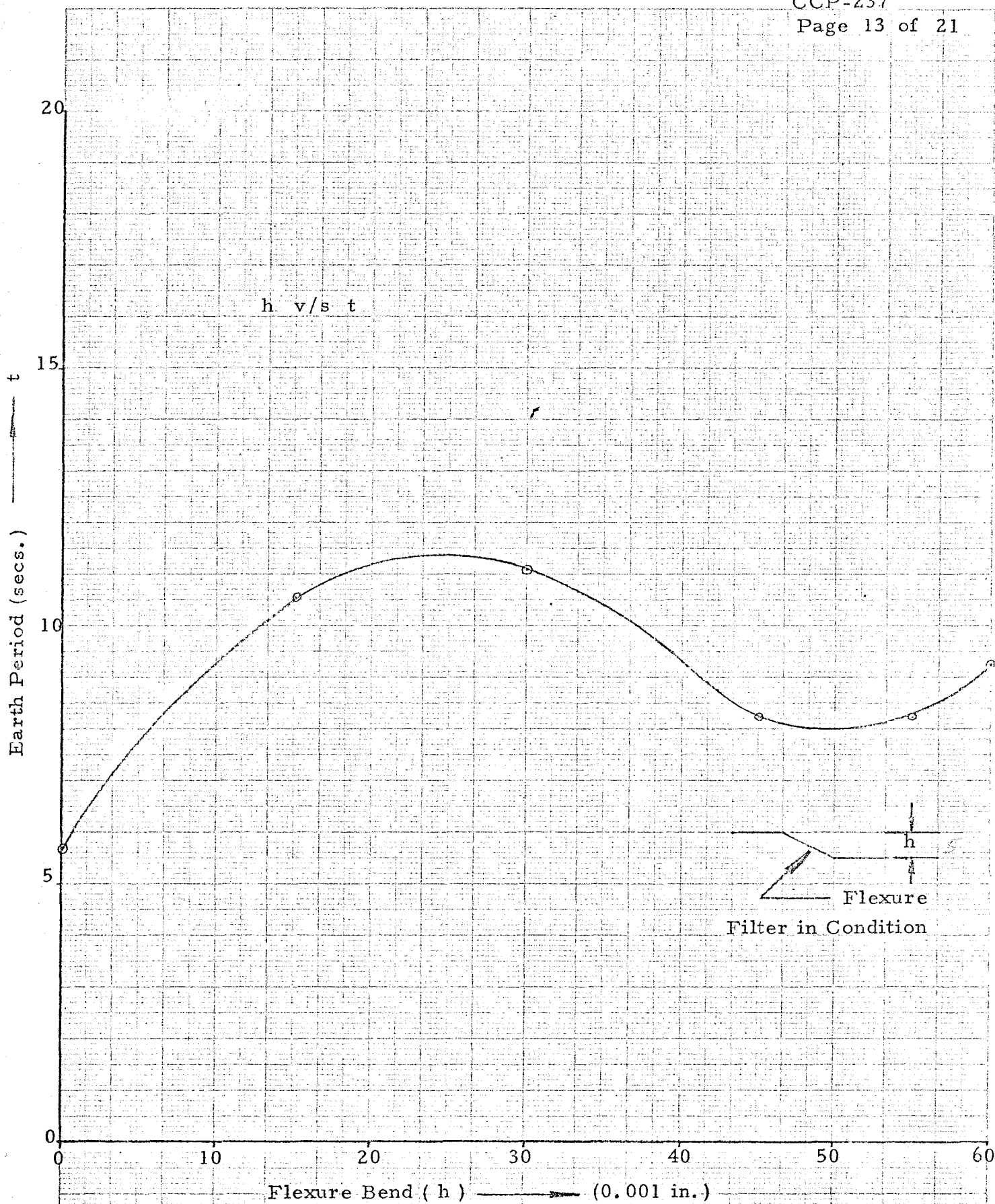


Figure 4 - Flexure Bend V/S. Earth Period

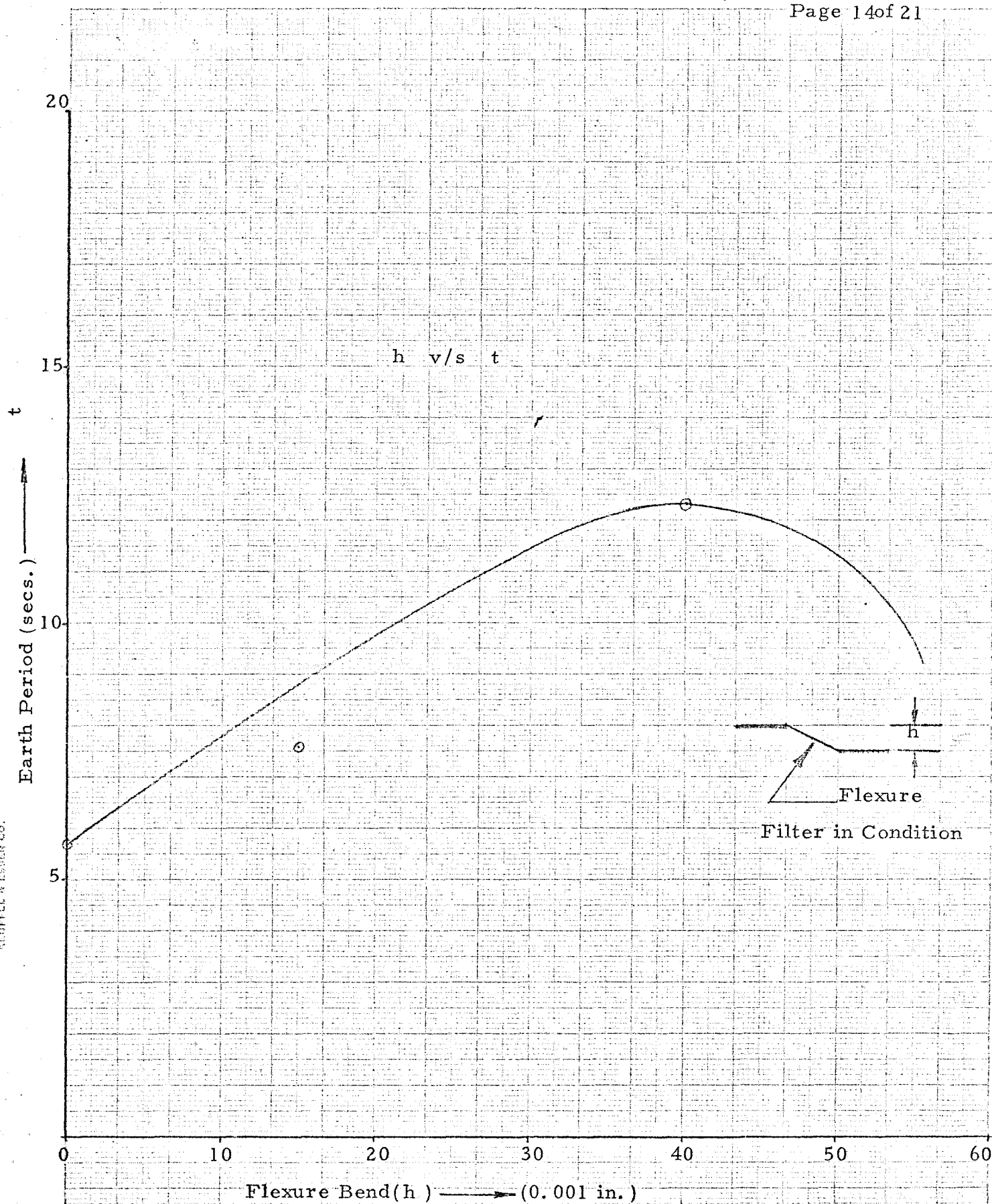


Figure 5 - Flexure Bend V/S. Earth Period

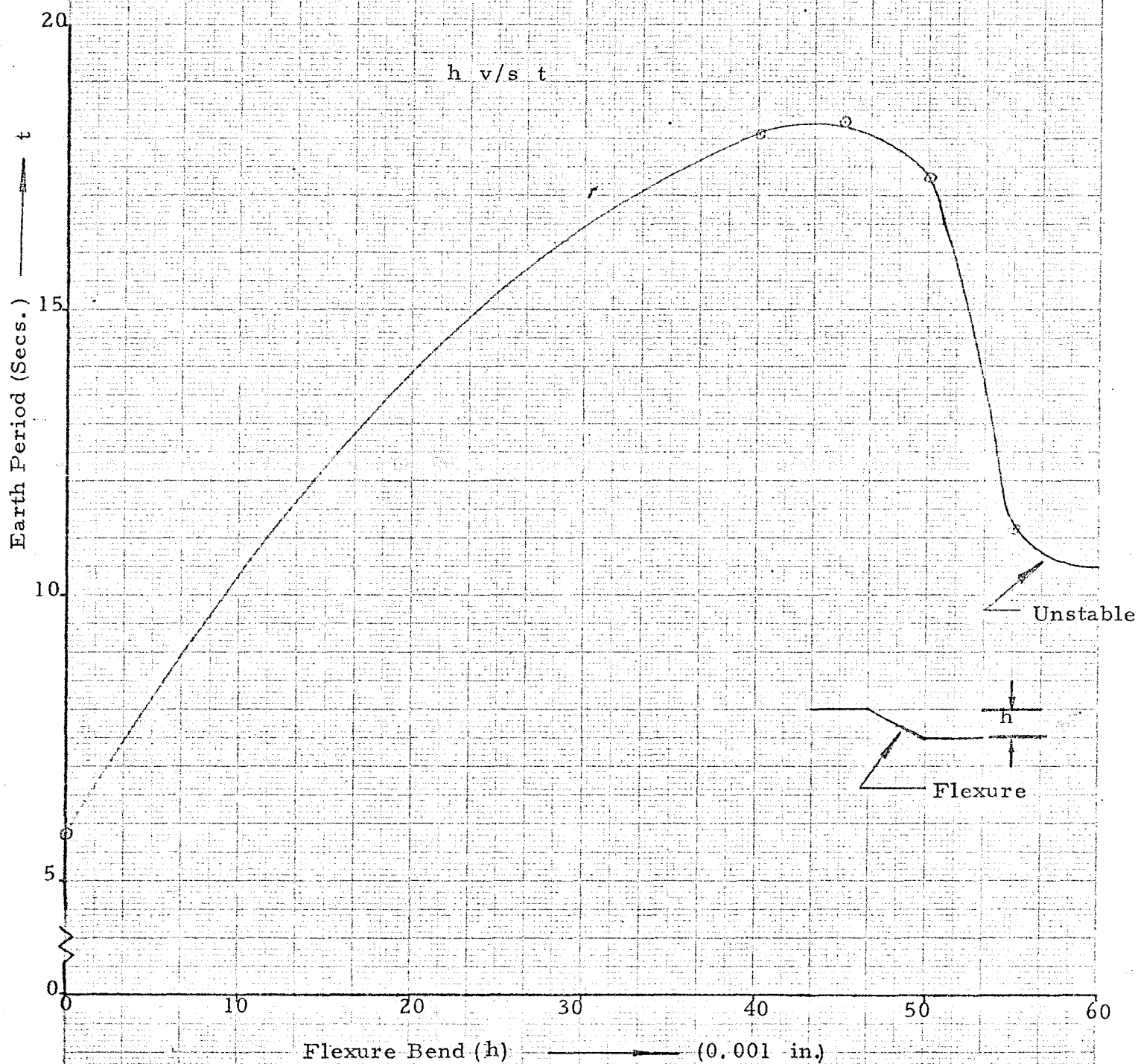


Figure 6 - Flexure Bend V/S. Earth Period

Figure 7
Flexures - Table 1
Item a

SSD-R-57 (c)

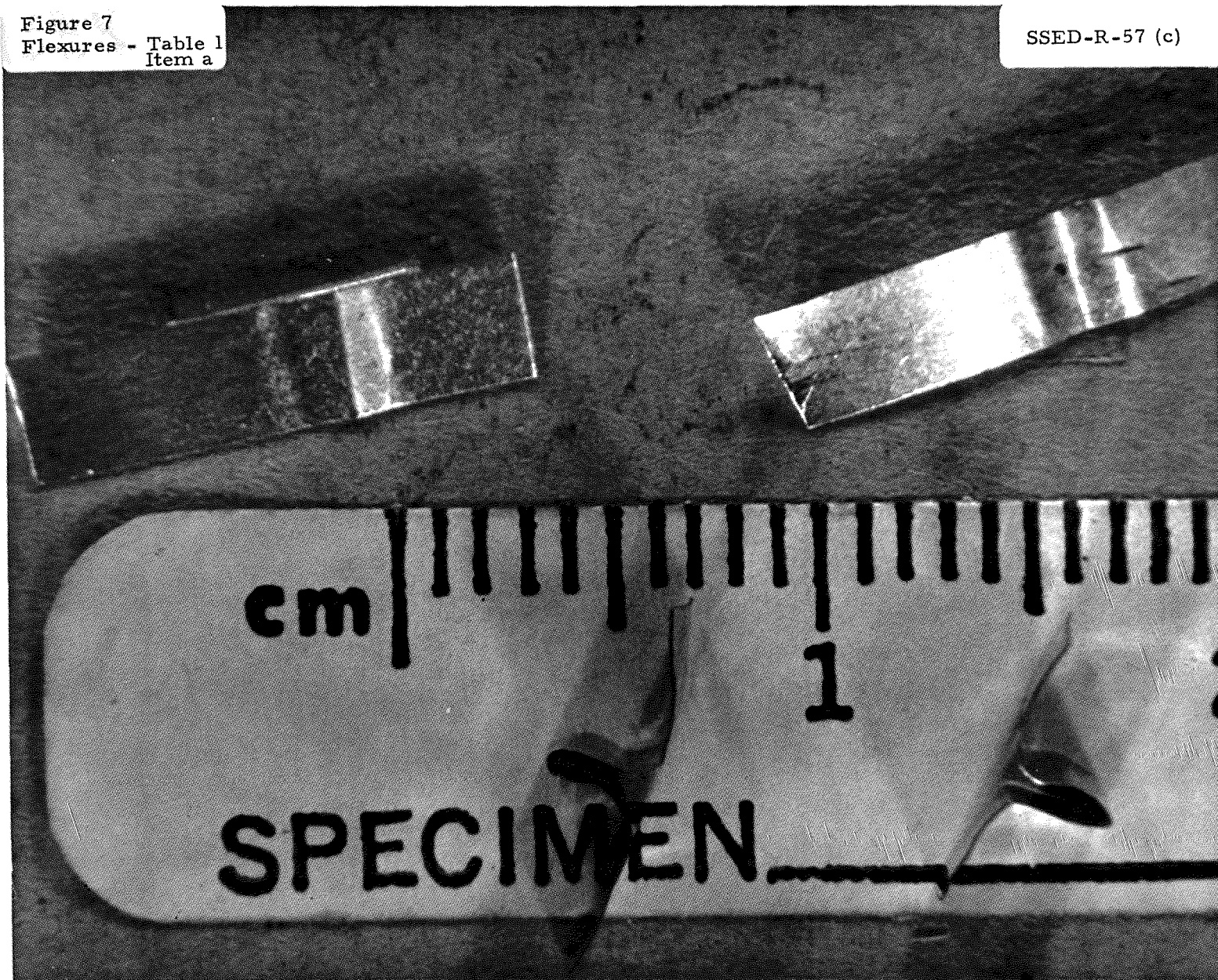
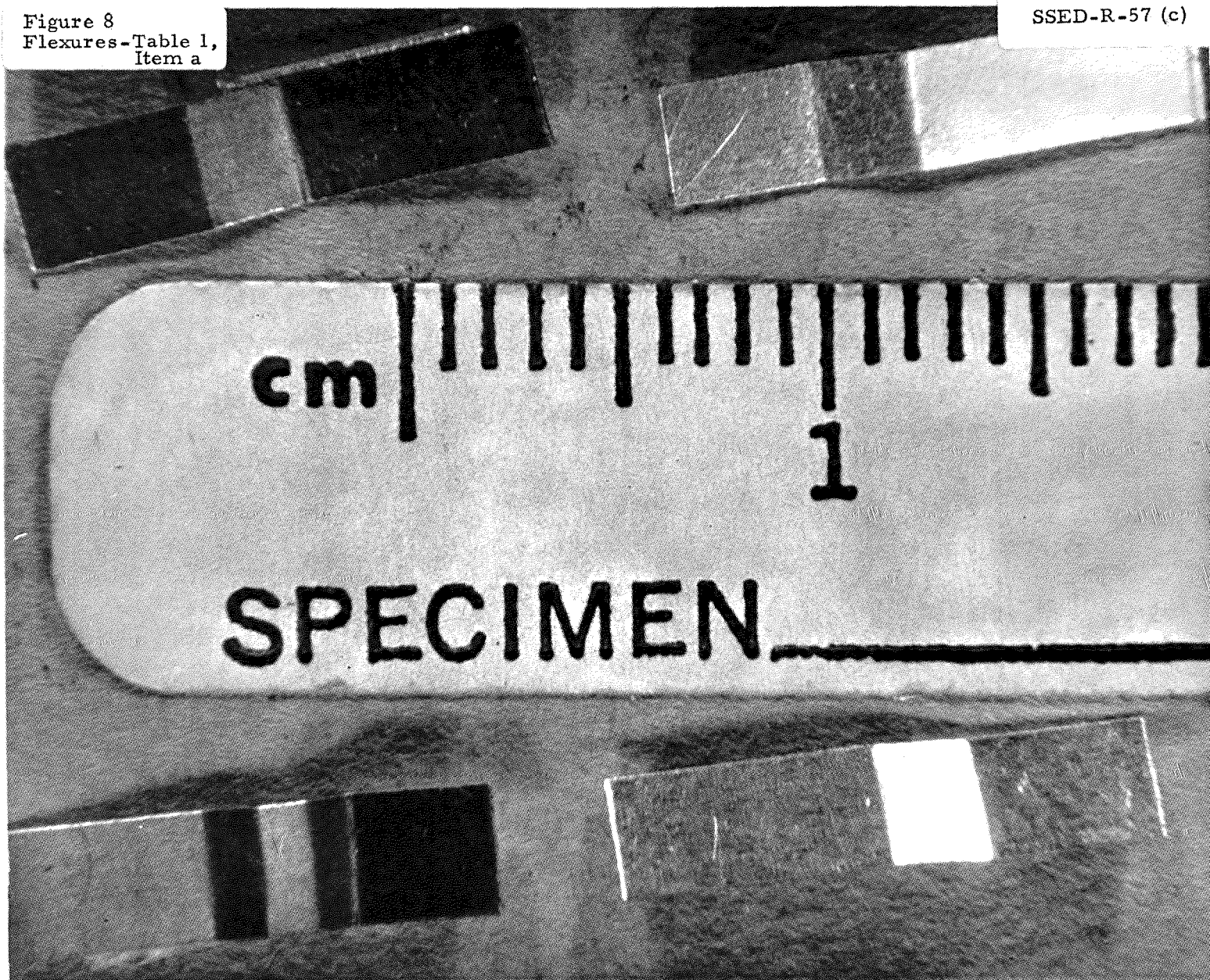
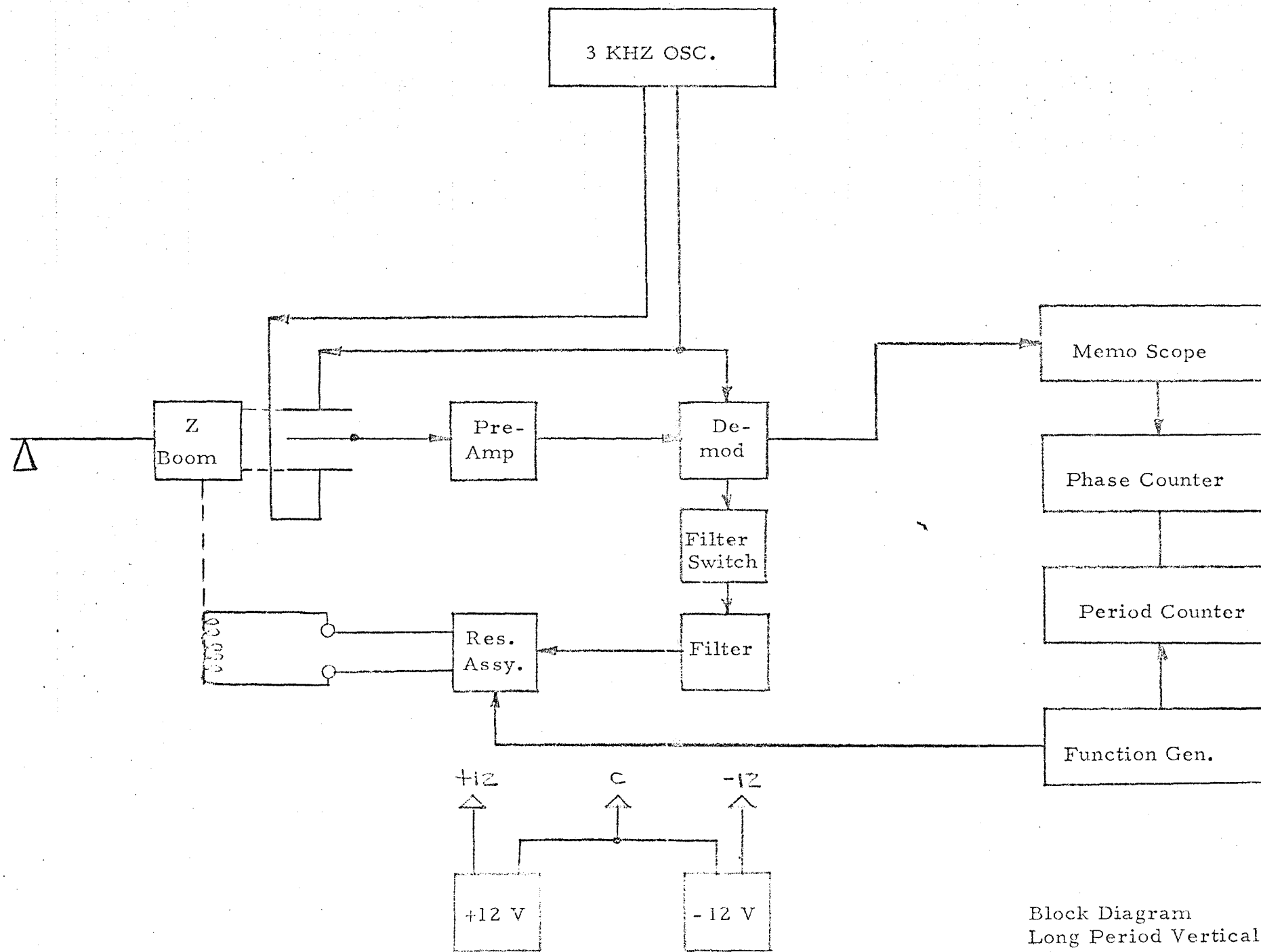


Figure 8
Flexures-Table 1,
Item a

SSSED-R-57 (c)





Block Diagram
Long Period Vertical
Period Measurements

Figure 9

Figure 10
Experiment Set Up

SSED-R-57 (c)



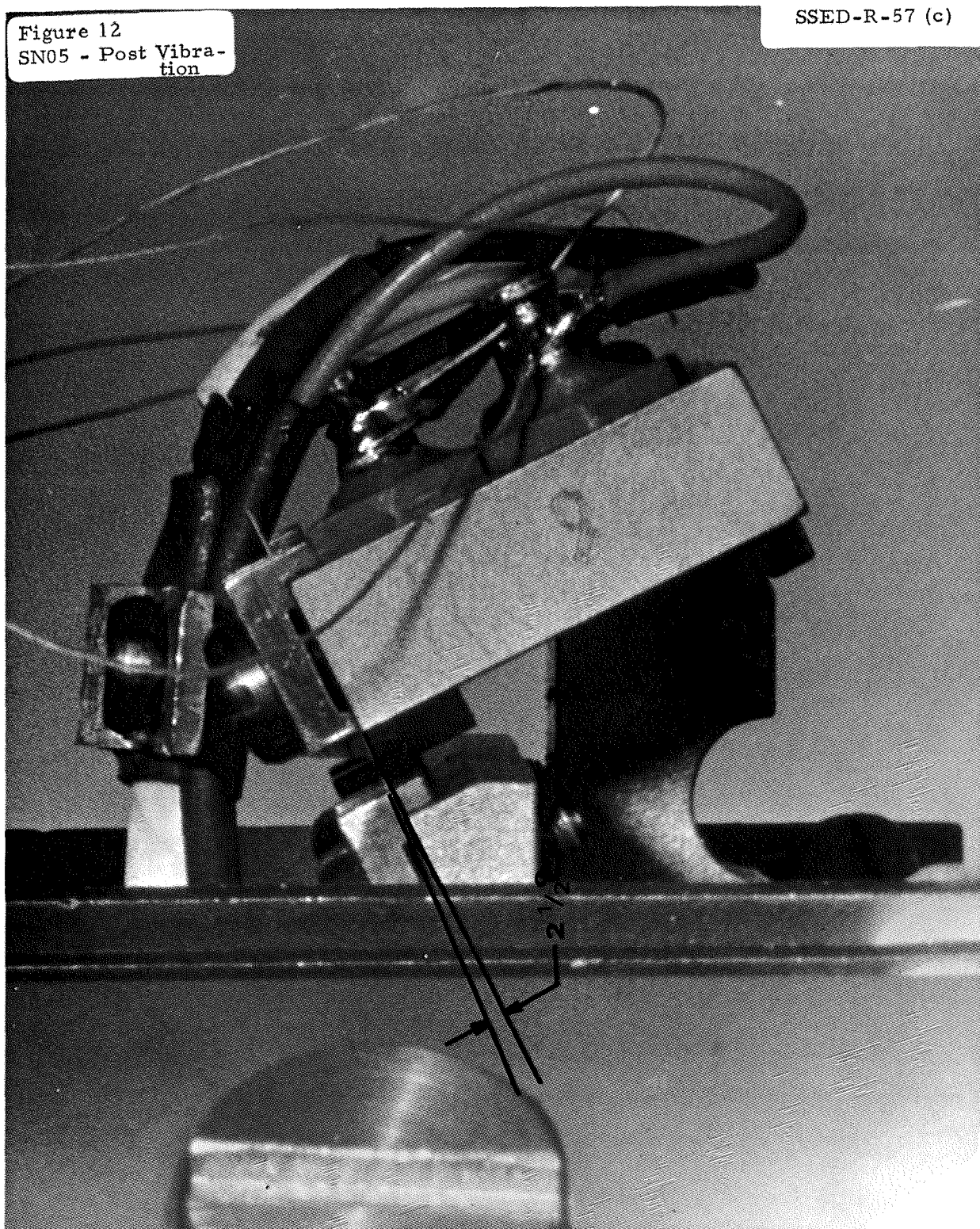
Figure 11
Experiment Set Up

SSSED-R-57 (c)



Figure 12
SN05 - Post Vibration

SSED-R-57 (c)





**Acrospace
Systems Division**

Investigation of PSE Anomalies

Apollo 12 Mission

NO. SSED- R-57 (d)	REV. NO.
PAGE 1	OF 36
DATE 28 May 1970	

This report provides the results of investigations of PSE anomalies from Apollo 12 mission. Reference 97/510-454, CCP-237, 16 February 1970.

TASK TITLE: Analyze Thermal Control Problem

Prepared by: J. Million
T. Million

Prepared by: M. Goodkin
M. Goodkin

Approved by: J. Lewko, Jr. *RL*
J. Lewko, Jr.

CONTENTS

<u>Paragraph</u>	<u>Title</u>	<u>Page</u>
1.0	INTRODUCTION	5
2.0	DISCUSSION	5
2.1	STATEMENT OF WORK	5
2.2	ANALYSIS	5
3.0	SUMMARY OF RESULTS	10
4.0	CONCLUSIONS AND RECOMMENDATIONS	12
5.0	REFERENCES	13

TABLES

<u>Table</u>	<u>Title</u>	<u>Page</u>
1	Summary of Power Distribution in the Heater Circuit	14
2	Summary of Measured Circuit Parameters	15
3	Manual Mode Power Dissipation--Watts	16
4	Transistor Specifications (Notes 1 and 4)	17

ILLUSTRATIONS

<u>Figure</u>	<u>Title</u>	<u>Page</u>
1	PSE Heater Block Diagram	18
2	Original Heater Circuit Configuration	19
3	New Heater Circuit Schematic	20
4	Duty Cycle vs AR3 Voltage	21
5	Heater Circuit Power vs AR3 Output	22
6	"W" Board Changes	23
7	Heater Element Positions	24
8	Heater Circuit Test Configuration	25
9	Q_{18} , Q_{24} , Q_{25} Potential vs Duty Cycle	26
10	System Power Distribution	27
11	Power Dissipation vs Duty Cycle (Q_{24} or Q_{25})	28
12	Power Dissipation vs Duty Cycle (Q_{13})	29
13	Power Loss In Test Fixture	30
14	Test Point B - T_3 Secondary	31
15	Test Points C and D	32
16	Test Points C and D Rise and Fall Times	33
17	Test Point E- Q_{18} Collector	34
18	Measurement of V_{CE} Test Point E- Q_{18} Collector	35
19	Test Point F - Ripple Voltage Across C_{24}	36

1.0 INTRODUCTION

This report describes the results of the study of the Apollo 12 PSS thermal anomaly. The PSS thermal control system did not maintain the sensor temperature within the require temperature range of $+108^{\circ}\text{F}$ to $+144^{\circ}\text{F}$, rather the temperature reference DL-07, indicated excursions of -75°F (lunar night) to $+143^{\circ}\text{F}$ (lunar day).

2.0 DISCUSSION

2.1 STATEMENT OF WORK

The following Statement of Work is taken from the MCP originally prepared for this Anomaly Study.

2.1.1 Analyze Thermal Control Problem

2.1.2 Coordinate electrical engineering effort with concurrent thermal design group activity.

2.1.3 Analyze incorporating additional heater or a replacement heater that will enable experiment power to increase by 2.5 to 3.0 w.

2.1.4 Make recommendations regarding circuit changes and method of implementation of design change.

2.1.5 Obtain a reliability review of proposed circuit design change.

2.2 ANALYSIS

The following section of this report provides the basis for a design that increases the available sensor heater power from 2.5 w to 5.5 watts in the AUTO-ON mode of operation. This value of heater power, 5.5 watts, was established as a result of reviewing all aspects of the PSS sensor thermal control system operation.

2.2.1 The PSE heater circuit shown in Figure 3.0 is a modified form of the original circuit shown in Figure 2.0. This modification now permits, in "Auto Mode", controlled heater power up to 5.5 watts to be delivered to the Sensor.

Curves to show the relationship of 29 volts supply current, duty cycle, and the output of temperature sensor amplifier AR3 (see block diagram in

Figure 1.0) are given in Figure 4.0. These curves indicate the maximum power in "auto" is available at 80% duty cycle, and the minimum controllable power is at 4%. Below 4%, supply current drops to 1.5 ma and heater power is essentially, zero, giving a heater "off" condition in the "auto" mode, to supplement that given by command.

This change has been implemented by replacing the transistors at Q18, and Q21 with ones of higher ratings, reactivating the current regulator circuit (and increasing its capacity), and changing the values of the heater elements and capacitor C24.

Figures 6.0 and 7.0 show the modification to the "W" board and the location of the added heater elements on the sensor.

Changes made to the circuit were done without changing its principle of operation on its electrical configuration from the basic heater circuit as originally designed.

Tests were performed to verify the circuit performance, and the results of the tests are included in this report.

2.2.2 Modified Circuit Description

In the modified heater circuit shown in Figure 3.0 the following changes were made, Transistors Q18 and Q21 have been changed from Type 2N2222A to 2N3499's (See Table 4 for specifications). This resulted in a larger case size as well as a higher current capacity. An additional 2N2102 transistor Q25, has been added to the current regulator to increase its current capability. To provide for better load distribution on Q24 and Q25 separate emitter resistors R38 and R39 have been used to replace the single R38 resistor. Heater elements have been added to parallel the present elements reducing the resistance from $290\ \Omega$ to $104.5\ \Omega$. To compensate for the change in time constant in the decoupling circuit (H1 and C24) an additional 47 mfd has been paralleled with C24 for a new value of 94 mfd.

Resistors R38 and R39 are critical in determining the current limit, and in turn the maximum power available from the circuit, consequently these will be selected in the "W" board test procedure for optimum results.

2.2.3 Calculations

2.2.3.1 Transistor Q₁₈ Power Dissipation

For the Q₁₈ power dissipation calculations it was assumed that Q₁₈ acted as a "perfect" switch. Current flowed only when Q₁₈ was "ON". Negligible current flowed when Q₁₈ was "OFF".

Test data used included the current through Q₁₈, measured with an ammeter, and the potentials at the collector and emitter of Q₁₈ and the duty cycle, measured with a CRO.

The current during the "ON" time of Q₁₈ was

$$I_{ON} = I_{\text{measured}} / \text{Duty Cycle}$$

The power dissipation during the "OFF" time of Q₁₈ was negligible. The power dissipation during the "ON" time was

$$P_{ON} = I_{ON} V_{CE(ON)}$$

Then the average power dissipation of transistor Q₁₈ was

$$\begin{aligned} P_{AVG} &= P_{ON} \cdot (\text{Duty Cycle}) \\ &= I_{ON} \cdot V_{CE(ON)} \cdot (\text{Duty Cycle}) \\ &= I_{\text{meas}} / (\text{Duty Cycle}) \cdot V_{CE(ON)} (\text{Duty Cycle}) \\ &= \frac{I_{\text{measured}} V_{CE(ON)}}{\text{Duty Cycle}} \end{aligned}$$

2.2.3.2 Transistors Q₂₄ and Q₂₅ Power Dissipation

The emitter resistors of Q₂₄ and Q₂₅, R₃₉ and R₃₈, were measured. The resistors were each 6.0 ohms. During the test, the potential across each resistor, R₃₉ and R₃₈, was measured with a digital voltmeter. The currents through R₃₉ and R₃₈, and thus through Q₂₄ and Q₂₅, respectively, were calculated by

$$I = E/R$$

The potential at the common collectors of Q₂₄ and Q₂₅ was obtained with a CRO. The potential was a ripple voltage around a DC level. The col-

lector-emitter potentials, of Q₂₄ and Q₂₅ were taken as the difference between the DC level and the drops across R₃₉ and R₃₈.

Then, the power dissipation was

$$P = I V_{CE}$$

for each transistor.

2.2.3.3. Duty Cycle

The rectangular waveform at the collector of Q₁₈ was displayed on a CRO. The pulse repetition time, PRT, and the pulse width, PW, during the "ON" time of Q₁₈ were measured.

The duty cycle was calculated as follows:

$$\text{Duty Cycle} = PW/PRT$$

2.2.3.4 Heater Elements Power Dissipation

The measured 29 volt supply current, I, was the average current through the two heater elements. Designating the resistances of the heater elements as R_{H1} and R_{H2}, the power dissipated in the heater elements was

$$P_H = I^2 (R_{H1} + R_{H2})$$

2.2.3.5 Survival Power Calculation

In the survival mode of operation a 290Ω ±10% heater element and a diode located in the CSE are placed in series with the 29 volt source and the PSE heater circuit. In the "Manual Mode" of operation, Heater Power is calculated as:

$$P_{\text{Heater Circuit-Survival}} = E_{29v} I_{AVE} - \left(I_{AVE} \right)^2 \left(290\Omega \right) = \left(I_{AVE} \right)^2 R_{\text{Heater Elem.}} + \frac{E_{R38}^2}{R_{38}} + \frac{E_{R39}^2}{R_{39}} + E_{Q24} I_{Q24} + E_{Q25} I_{Q25}$$

(where E_{R38}, E_{R39}, E_{Q24}, and E_{Q25} are voltage drops across subscript elements.)

Power Closure: To determine distribution of power in the heater circuit, the following relationship was used for a given value of duty cycle:

$$P_{\text{circuit power}} = E_{29v} \times I_{\text{ave}} = I_{\text{ave}}^2 (R_{\text{heaters}}) + E_{Q18} I_{\text{ave}} + E_{Q24} I_{Q24 \text{ ave}} \\ + E_{Q25} I_{Q25 \text{ ave}} + \frac{E_{R38}^2}{R38} + \frac{E_{R39}^2}{R39} + P_{\text{Lumped Losses}} + P_{\text{Test Fixture Losses}}$$

Results of these calculations are tabulated in Table 1 and plotted as a function of duty cycle in Figure 10.0.

To separate circuit power from fixture power, the above equation was solved for $P_{\text{Test Fixture Losses}}$ as

$$P_{\text{Test Fixture Losses}} = P_{\text{circuit power}} - (P_{\text{Lumped}} + P_{\text{Heaters}} + P_{Q18} + P_{Q24} + P_{Q25} \\ + P_{R38} + P_{R39})$$

A plot of this power as a function of duty cycle is shown in Figure 13.0.

2.2.3.6 Transistor Power Dissipation Derating

For both transistors 2N2102 and 2N3499, the following approach was used during the circuit design for component selection. The dissipation ratings based on case temperature were used, since the objective of the heater circuit is to maintain the Passive Seismometer at a stable temperature of approximately 52°C.

Calculation:

Maximum transistor dissipation at 25°C:

$$P_{D25} = 5 \text{ watts}$$

Derating factor for temperature:

$$D_T = 28.6 \text{ mW/}^\circ\text{C}$$

Derating factor for vacuum

$$D_V = 0.5$$

Maximum allowed dissipation derated for operating environment:

$$\begin{aligned} P_D &= (P_{D25} - D_T \quad T) D_V \\ &= 5W - (28.6 \text{ mW/}^\circ\text{C}) (52^\circ\text{C} - 25^\circ\text{C}) \quad 0.5 \\ &= \underline{2.1 \text{ watts.}} \end{aligned}$$

2.2.4 Test Description

The circuit parameters were measured in the lab using an engineering model of the PSE. The test configuration is shown in Figure 8. Heater elements were simulated by using two wire wound resistors located on the test fixture. Decade boxes were used to vary the input to the thermal bridge amplifier, AR3, which in turn controlled the duty cycle at the VCO (Ref. Figure 1). For each "sensor" resistance valve, the following measurements were made (Table 2):

- a. Current from 29 volt supply
- b. Potentials at the collector and emitter of Q₁₃
- c. Potentials across R₃₈ and R₃₉
- d. Temperatures of Q₁₃ and Q₂₄
- e. Duty cycle
- f. AR3 output (thermal sensor amplifier).

3.0 SUMMARY OF RESULTS

The purpose of testing the design was to verify that the modified circuit, would function in the same manner as the original circuit, but would supply 3 watts of additional power. The results of the tests are shown in Figures 9, 10, 11 and 12. These curves show that the measured circuit power at 80% duty cycle was over 5.5 watts.

To determine the functioning of components in the new design, the power distribution was analyzed in Figure 10. From these curves it is evident that the heater elements located on the sensor case (Figure 7) will receive the greater portion of the increased power (60.6% at 80% duty cycle). The next largest dissipation (22.6%) is in the regulator transistors Q₂₄ and Q₂₅.

Distribution of this power is shown in Figure 11. This plot indicates these transistors must be capable of operating from less than 15 milliwatts to a maximum of 620 milliwatts in the "Auto Mode". A temperature profile of the Q_{24} case parallels the dissipation curve of both transistors, indicating the relationship of the two quantities. A test in the "Manual Mode", showed a power of 790 milliwatts as a maximum power in each transistor for this configuration.

The temperature and power profile of Q_{18} (Figure 12) shows a smaller variation with duty cycle and a lower maximum dissipation.

The difference between the "corrected power" curve and the "Heater Power + Q_{18} + Q_{24} + Q_{25} " curve (Figure 10) is the dissipation attributed to the rest of the PSE heater circuit components shown in Figure 3. The difference between the "Nominal Measured Circuit Power" and the "Corrected Power" plotted in Figure 13, is believed to be a reactive effect due to C_{24} and the inductance in the 30 ohm wire wound resistor used to simulate the parallel 64 ohm heater elements in the modified circuit.

The "frequency" curve in Figure 13 is the lowest frequency component in the "ON" time pulse at the collector of Q_{18} .

The peak in the power curve in Figure 13 indicates resonance in the AC loop, also illustrated in that figure. It was calculated that resonance would occur at a duty cycle of 21.2% if the 30 ohm "heater element" had an inductance of about $1/4$ Henry. The inductance of the 30 ohm "heater element" was found by measurement with a bridge to be $1.5 \mu\text{H}$.

Because of the inductance in the resistors used to simulate the heater elements, the selection of resistors R_{38} and R_{39} will be done in a DC test in the "Manual On" mode, and a wider tolerance to allow for stray resistance in tests fixtures for the in-process test for the W board (P/N 2338786), will be made. This procedure will allow a more accurate determination of power that will be available when the non-inductive heater elements in the sensor replace the test fixture resistors after final assembly of the instrument.

Photos in Figures 14 through 19 show that the basic waveforms have remained the same after modification, changing only to reflect the increased power in the Q_{18} collector circuit.

Comparison of the control curves of Figure 4 indicate that the duty cycle has remained essentially the same and the current available has more than doubled to supply the increased power.

Changing the value of capacitor C_{24} has allowed the retaining of its decoupling function by compensating for the change in heater element resistance. Tests indicate the amplitude of the ripple is larger, but the waveforms are unchanged.

Power data taken on Q_{24} and Q_{25} transistors indicate a better division of power with the addition of the emitter resistor R_{38} than could be expected with a single emitter resistor.

The measured power indicated in Table 1 as 5.52 watts and corrected to 5.321 was the result of setting the desired power in the "auto mode". This method of setting desired maximum power has been modified for the reasons previously discussed.

4.0 CONCLUSIONS AND RECOMMENDATIONS

As a result of the design study and test of the modified heater circuit the following recommendations are made:

1. Transistors Q_{24} and Q_{25} , because of the amount of power they are required to dissipate, should be provided with heat sinks. This will ensure increased reliability.
2. The heater elements, now composed of four separate elements should be replaced by two of the appropriate size, and located in the position of the present 145 ohm heaters in other sensors.
3. Allow a wider tolerance for readings in testing the "W" board in the "auto mode" to allow for test fixture, reactive effects.
4. Set the desired maximum power level in the "Manual On" mode in the in-process test in the "W" board.
- 5., Evaluate the thermal stability of transistors Q_{18} , Q_{24} , and Q_{25} . This should be done for the worst case condition of the "Manual On" and using 29 volt power as the source.
6. Present limits on the ALSEP 29 volt circuit breaker have necessitated the reactivation of the current regulator. The results of the tests that have been made indicate that 22.6% of the heat power supply by the heater is being done so by use of the regulation transistors' case dissipation. Higher efficiency in current operation could result if more of the heat were supplied by the heater elements. To provide for this, increasing the

current capability of the breaker and again deactivating the regulation circuit, along with proper selection of heater resistance values should be considered in future designs. From this change a more uniform distribution of heat throughout the instrument (by conduction) should result because better coupling of the heat source (the elements) to the case will be provided.

5.0 REFERENCES

1. Acceptable Parts List; BSR 2857; February 13, 1970.
2. Memorandum Earth Sciences - Teledyne 640-8-0043, 21 March 1968 from R. Smith.
3. Teledyne Document T-13102.
4. Motorola Semiconductor Products Specification Sheet for a Type 2N2222A.
5. Motorola Semiconductor data book; Page 8-161, 2nd Edition.
6. Apollo 12 PSS Problems, Anomalies and Preliminary Action Plan SSED-346, 10 December 1969.
7. Teledyne Document T-13071, 234373 Rev. D.
8. Bendix Document 2338817, 2344707, 2344708.
9. BxA Minutes, 8 May 1970, SSED-443.
10. Investigation of PSE Anomalies Apollo 12 Mission Interim Report SSED-R-57 (d), 21 April 1970.
11. Internal Memorandum Apollo 12 Anomaly Study SSED-415, 7 April 1970.
12. MCP Task Statement SSED-230, 8 January 1970, Investigation of Apollo 12 Anomalies.

"On" Time Lowest Freq. Comp- onent (KHz)	Duty Cycle (%)	Circuit Current I (mA)	Circuit Power $I \times 29V$ (Watts)	Heater Element Power $I^2 \times R_H$ (Watts)	Q_{18} Power $I_C \times V_{CE}$ (mW)	Q_{24} Power $I_C \times V_{CE}$ (mW)	Q_{25} Power $I_C \times V_{CE}$ (mW)	R_{38} Power E^2/R (mW)	R_{39} Power E^2/R (mW)	Misc. Lumped Power ($R_{36}, CR_5,$..., $CR_8,$ etc.) (mW)	Cor- rected Total Power (Watts)	AR3 Output (mV)	Test Fixture Power Loss (Watts)
3	78.8	190	5.52	3.74	190	580	620	56	48	87	5.321	3	0.199
	69.8	185	5.36	3.54	185	490	520	54	47	87	4.923	21	0.237
5.55	54.6	178	5.16	3.29	178	380	410	50	44	87	4.439	41	0.721
7.15	42.5	172	4.99	3.06	2.58	210	210	45	41	87	3.911	56	1.079
	33.9	163	4.73	2.75	244	120	120	39	36	87	3.396	73	1.334
11.05	27.2	140	4.06	2.03	252	88	89	28	27	87	2.601	87	1.459
15.85	21.2	115	3.34	1.37	23	71	71	19	18	87	1.659	102	1.681
	17.5	99	2.87	1.02	238	65	64	14	15	87	1.503	117	1.367
25.0	12.1	82	2.38	0.696	252	22	22	9.4	9.5	87	1.097	135	1.283
	10.6	68	1.97	0.478	282	17	16	6.7	7.0	87	0.894	150	1.076
33.3	9.1	59	1.71	0.360	248	18	18	4.9	4.9	87	0.741	165	0.969
	7.6	50	1.45	0.258	215	14	14	3.6	3.7	87	0.595	180	0.855
50.0	6.1	40	1.16	0.165	212	12	11	2.2	2.3	87	0.492	200	0.668
	5.5	37	1.07	0.142	196	11	11	2.1	2.1	87	0.451	208	0.619
	4.6	34	0.985	0.110	194	11	11	1.6	1.6	87	0.416	209	0.569
	4.2	32	0.928	0.106	182	11	11	1.4	1.5	87	0.400	215	0.528
83.3	3.6	30	0.870	0.094	165	14	14	1.4	1.4	87	0.347	220	0.523
	0	1.4	0.0406	0.0002	---	0.8	0.7	0.004	0.004	--	-----	222	-----

Table 1 - SUMMARY OF POWER DISTRIBUTION IN THE HEATER CIRCUIT

MEASURED														CALCULATED			
AR3 Out- put	Duty Cycle (PW/PRT x 100)	29V Supply Current	Collector Potential Q ₁₈ (Volts)		Collector Potential Q ₂₄ , Q ₂₅ (Volts)		Temperature (°C)		Emitter Potential (mV)		Current (mA)						
(mV)	(%)	(mA)	Min.	Max.	Avg.	PK-PK	Q ₁₈	Q ₂₄	Q ₂₄	Q ₂₅	Q ₂₄	Q ₂₅					
3	78.8	190	8	15.5	7	0.2	37.4	55.4	539	581	90	97					
21	69.8	185	7	15	6	0.3	37.5	53.9	532	569	89	95					
41	54.6	178	6	14	5	0.4	37.9	49.5	516	550	86	92					
56	42.5	172	4.5	16	3	0.4	38.8	44.3	498	518	83	86					
73	33.9	163	3.5	17	2	0.4	40.6	36.8	465	481	78	80					
87	27.2	140	3.5	18.5	1.7	0.04	40.6	33.0	405	412	68	69					
102	21.2	115	1.8	20	1.6	0.02	40.6	31.5	335	336	56	56					
117	17.5	99	4	22	1.6	0.04	41.1	30.6	297	293	50	49					
135	12.1	82	4	22	0.8	0.03	40.9	30.2	239	238	40	40					
150	10.6	68	5	25	0.7	----	40.7	29.7	204	200	34	33					
165	9.1	59	5	25	0.8	----	39.9	29.2	171	171	29	29					
180	7.6	50	5	25.5	0.7	----	39.5	29.0	149	147	25	25					
200	6.1	40	6	26	0.7	----	38.3	28.6	118	116	19.6	19.3					
208	5.5	37	6	26	0.7	----	37.5	28.4	113	111	18.8	18.5					
209	4.6	34	6.5	26.2	0.8	----	36.5	28.2	99	98	16.5	16.3					
215	4.2	32	6.5	26.5	0.8	----	36.4	28.2	94	91	15.6	15					
220	3.6	30	6.5	26.5	1.0	----	30.2	27.7	92	90	15.3	15					
222	0.0	1.4	29	29	1.0	----	27.5	26.9	4.8	4.5	0.8	0.7					

Table 2 - SUMMARY OF MEASURED CIRCUIT PARAMETERS

MODIFIED CIRCUIT						ORIGINAL CIRCUIT	
OPERATING WITH 29 VOLT SUPPLY			OPERATING WITH SURVIVAL POWER			OPERATING WITH 29 VOLT SUPPLY	OPERATING WITH SURVIVAL POWER
Total Circuit	Q ₂₄	Q ₂₅	Total Circuit	Q ₂₄	Q ₂₅	Total Circuit	Total Circuit
5.57	0.790	0.790	0.628	0.046	0.046	2.9	0.725

Table 3 - MANUAL MODE POWER DISSIPATION -- WATTS

Item	2N2222A	2N3499	2N2102 (Note 4)
Power (mW)	500	1000	5000 (Note 5)
I _c (ma)	500	500	---
BV _{CBO} Max (Vdc)	75	100	120
BV _{CEO} Max (Vdc)	50	100	65
BV _{EBO} Max (Vdc)	6	6	7
h _{FE} Max	100-300	100-300	10-120
I _C Max (ma)	150	150	1A
V _{CE} (sat) Vdc)	0.4	0.6	0.5
f (MHz)	250 (ft)	150 (ft)	120 (ft)
hfe	----	1.5	----
JEDEC Outline	TO-18	TO-5	TO-5
MIL-S-19500	255	366	
	(Note 2)	(Note 3)	
hFE	50-60	40	40

1. Acceptable Parts List, February 13, 1970, BSR 2857, P53.
2. Specification Sheet for 2N2222A, Motorola Semiconductor Products
3. Motorola Semiconductor Data Book, Page 8-161, 2nd Edition
4. Specification Sheet for 2N2102, 2N1613, Radio Corp. of America
5. Dissipation at Case Temperature up to 25°C.

Table 4 - TRANSISTOR SPECIFICATIONS (Notes 1 and 4)

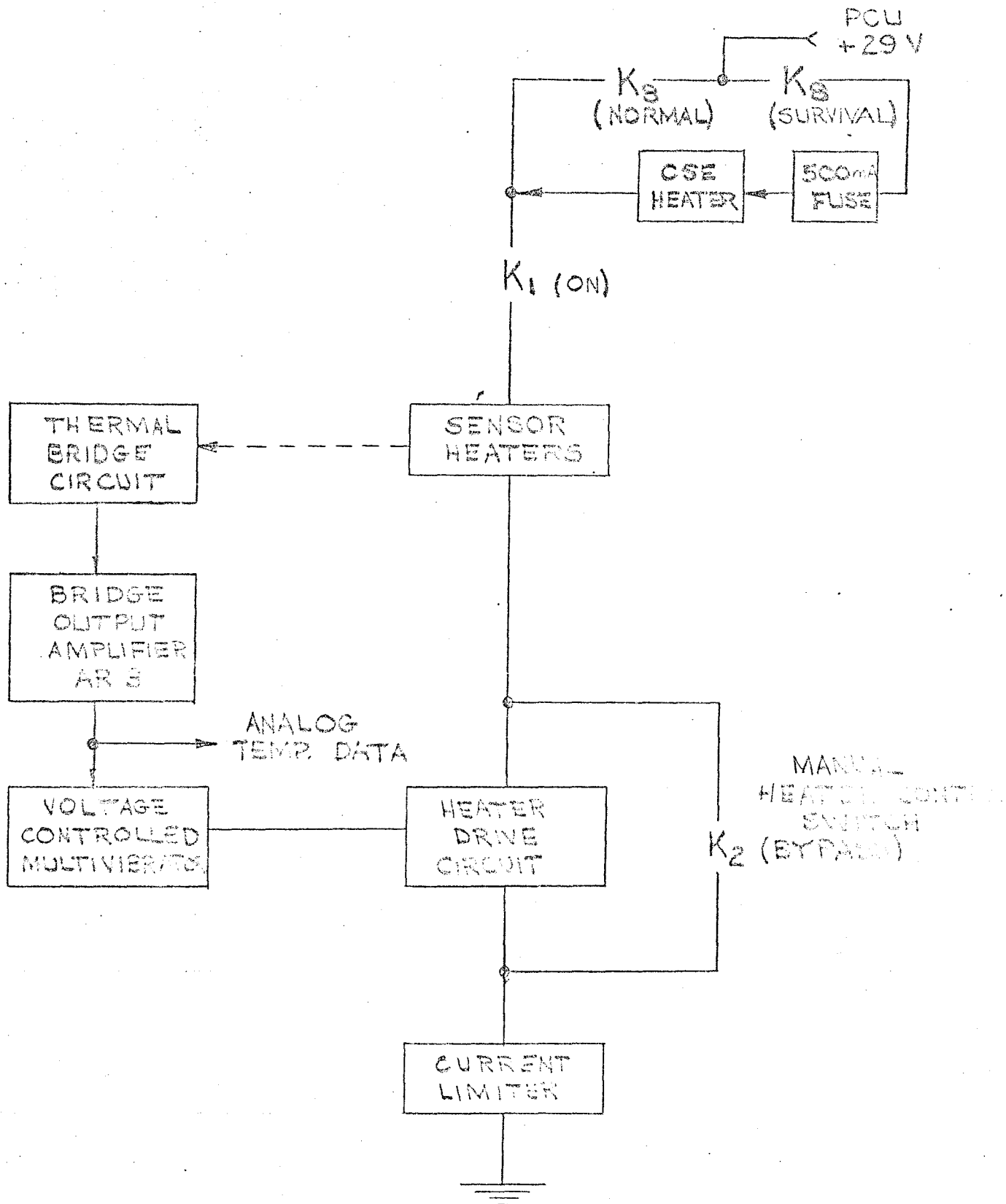


Figure 1.0 - PSE Heater Block Diagram

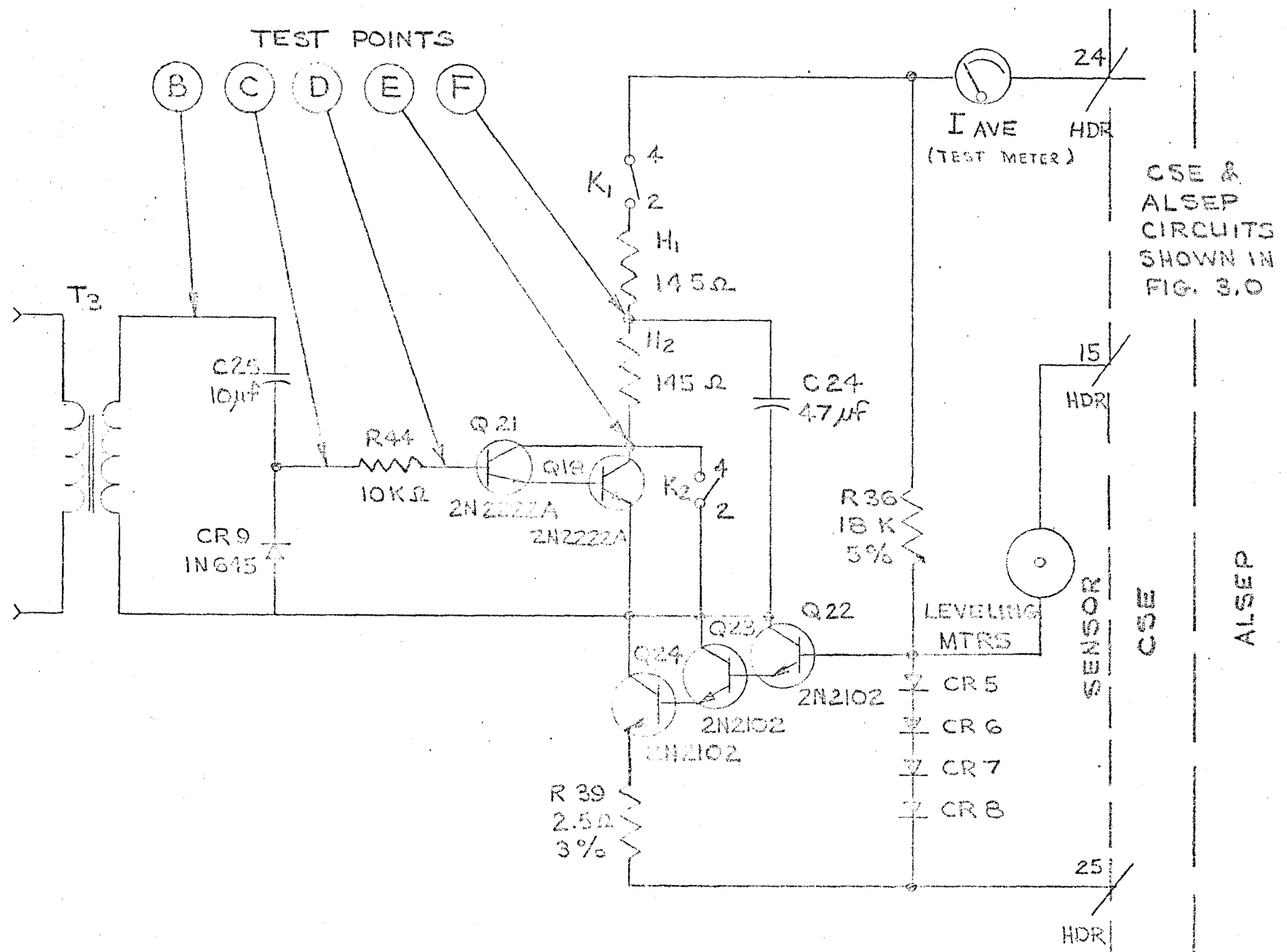
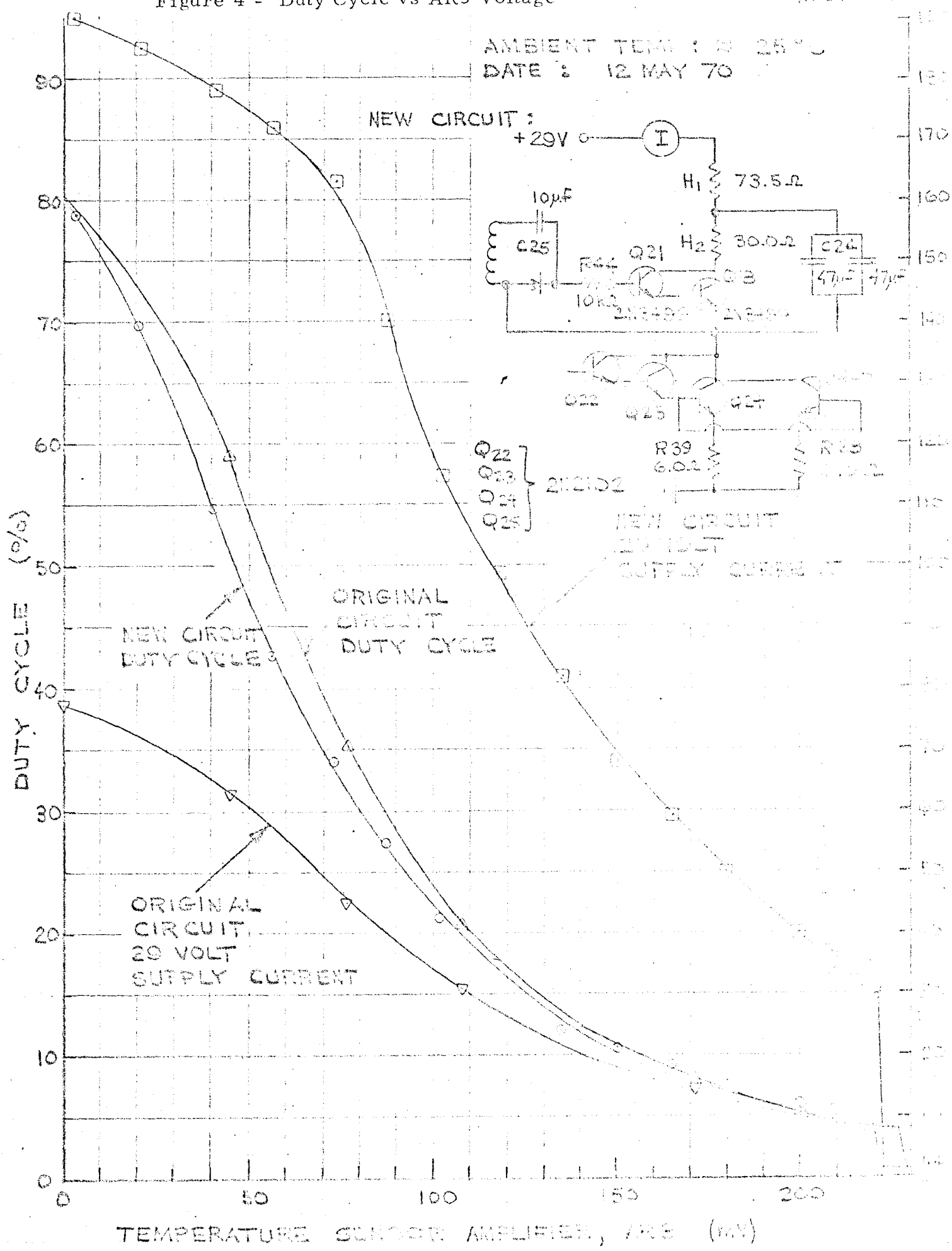


Figure 2.0 - Original Heater Circuit Configuration

Figure 4 - Duty Cycle vs AR3 Voltage

AMBIENT TEMP : 25 °C
DATE : 12 MAY 70



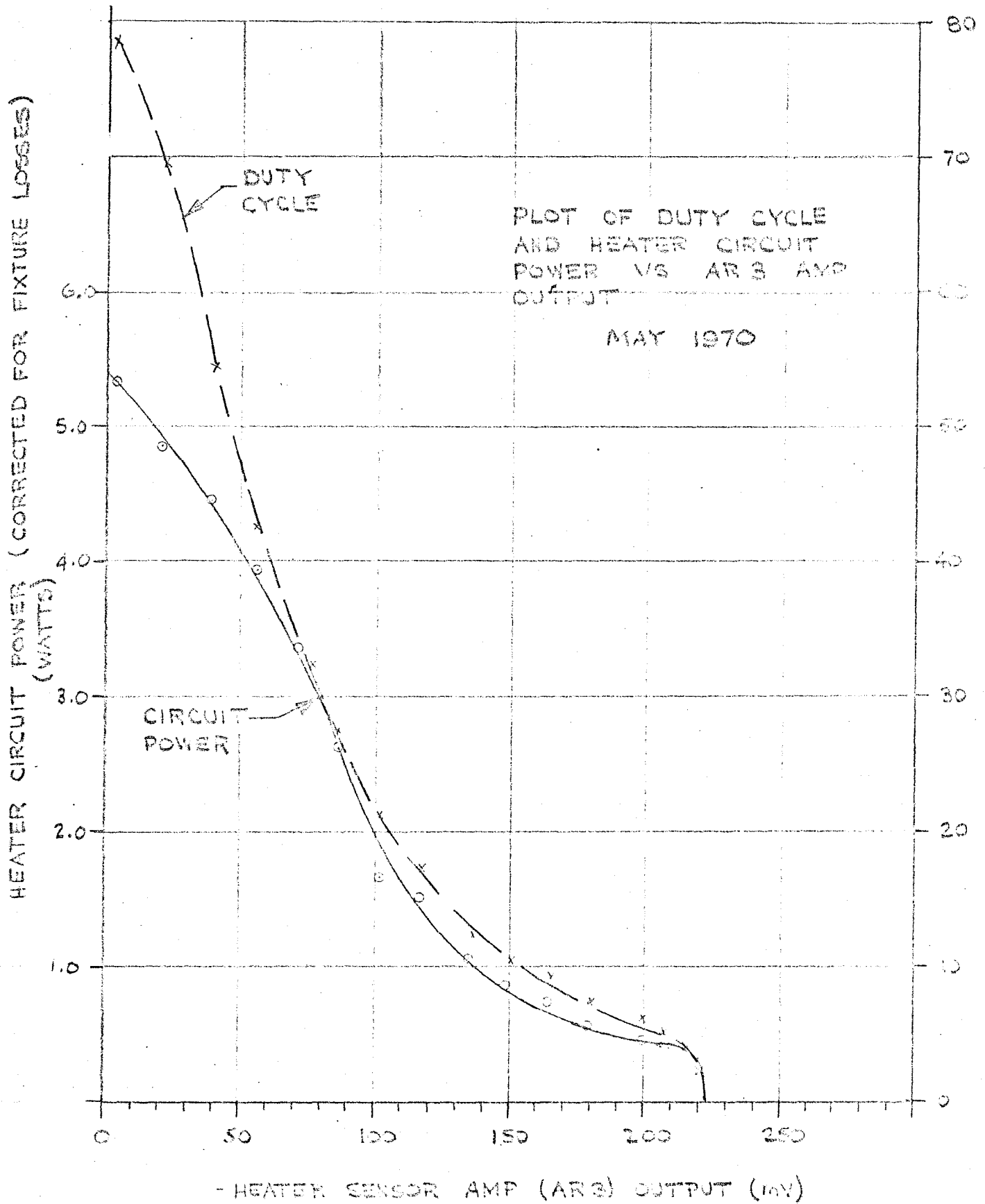


Figure 5.0 - DUTY CYCLE (%)

Figure 5 - Heater Circuit Power vs AR3 Output

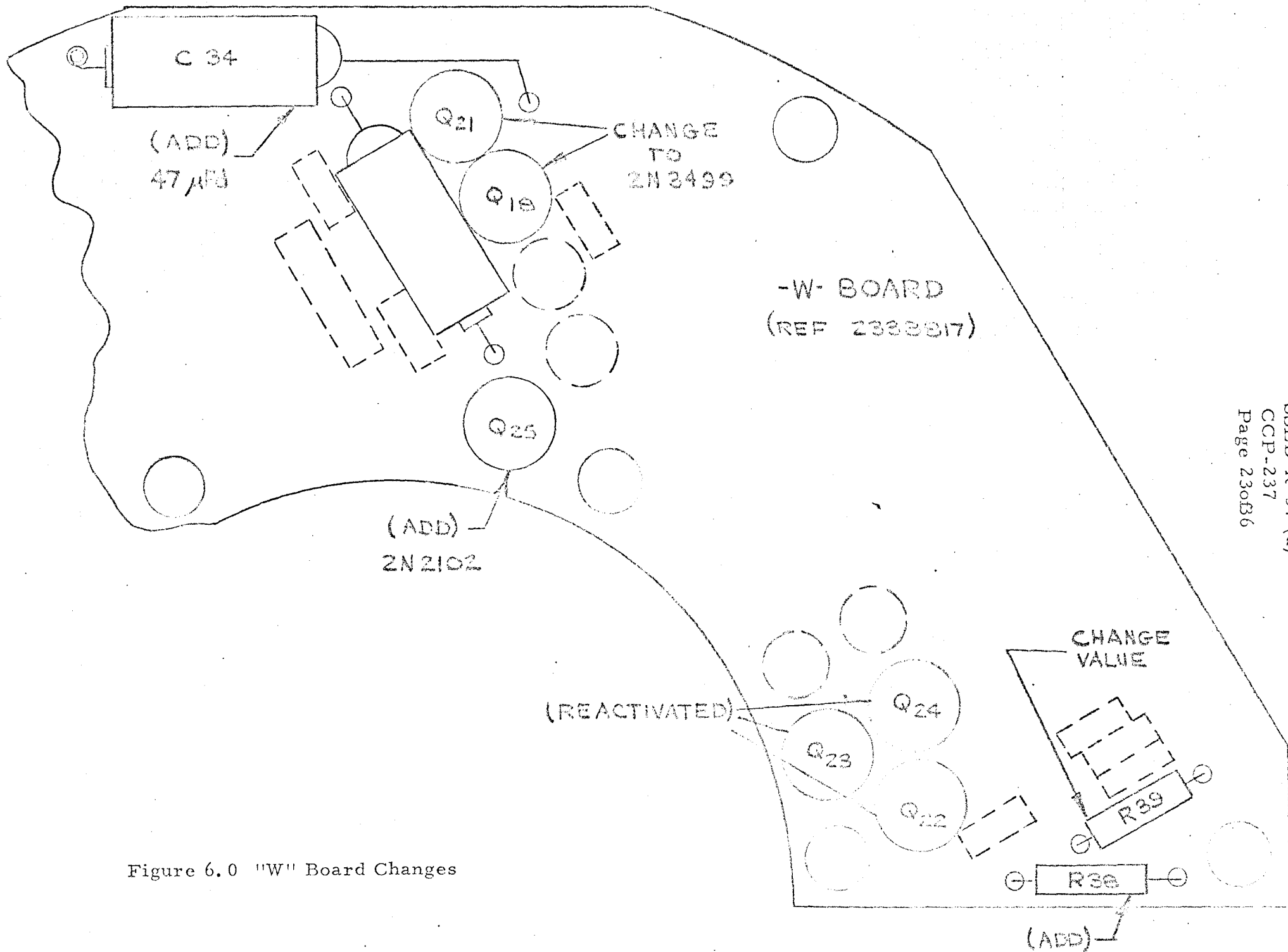
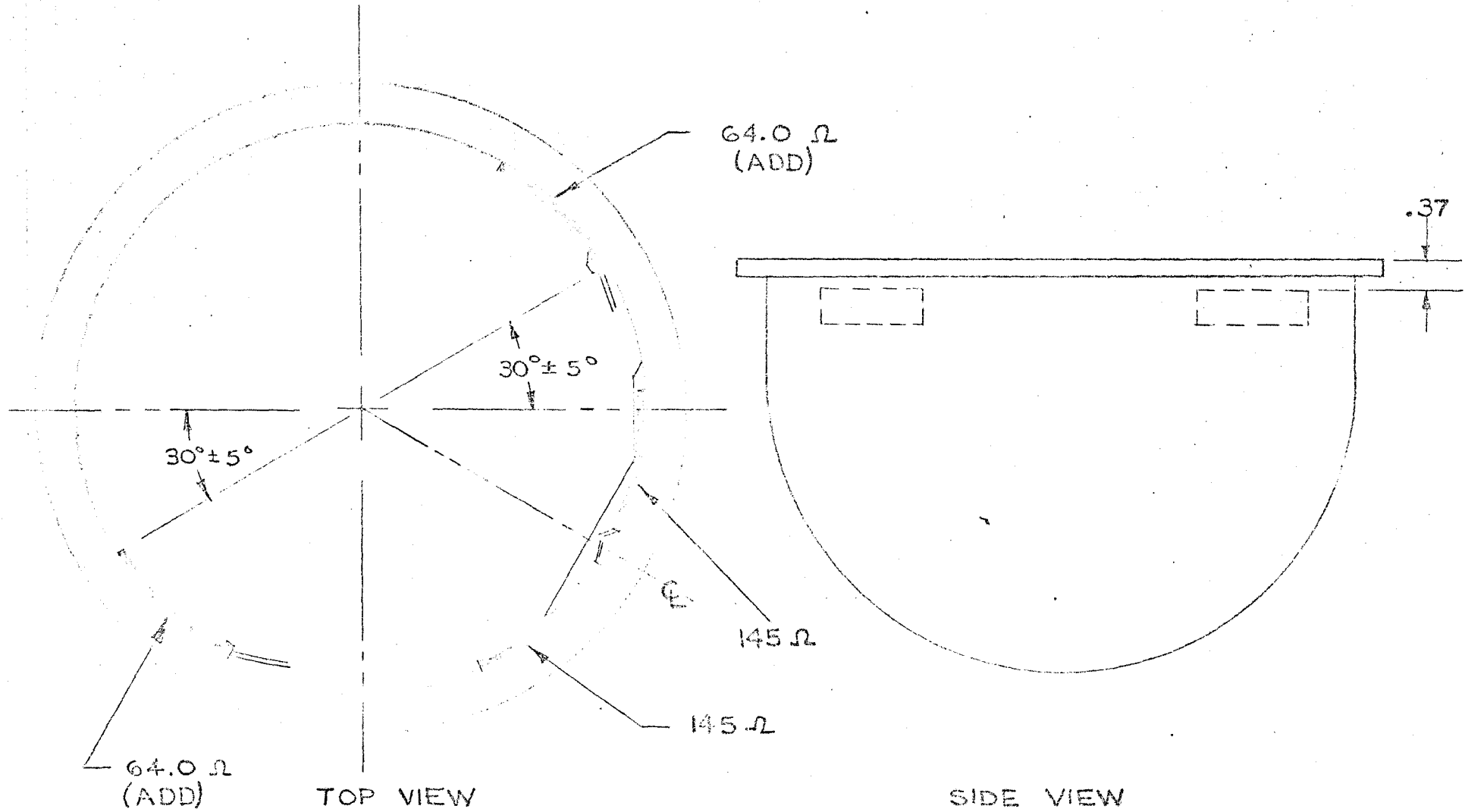


Figure 6.0 "W" Board Changes



PSS SENSOR

Figure 7.0 - Heater Element Positions

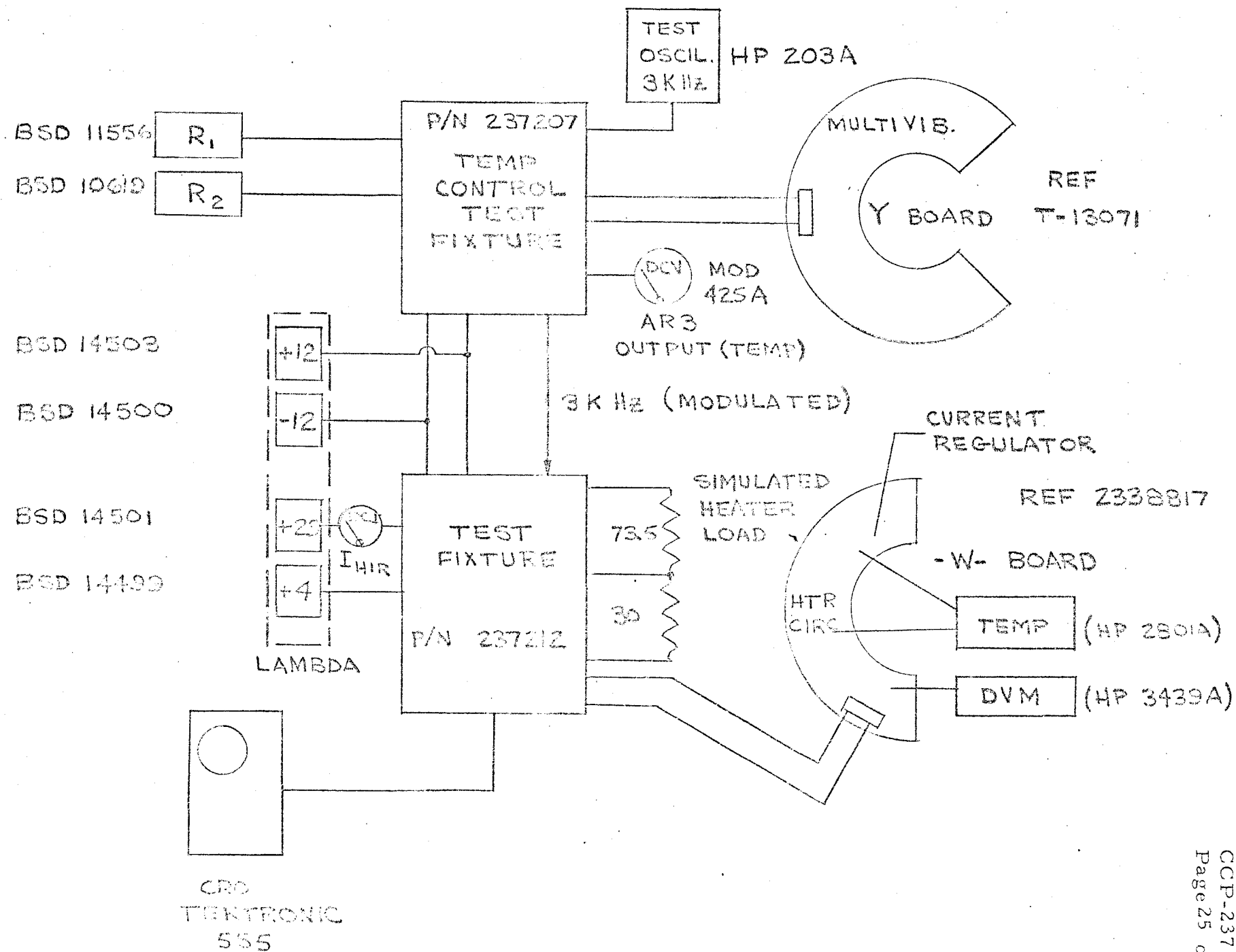
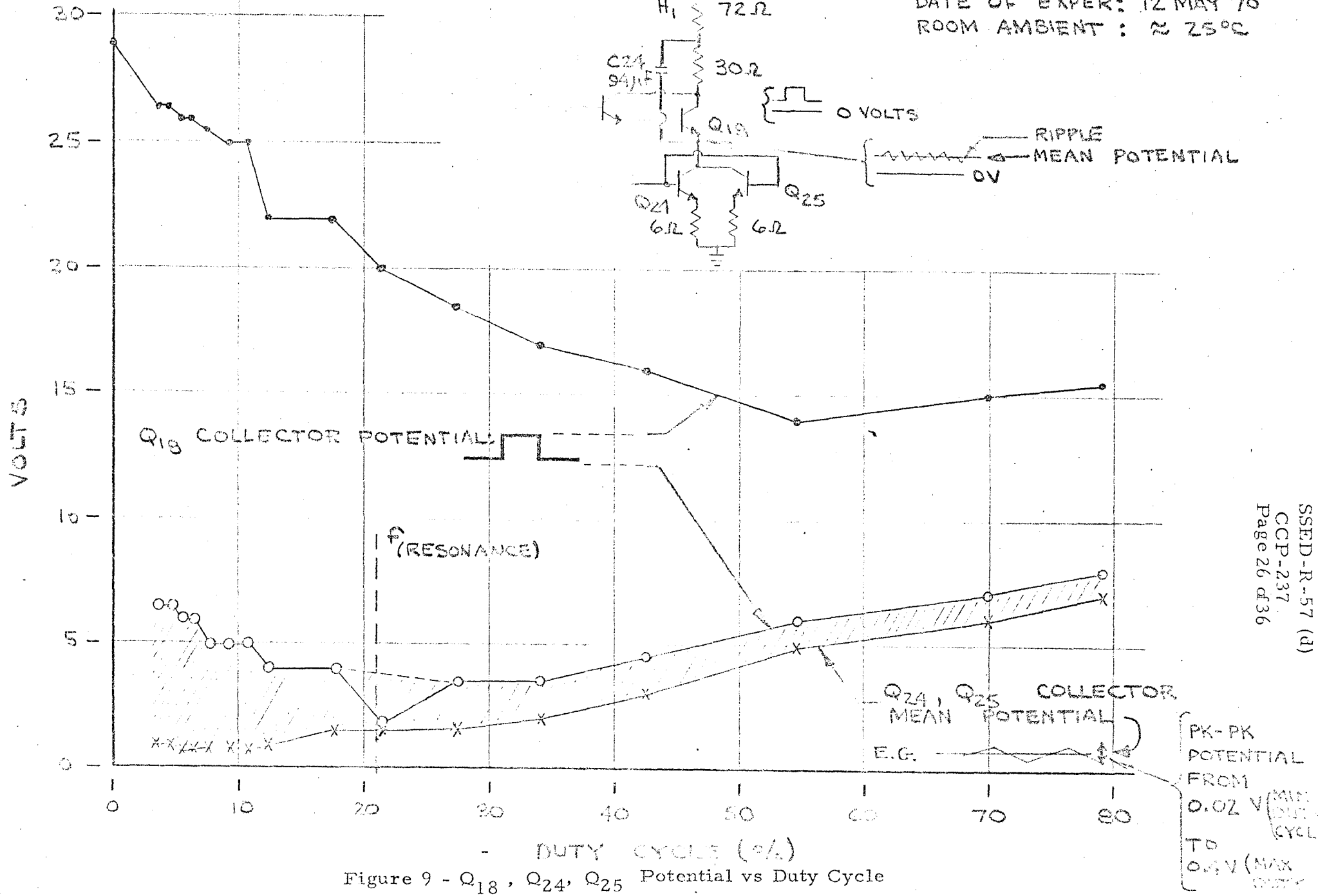


Figure 8.0 - Heater Circuit Test Configuration

Q18, Q24, Q25 POTENTIALS VS DUTY CYCLE

DATE OF EXPER: 12 MAY 70
ROOM AMBIENT : $\approx 25^{\circ}\text{C}$



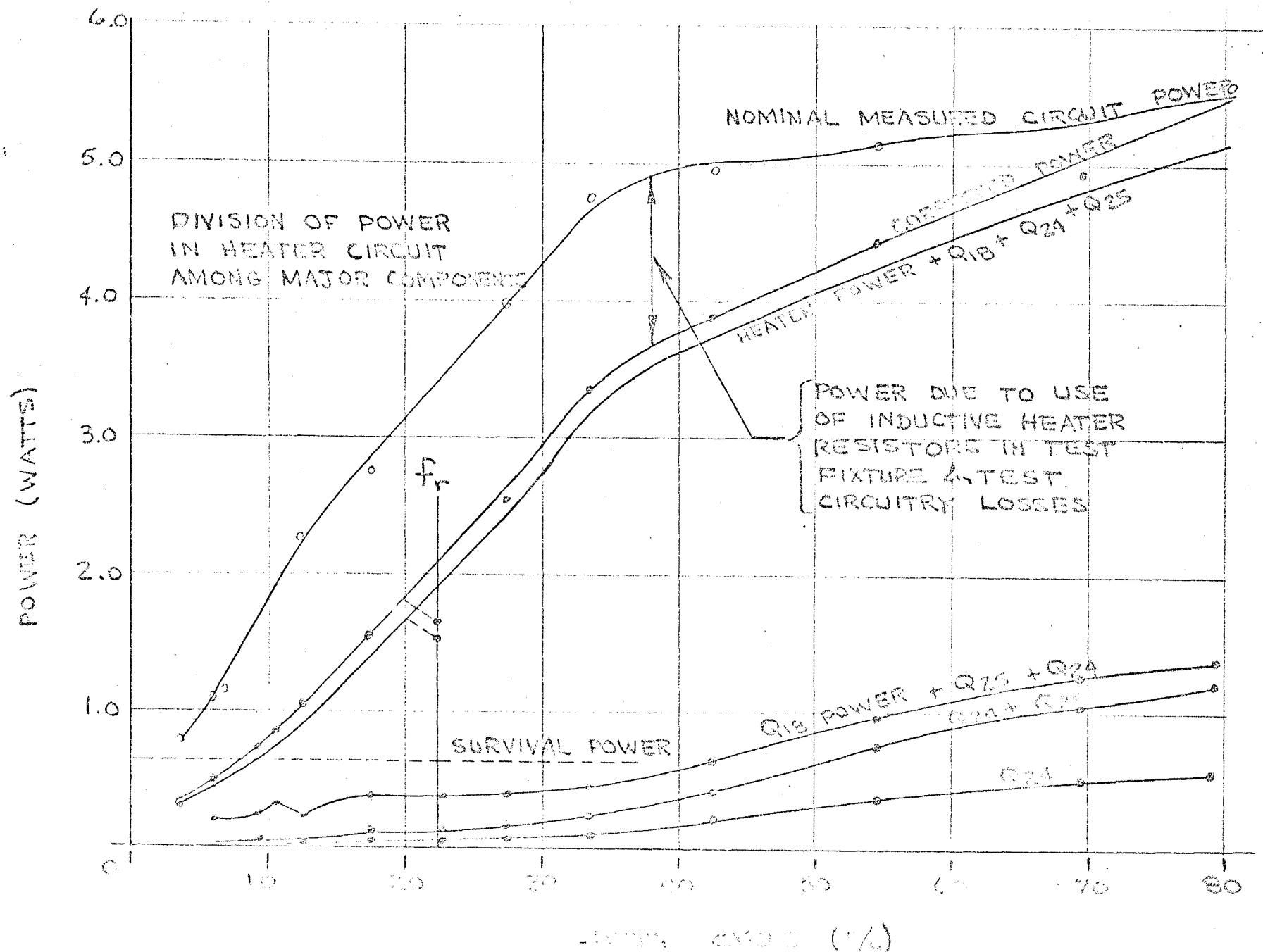


Figure 10 - System Power Distribution

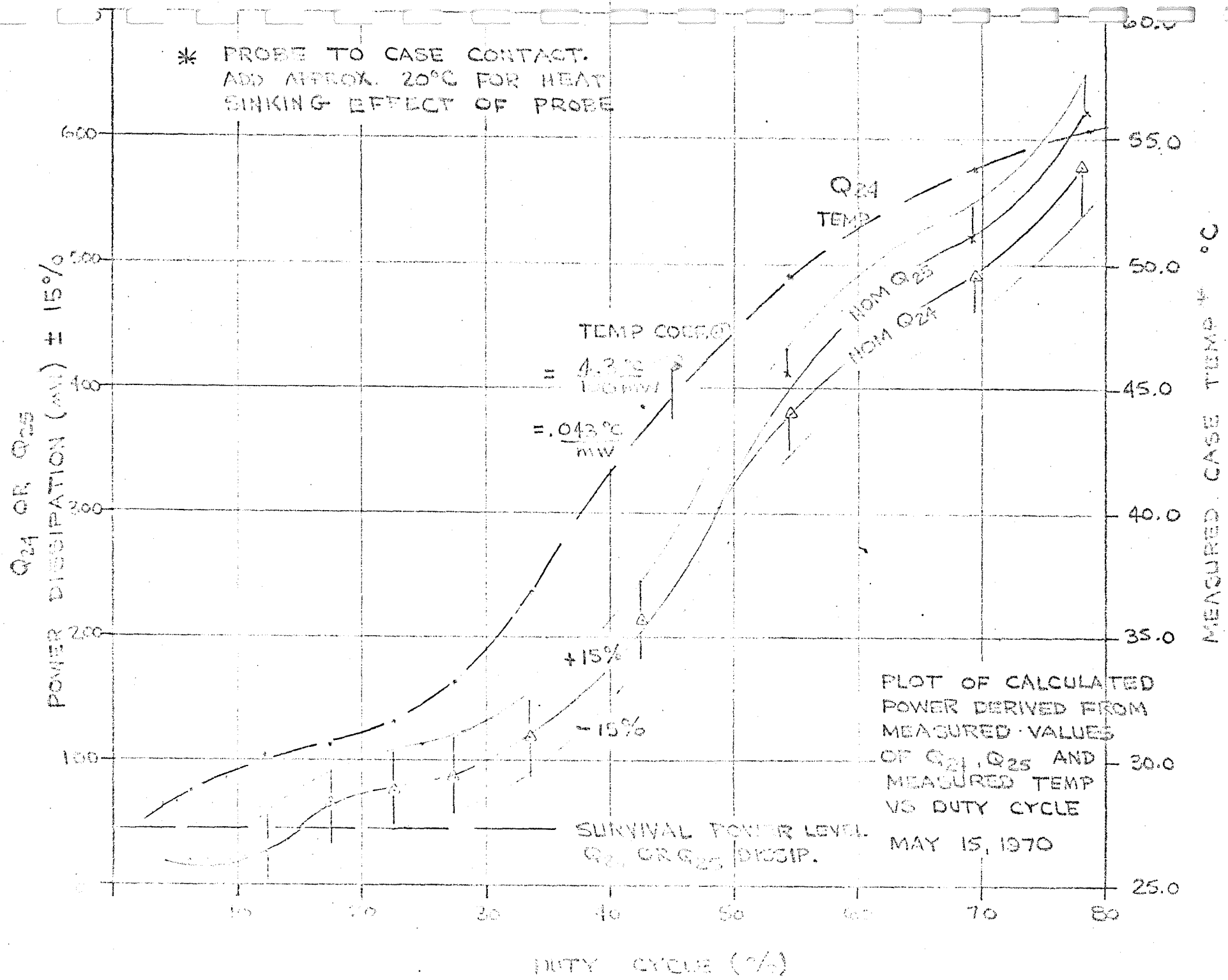


Figure 11 - Power Dissipation vs Duty Cycle (Q_{24} or Q_{25})

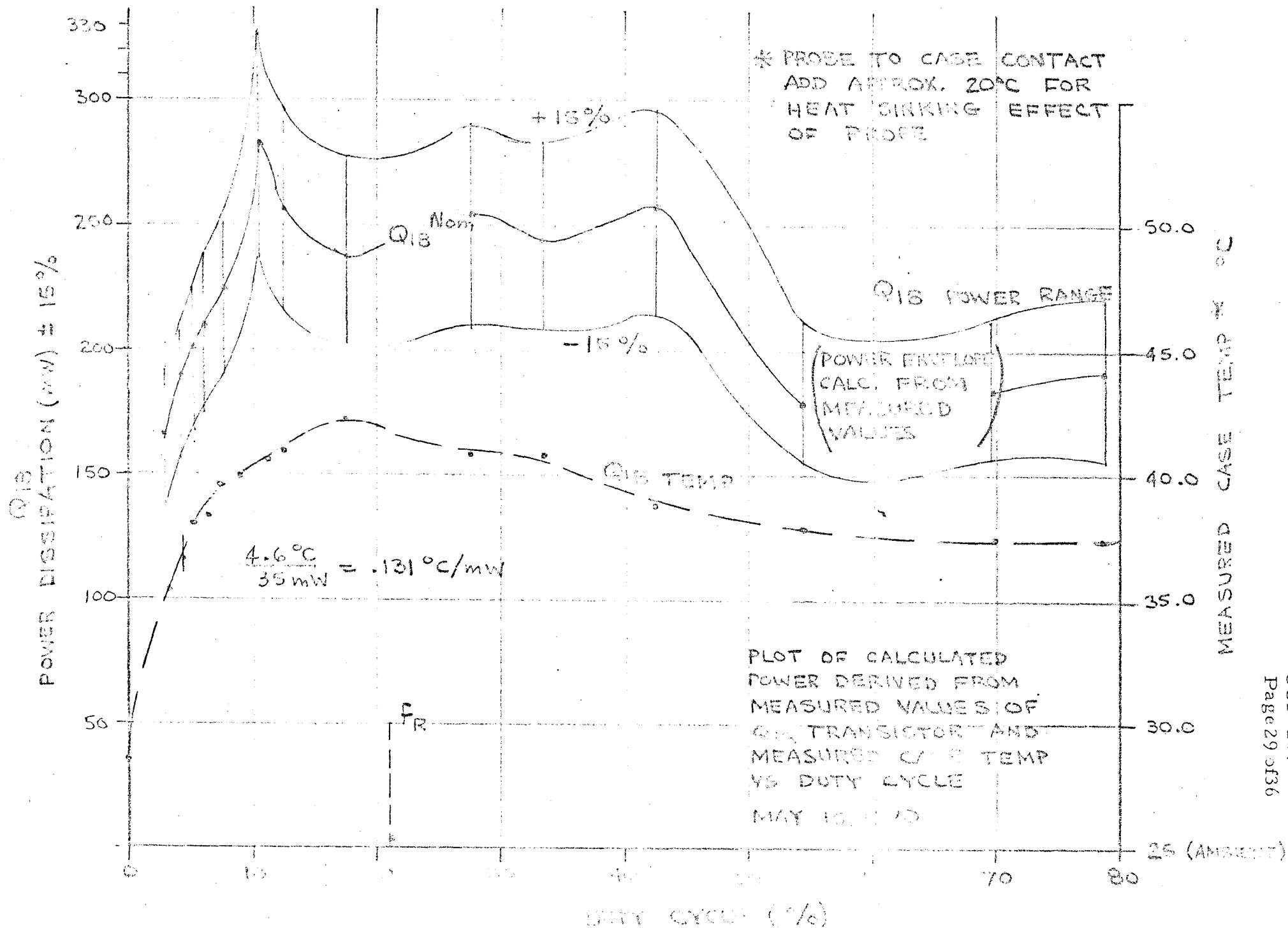


Figure 12 - Power Dissipation vs Duty Cycle (Q₁₃)

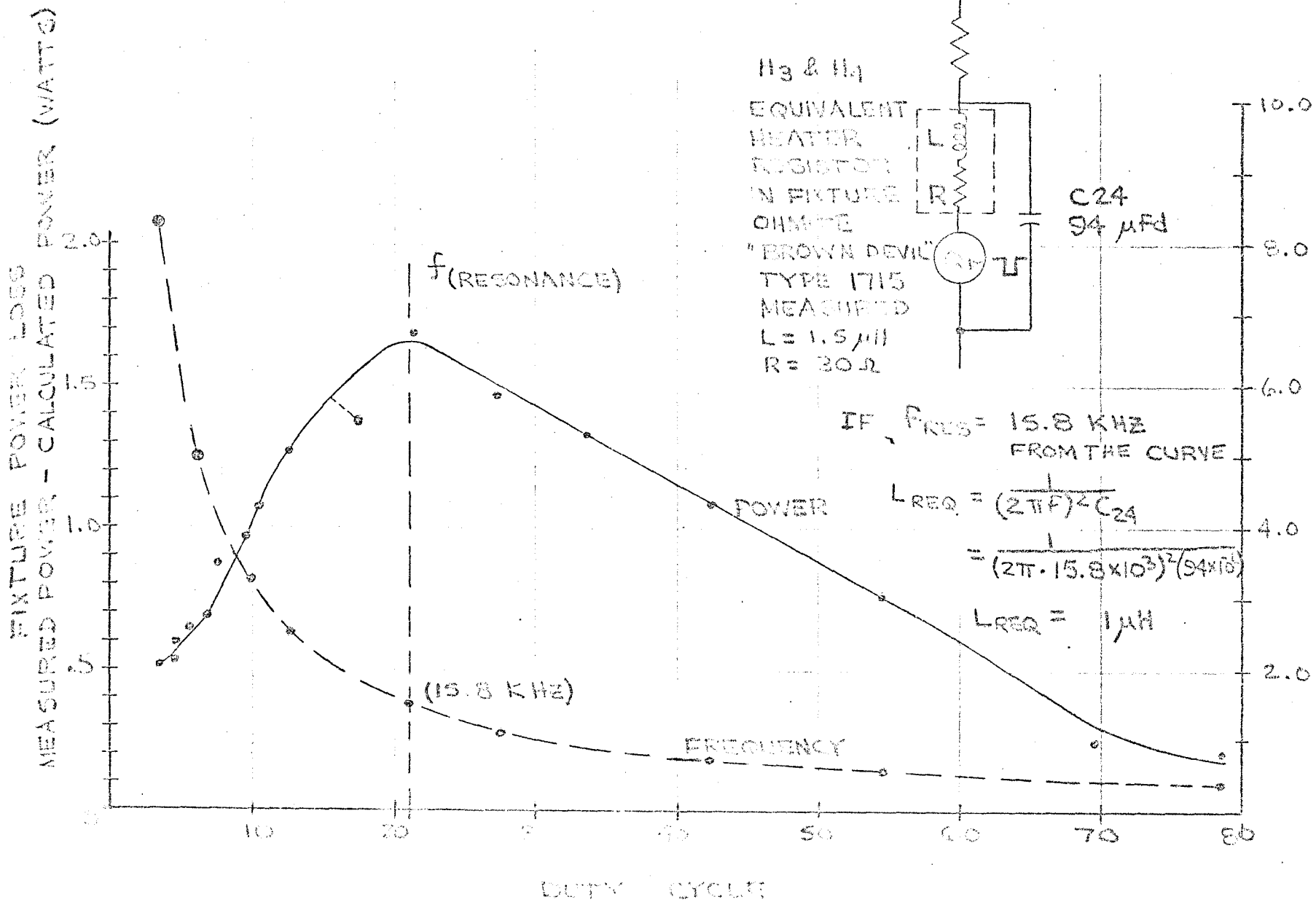
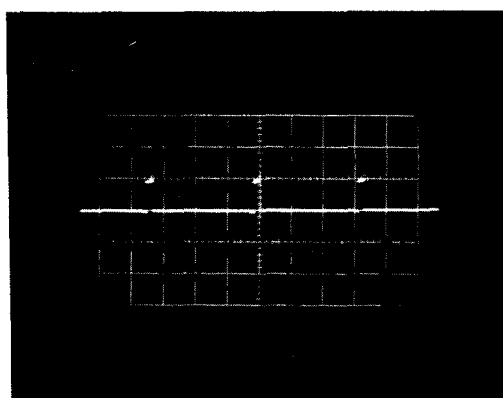


Figure 13.0 - Power Loss In Test Fixture

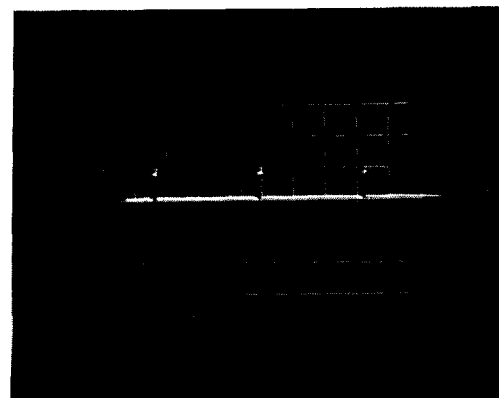
TEST POINT B - T₃ SECONDARY



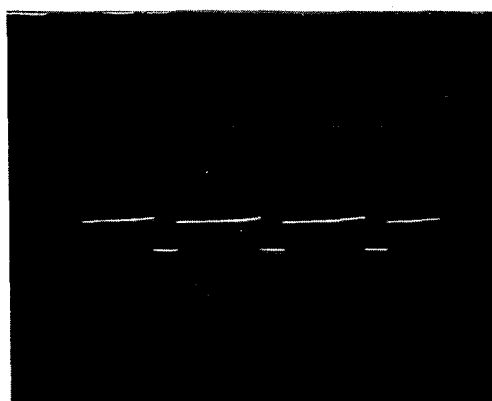
Original Circuit

Minimum
Duty
Cycle

5 volts/cm
100 μ sec/cm

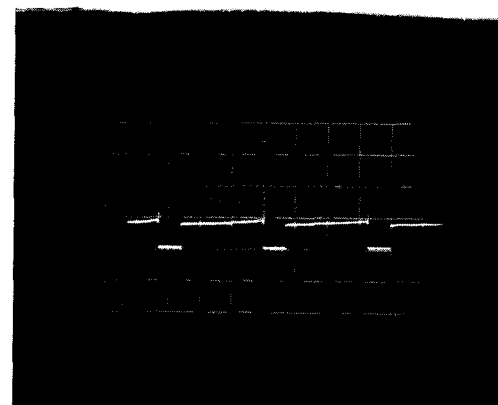


Modified Circuit



Time ←

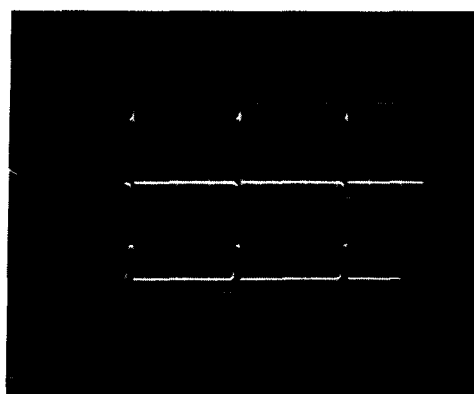
Maximum
Duty
Cycle



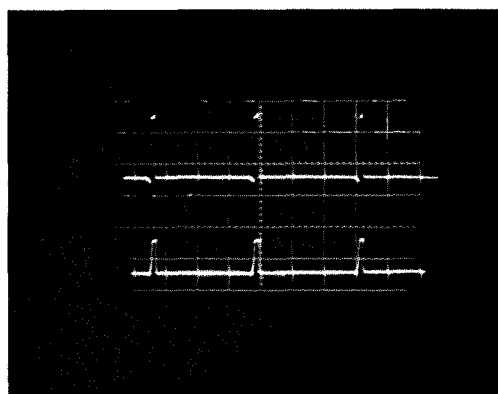
Time ←

Figure 14.0

TEST POINTS C AND D



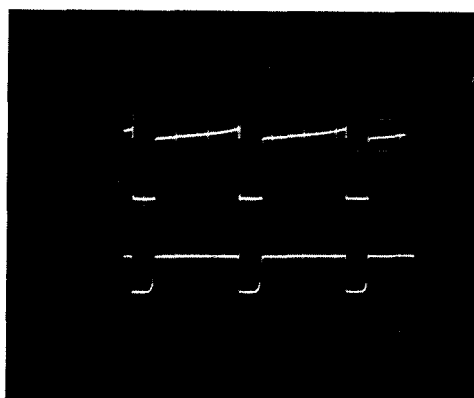
Minimum
Duty
Cycle



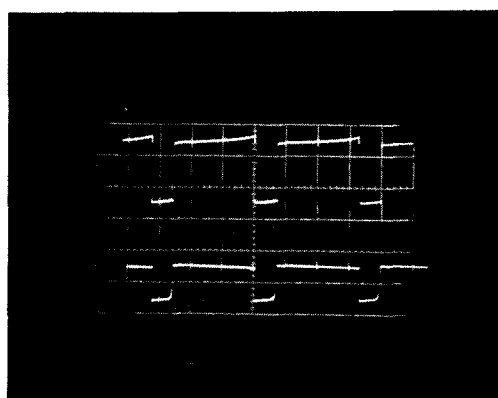
Original Circuit

2 volts/cm
100 μ sec/cm

Modified Circuit



Maximum
Duty
Cycle

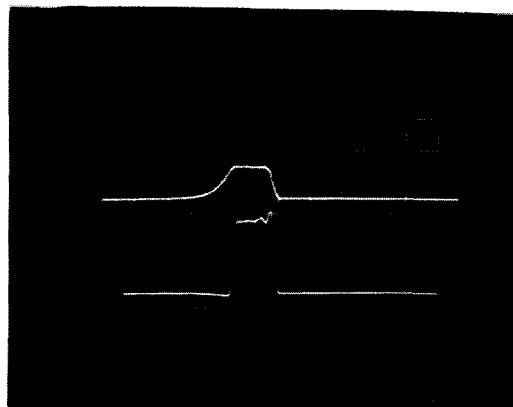


In Each Photograph-
Top Waveform: Test Point C
Bottom Waveform: Test Point D

Note: Center and bottom
reticle lines are
 $V = 0$ reference for
Respective traces.

Figure 15.0

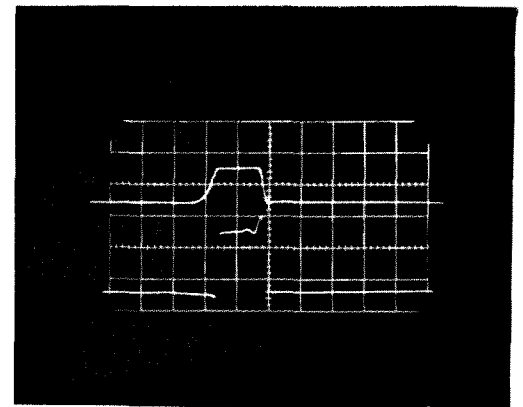
TEST POINTS C AND D RISE AND FALL TIMES



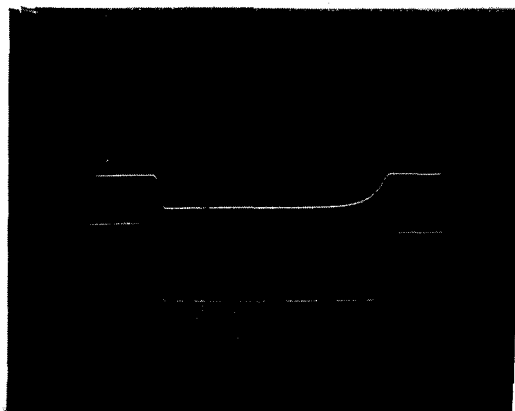
Original Circuit

Minimum
Duty
Cycle
Test Point D
Test Point C

2 v/cm
10 μ sec/cm

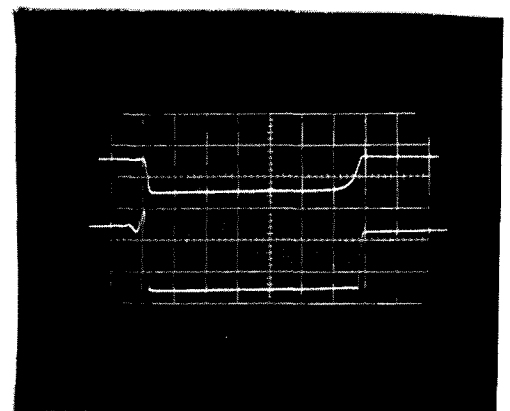


Modified Circuit



Time \rightarrow

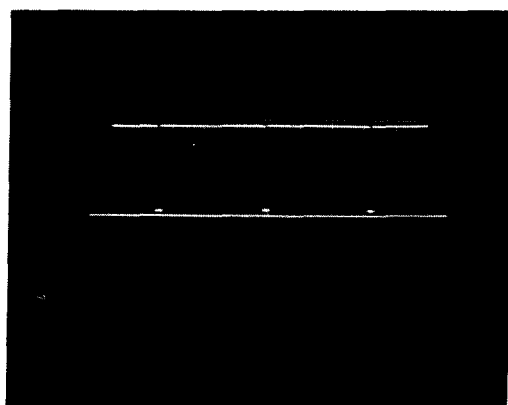
Maximum
Duty
Cycle
Test Point D
Test Point C



Time \leftarrow

Figure 16.0

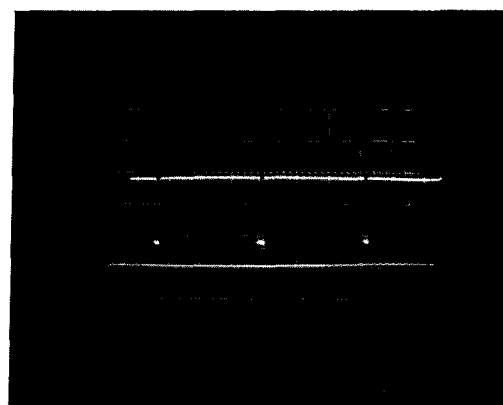
TEST POINT E- Q_{18} COLLECTOR



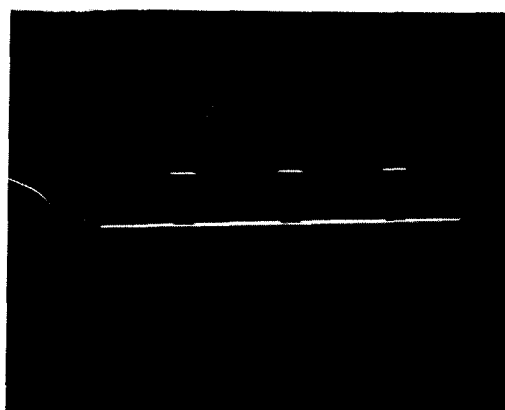
Original Circuit

Minimum
Duty
Cycle

10 volts/cm
100 μ sec/cm

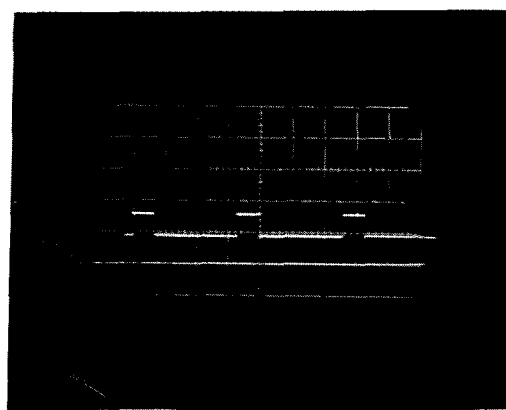


Modified Circuit



Time ←

Maximum
Duty
Cycle

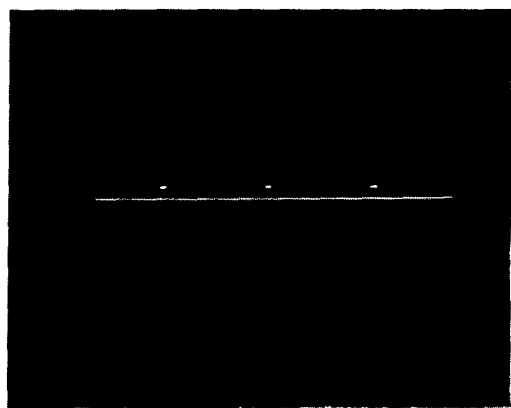


Time ←

NOTE: Unbroken trace
V = 0 Reference

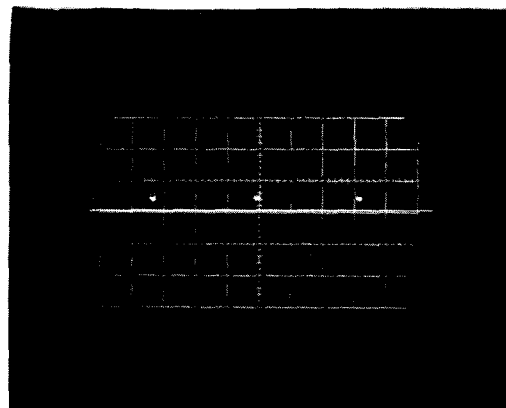
Figure 17.0

MEASUREMENT OF V_{CE}
TEST POINT E - Q₁₈ COLLECTOR

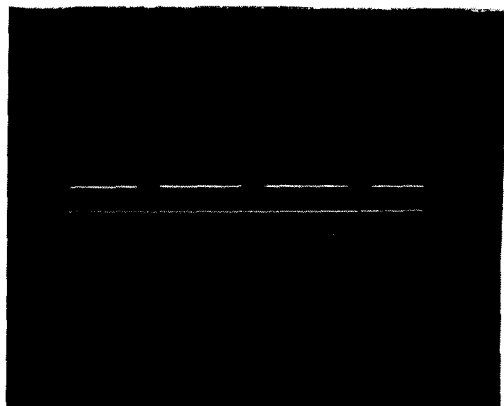


Minimum
Duty
Cycle

Original Circuit
1 v/cm
100 μ sec/cm

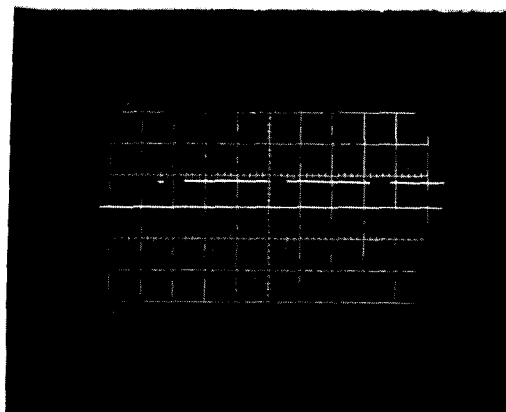


Modified Circuit
10 v/cm
100 μ sec/cm



Maximum
Duty
Cycle

Time \rightarrow

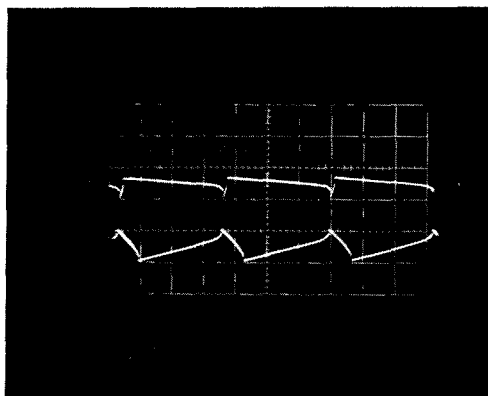


Time \rightarrow

Figure 18.0

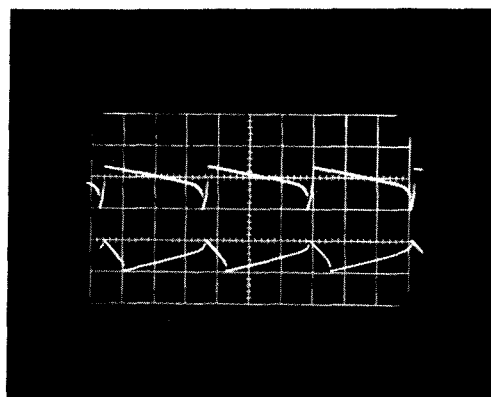
TEST POINT F - RIPPLE VOLTAGE ACROSS C_{24}

Original Circuit



Time \leftarrow

Modified Circuit



Time \leftarrow

IN EACH PHOTOGRAPH:

TOP: Minimum Duty Cycle

BOTTOM: Maximum Duty Cycle

SCOPE SETTINGS:

200 mV/cm

100 μ sec/cm

Figure 19.0



Investigation of PSE Anomalies
Apollo 12 Mission

Aerospace
Systems Division

NO.	REV. NO.
SSFD- R-57 (e)	
PAGE <u>1</u>	OF <u>13</u>
DATE 28 May 1970	

This report provides the results of investigations of PSE anomalies from Apollo 12 mission. Reference 97/510-454, CCP-237, 16 February 1970.

TASK TITLE: Analyze Thermal Shroud Design

Prepared by: D. Dewhirst
D. Dewhirst

Prepared by: R. D. Johnson
R. Johnson

Approved by: J. Lewko, Jr.
J. Lewko, Jr.

CONTENTS

<u>Paragraph</u>	<u>Title</u>	<u>Page</u>
1.0	INTRODUCTION	4
2.0	DISCUSSION	4
2.1	STATEMENT OF WORK	4
2.2	ANALYSIS	4
3.0	SUMMARY OF RESULTS	10
4.0	CONCLUSIONS AND RECOMMENDATIONS	10
5.0	REFERENCES	11

ILLUSTRATIONS

<u>Figure</u>	<u>Title</u>	<u>Page</u>
1	The Moment of ΔF about Point X Is Minimized by Running Cable Below PSE.	12
2	Labyrinth Skirt Configuration	13

1.0 INTRODUCTION

This task has been performed to determine the magnitude of the forces exerted by the electronic cable assembly on the PSE, and to determine the contributions of the skirt to the noise anomaly observed at terminator crossing.

2.0 DISCUSSION

2.1 Statement of Work

The following statement of work is taken from the MCP originally prepared for this anomaly study.

2.1.1 Analyze Thermal Shroud Design

2.1.2 Analyze design (Ultra Insulation/Easton Precision Tube) of skirt multi layer tie down. Consider the following,

- a) Multi use of mono filament to increase individual layer tie down.
- b) Perforated mylar (modification) to provide a means to permit outgassing between layers.

2.1.3 Analyze use of additional skirt deployment tabs. Consider addition of ballast to weigh down the edges of the skirt.

2.1.4 Conduct a stowage/deployment test on a non flight thermal shroud to determine if any mechanical problems exist due to the addition of material to the edge of the skirt.

2.1.5 Prepare recommendations for a design mod kit to thermal shroud.

NOTE: ALSEP to provide a test model thermal shroud to support above.

The following task has been undertaken as a result of Letter BG 931/L115-70/T94, 20 February '70, Attachment 1, para 5.0, Noise at Terminator Crossing.

2.1.6 Analyze shroud design to devise a method of shroud modification to eliminate possible shroud problem due to strain accumulation and release.

2.2 Analysis

The ideal support for the PSE is three legs forming a simple tripod.

A tripod is statically determinate, which means that the forces of the ground on the three legs could change only by a shift in the center of gravity of the PSE assembly.

Both the thermal shroud and the electronic cable assembly add redundant "supports" to the PSE tripod in that they can transmit loads from the ground to the instrument, or can transmit their own weight forces to either the PSE or the ground in varying amounts. This problem could be alleviated by either decoupling the two items from the PSE or by lowering their weight and stiffness. It may not be feasible to decouple the cable assembly from the instrument. However, running the cable beneath the experiment would minimize the change in moment on the instrument for a given change in cable force. See Figure 1.

The calculations which follow investigate conditions under which anomalous moments can be exerted on the PSE. Included are:

2.2.1 Forces exerted by the electronic cable assy on the PSE

(Reference pages through).

2.2.1.1 Change in cable length supported.

2.2.1.2 Change in curvature of cable.

2.2.2 Effects of skirt on terminator anomaly.

(Reference pages and)

2.2.2.1 Griffin modification

2.2.1 Calculate Forces Exerted By Electronic Cable Assy. On PSE.

Two possibilities are presented: 1) a moment on PSE due to the length of cable supported and 2) a moment on the PSE due to a change in curvature in the cable.

2.2.1.1 Determine threshold value of change of cable length which will cause signal by PSE

$$\text{Weight of P-35 cable per inch} = W = W_{cu} + W_{pl}$$

where W_{cu} = weight of copper in cable

W_{pl} = weight of plastic in cable

$$W_{cu} = 30 \times .002 \times .025 \times .32 \frac{\text{lb}}{\text{in}^3} = .00048 \text{ lb/in.}$$

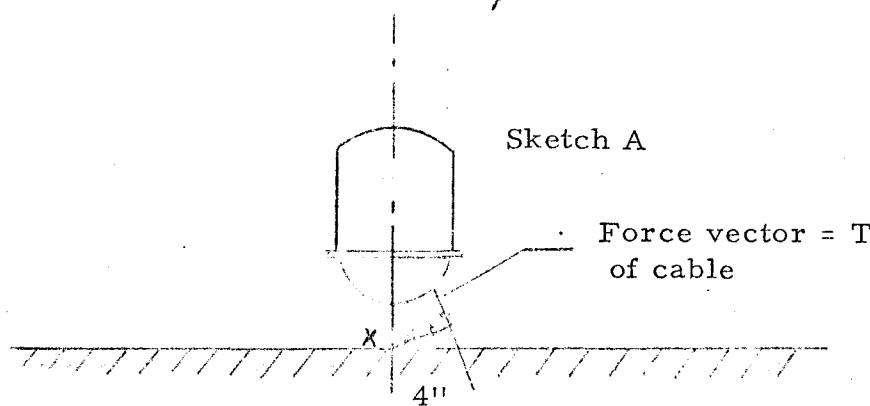
$$W_{pl} = \frac{2}{27} \frac{\text{lb}}{\text{ft}^2} \times \frac{1 \text{ ft.}^2}{144 \text{ in}^2} \times 1.65 \text{ in.} = \frac{.000846}{144}$$

$$W = .001326 \text{ lb/in}$$

Weight of P-30 cable per inch = $(.024/.010) (.001326) = .00318$

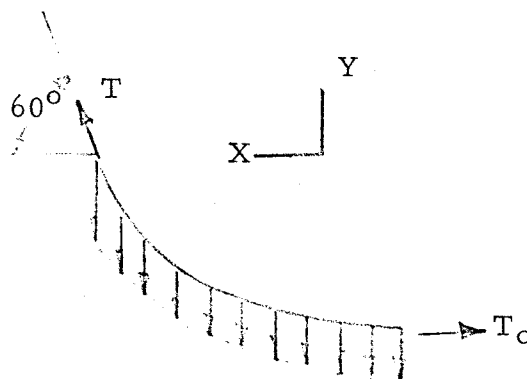
∴ Unit cable weight = $.001326 + .00318 = .00451 \text{ lb/in.}$

a) $M = 4T$ = moment of force exerted by cable about point X:



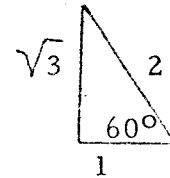
Assume cable hangs in catenary making an angle of 60° with the horizontal at a moment arm of 4 inches. See sketch A.

Let L = length of cable



$$T_x = T_o$$

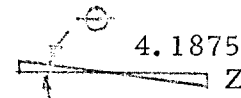
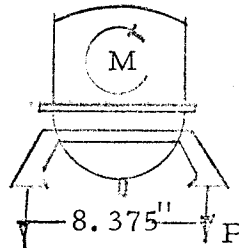
$$\frac{T_y}{T_x} = \frac{\sqrt{3}}{1} \quad \text{and} \quad \frac{T_y}{T_x} = \frac{\sqrt{3}}{2}$$



$$T_y = .00318 \frac{\text{lb}}{\text{in}} \times L \text{ in.}$$

$$b) \quad T = \frac{2}{\sqrt{3}} T_y = \frac{1}{.866} \times .00318 \times L = .00367 L$$

Determine threshold moment as function of threshold rotation:



$$\theta = \arctan \frac{Z}{4.1875} = \arctan \frac{.1}{4.1875} = \tan^{-1} .0239 = .024 \text{ radians}$$

$$M = 8.375 P = 8.375 p (4.5) = 8.375 (3 \times .1^1) (4.5) = 11.3$$

$$c) \quad K = \frac{M}{\theta} = \frac{11.3}{.024} = 470 \text{ lb.-in/radian}$$

Threshold rotation is 5×10^{-8} radians

Therefore threshold moment is.

$$d) \quad M = K \theta = 470 \times 5 \times 10^{-8} = 2.35 \times 10^{-5} \text{ lb.-in}$$

From eqs a, b, and d:

$$4 (.003675 L) = 2.35 \times 10^{-5}$$

$$e) \quad L = \frac{2.35}{4} \times \frac{1}{367.5} = .0016 \text{ in.}$$

2.2.1.2 Eq. e assumes no change in cable curvature. However, because the cable has a finite bending stiffness, a change in curvature does produce a moment on the instrument. The following calculations determine the change in curvature to produce a change in moment equal to the threshold value of Eq. d.

Determine bending stiffness of cable:

$$I_{cu} = \frac{1}{12} b h^3 = \frac{1}{12} (30 \times .002) (.025)^3 = 77.9 \times 10^{-9}$$

where: I_{cu} = Moment of Inertia of copper

$$(EI)_{cu} = 17 \times 10^6 \times 77.9 \times 10^{-9} = 1.323 \text{ lb} - \text{in}^2$$

E_{cu} = Modulus of Elasticity of Copper

$$(EI)_{FEP} = 70,000 \left(\frac{1}{12} \right) 1.65 [(.006)^3 - (.002)^3]$$

where: I_{FEP} = Moment of Inertia of FEP plastic

E_{FEP} = Modulus of Elasticity of FEP plastic

$$= 2 \times 10^{-3}$$

$$\begin{aligned} *(EI)_{Mylar} &= 550,000 \left(\frac{1}{12} \right) (1.65) [(.01)^3 - (.006)^3] = .0591 \\ &= 59 \times 10^{-3} \end{aligned}$$

where I_{Mylar} = Moment of Inertia of Mylar

E_{Mylar} = Modulus of Elasticity of Mylar

negligible

$$f) EI = (EI)_{cu} + (EI)_{FEP} + (EI)_{Mylar} = \underline{61 \times 10^{-3} \text{ psi}}$$

Cables P-30 and P-35 are tied together at only one point. Approximating their effective EI yields:

$$EI = \left[1 + \left(\frac{.024}{.010} \right)^3 \right] \times 61 \times 10^{-3}$$

* Type A Mylar ($E = 5.5 \times 10^6$ psi)

$$= (1 + 13.8) \times 61 \times 10^{-3}$$

$$= 14.8 (61) \times 10^{-3}$$

$$= .904 \text{ lb} - \text{in}^2$$

$$g) \quad EI \left(\frac{1}{R_{\text{final}}} - \frac{1}{R_{\text{initial}}} \right) = M$$

R = Radius of curvature

For initially flat cable, $R_{\text{in}} = \infty$. From eqs g, f and d,

$$.904 \left(\frac{1}{R_{\text{final}}} \right) - 0 = 2.35 \times 10^{-5}$$

$$h) \quad R_f = \frac{.904}{.0235 \times 10^{-3}} = 38,500 \text{ in.}$$

2.2.2 Determine Influence of PSE Skirt Using Griffin's Auxiliary Ring Concept - Reference 4.

2.2.2.1 Calculate weight of PSE skirt necessary to cover annular area 60" O.D., 10.75" I.D.

$$\text{Area} = 2827.50 - 90.76 = 2736.74 \text{ in}^2$$

$$W = \text{Weight} = 2736.74 \times \left[\begin{array}{cc} t & p \\ .002 & (.076) \\ \text{teflon} & \end{array} + \begin{array}{cc} t & e \\ .0055 & (.05) \\ \text{mylar} & \end{array} \right]$$

$$W = 2736.74 \times \left[.000152 + .000275 \right]$$

$$i) \quad W = 1.168 \text{ lb.}$$

2.2.2.2 Calculate change in weight supported by one point on ring to produce threshold moment.

Radius of ring is moment arm of weight = 5.375 in.

$$\Delta W \times (5.375) = 2.35 \times 10^{-5}$$

$$\Delta W = .437 \times 10^{-5} \text{ lb.}$$

$$j) \quad \frac{\Delta W}{W} \times 100 = \frac{.437}{1.168} \times 10^{-3} = .000375\%$$

is the percentage of shroud weight needed to cause detectable instrument rotation.

3.0 SUMMARY OF RESULTS

3.1 The interpretation of Eq e is that for the assumed cable configuration, i. e. 4 in. moment arm and 60° angle, and for no change in bending moment on the cable, an increase in the supported cable length of .0016 in. is sufficient to cause an anomalous signal. This change in length could be due to time dependent material effects (creep, relaxation) or due to thermal expansion.

3.2 The interpretation of Eq h is that a change in curvature from the flat condition to a radius of approximately 38,500 in will cause an anomalous signal. This is a small change in curvature and could be caused by changes in temperature or by changes in material properties. The effects of Eq e and Eq h may to some extent compensate one another.

3.3 The auxiliary ring concept effectively makes the shroud spring constant nearly zero and therefore minimizes the anomaly due to thermal expansion discussed in Reference 1. However, equation j shows that if the change in weight supported by one of the ring tie lines changes by .000375%, an anomalous signal can be picked up by the PSE.

4.0 CONCLUSIONS & RECOMMENDATIONS

With regard to the electronic cable assembly, it is concluded that the cable can exert an anomalous moment on the PSE if the change in supported length is as small as .0016 inches. Running the cable beneath the instrument would minimize this effect. See Figure 1.

With regard to the PSE skirt, it is concluded that a completely detached skirt is the only sure method of preventing anomalous signals from that source. Two methods of detaching the skirt are the dome configuration (Ref. SSED-436) and the labyrinth configuration, Figure 2.

5.0 REFERENCES

1. Interim Report, Investigation of PSE Anomalies, Apollo 12 Mission, SSED-R-57 (e).
2. Apollo 12 PSS Anomalies, SSED-P-1057 (a), J. Lewko, 1-8-70.
3. Identification of Apollo 12 PSS Problems, Anomalies and Preliminary Action Plan, SSED-346, J. Lewko/D. Breseke, 12-10-69.
4. 70-210-135, J. Griffin, Jr. to J. McNaughton, 5 May 1970
Subject: Concept to Reduce the Influence of PSE Skirt Thermal-Mechanical Stressing on Sensor Data

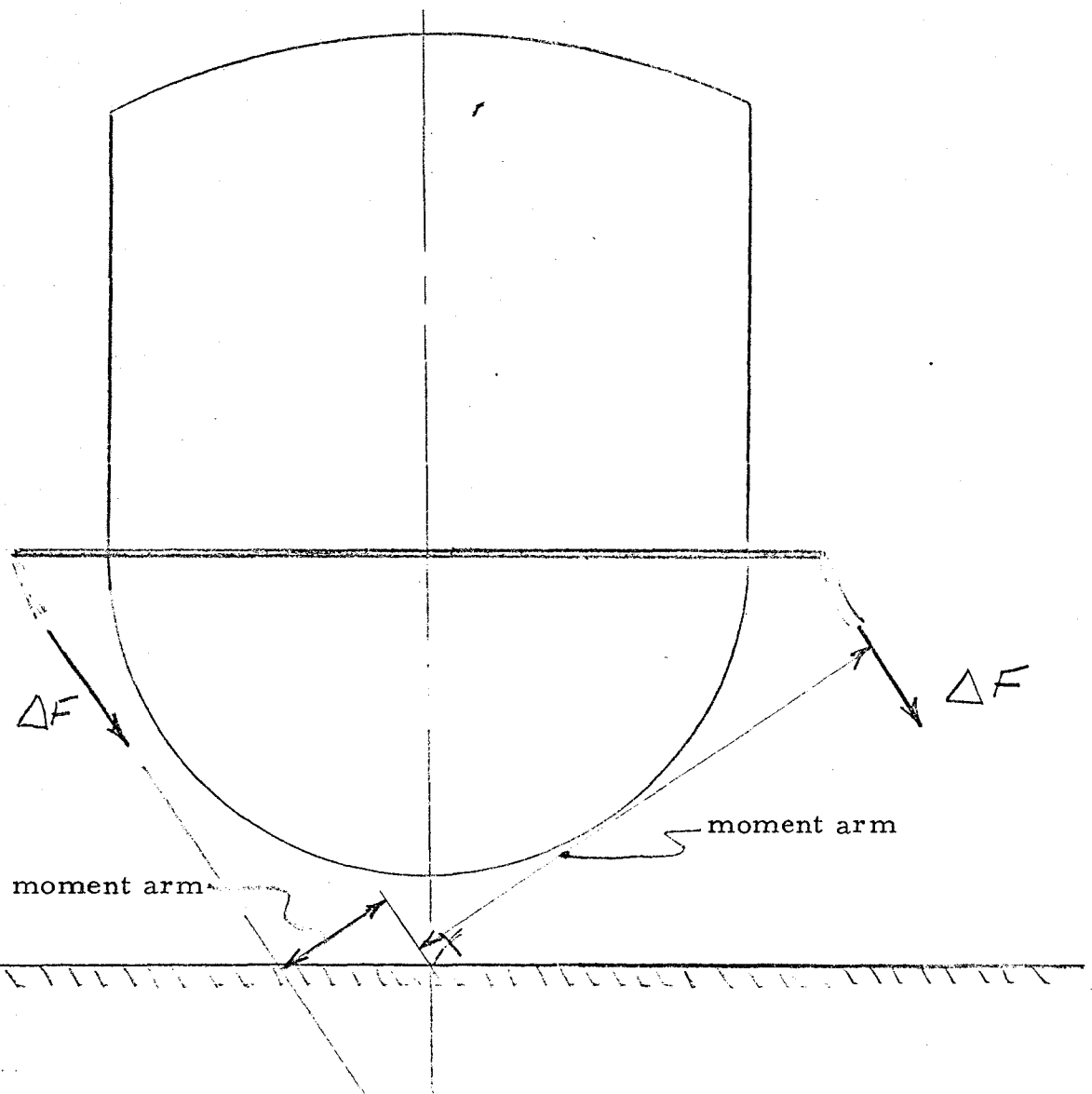


Figure 1. - The Moment of ΔF about Point X Is Minimized by
Running Cable Below PSE.

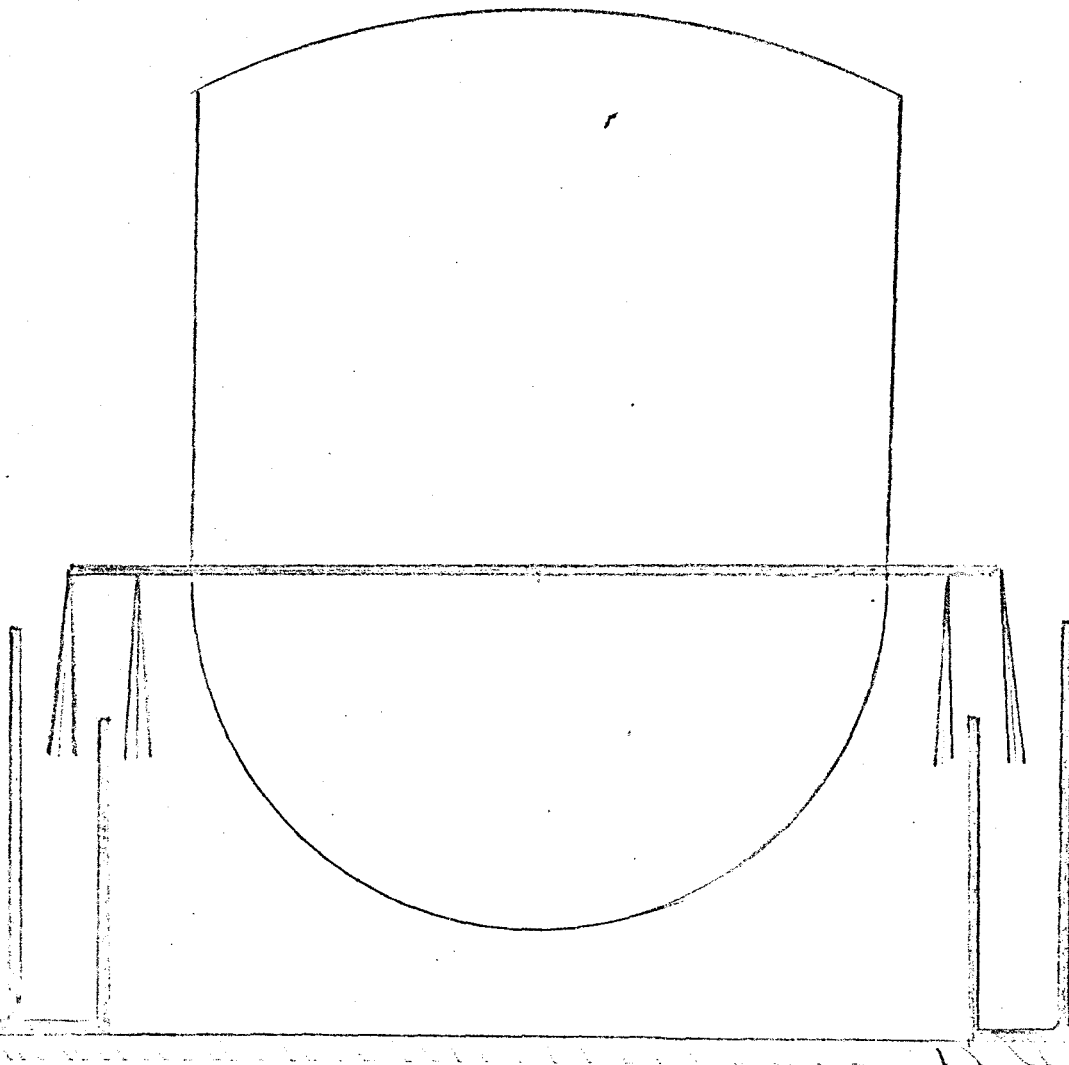


Figure 2. Labyrinth Skirt Configuration

Bendix

**Aerospace
Systems Division**

Investigation of PSE Anomalies
Apollo 12 Mission

SSSED-R-
57 (f)

PAGE 1 OF 14

DATE 28 May 1970

This report provides the results of investigations of PSE anomalies from Apollo 12 mission. Reference 97/510-454, CCP-237, 16 February 1970.

TASK TITLE: Analyze Design of PSS Leveling Stool Foot Pads.

Prepared by:

M. Asnani

M. Asnani

Prepared by:

R. Gibson

R. Gibson

Approved by:

J. Lewko, Jr. *RF*

J. Lewko, Jr

CONTENTS

<u>Paragraph</u>	<u>Title</u>	<u>Page</u>
1	INTRODUCTION	5
2	DISCUSSION	5
2.1	Statement of Work	5
2.2	Analysis	5
3.	SUMMARY OF RESULTS	6
4.	CONCLUSIONS AND RECOMMENDATIONS	7
5.	REFERENCES	8

LIST OF ILLUSTRATIONS

<u>Figure</u>	<u>Title</u>	<u>Page</u>
1	Lunar Soil Depth v/s Static Bearing Pressure	9
2	PSS Sensor Base/Leveling Stool Physical Relationship	10
3	Foot Pad Configuration-Astronaut Tool Location	11
4	Foot Pad Configuration - Remaining Two Legs	12
5	Beryllium Insert and Glass Epoxy Buttons	13
6	Completed Stool Assembly	14

TABLES

<u>Table</u>	<u>Title</u>	<u>Page</u>
1	Design Constraints for Leveling Stool Foot Pads	5
2	Summary of Tests Conducted at MSC, Houston on 5/20/70 Utilizing the Modified Stool Design	8

1.0 INTRODUCTION

Thermal data received from SN05 indicates a potential for the bottom of the sensor to contact the lunar surface. One probable cause of this may be due to the PSS leveling stool foot pads not being large enough to prevent continuous settling of the sensor into the lunar surface after deployment. The foot pads, the thermal isolator buttons and the foot design were modified resulting in a positive clearance of 0.425 in. to 0.925 in.

2.0 DISCUSSION

2.1 Statement of Work

2.1.1 Analyze design of PSS leveling stool foot pads and consider the design of the pin that is inserted into the lunar surface; a conical shaped pin is to be considered.

2.1.2 Analyze the size of the leveling stool foot pad in view of the fact the Apollo 12 PSS sensor continues to be settling after deployment.

2.1.3 Make a recommendation for appropriate redesign of the foot pad.

2.1.4 Analyze the design of the isolator pads on the ring of the leveling stool.

2.1.5 Propose to test the redesigned leveling stool at the MSC lunar surface simulator. This test will require the use of a dummy weight sensor simulator.

2.2 Analysis

2.2.1 Foot Pad Design Analysis

An analysis of both the current and proposed foot pad design was made. Table 1 lists the constraints under which the current foot pad design was made.

Item	Quantitative Value
1. Lunar Gravity	1/6 Earth Gravity
2. Earth Weight of Sensor	22 Lbs.
3. Lunar Weight of Sensor	3.7 Lbs.
4. Total Foot Pad Area	6.1 in ²
5. Pad Pressure on Lunar Surface	0.606 psi

Table 1 - Design Constraints for Leveling Stool Foot Pads

Assumptions

1. No impact or shock loading during deployment of PSE on the stool.
2. Astronaut does not lean on the sensor.

With these assumptions the stool will sink approximately 7.6 mm or 0.292 in (Ref. Figure 1). The total clearance between the bottom of the sensor and lunar surface is 0.44 in. (Ref. Figure 2). Thus, under static load conditions, the system attains a positive clearance of 0.148 inches. (The difference between 0.44 and 0.292).

During deployment, the astronaut firmly places the leveling stool on the lunar surface, and levels the sensor after it has been placed on the stool. The assumption regarding static deployment is questionable. For example, considering the impact/shock loading, coupled with the possibility of the astronaut leaning on the sensor, which induces extra forces on the stool, the loads could be increased at least four times, which will increase the foot pad pressure on the lunar surface to 2.424 psi. Referring to Figure 1, a clearance of 22.4 mm or 0.88 in. is required to withstand this pressure before the bottom of the sensor touches the lunar surface. These results indicate that the base is probably touching the lunar surface unless the astronaut formed a large enough depression beneath the sensor at the time of deployment. It is believed that the astronauts did provide a hole for the sensor as part of the deployment procedure for the PSE.

3.0 RESULTS

A new conceptual design is shown in Figures 3, 4 and 5. The total surface area of the foot pads is 12.25 sq. in. Using the same loads with a safety factor of 4, sensor pressure on the soil is 1.21 psi instead of 2.424, a decrease by a factor of 2.0. Referring to Figure 1, the stool will then penetrate approximately 13.0 m.m. (i. e. 0.515 inches); the interference, now would be 0.075 inches. A positive clearance of 0.425 to 0.925 in. is obtained by redesigning the buttons and the inserts in the stool, as shown in Figures 5-1, 5-2(a) and 5-2(b). A positive clearance of 0.425 in. is obtained if the button design shown in Figure 5-2(a) is used, and a positive clearance of 0.925 in. is obtained if the button design shown in Figure 5-2(b) is used. Thus, a total clearance of 0.425 in. to 0.925 in. is obtained with the foot pad design change shown in figures 3 and 4 coupled with insert and button design change shown in Figures 5-1, 5-2(a) and 5-2(b). The above positive clearance between the sensor and the lunar surface is based on a conservative design estimate of all anticipated loads.

The modified foot pads and insulating button inserts would be made of beryllium to minimize thermal stresses. The new foot pads can be physically

*Lunar soil constants are obtained from figure 1.

attached by thermally conducting epoxy to the old foot pads and a mechanical attachment achieved with 3 screws to provide additional rigidity at the interface point. The insulating button inserts can be screwed in the stool and secured to withstand vibrations. The insulating buttons will be epoxied in the beryllium inserts.

4.0 CONCLUSIONS AND RECOMMENDATIONS

The test results, summarized in Table 2, show that with the redesign of the foot pads and buttons, a positive clearance will be obtained in a very fluffy soil, if the soil is moderately compacted. It is therefore recommended that the new foot pads, inserts and button sizes be incorporated in future units as shown in Figures 3, 4, and 5. A typical completed assembly is shown in Figure 6.

5.0 REFERENCES

1. Interim Report, SSED R-57 (f), 21 April 1970.

Table 2 - Summary of Tests Conducted at MSC, Houston
on 5/20/70 Utilizing the Modified Stool Design

Soil	Pads	Buttons	Extra Pressure Applied	Clearance (Between the bottom of the sensor & soil)
1. Compact	New foot pads	Long buttons	None	2.5 in.
2. Very loose (fluffy up to 6 in. depth)	New food pads	Long buttons	None	Interference (base touching the soil)
3. Loose soil as in 2. (moderately compacted)	New foot pads	Short	None	1.5 in.
4. Loose soil (fluffy up to 3 in. in depth) (moderately compacted)	New foot pads	Long	None	1.875 in.
5. Loose soil as in 4. (not compacted)	New foot pads	Short	Excess of 5 lbs	Very close, not touching
6. Loose soil as in 4. (not compacted)	New foot pads	Long	None	1.625 in.
7. Loose soil as in 5.	New foot pads	Long	None	1.625 in.
8. Loose soil as in 4.	New foot pads	Short	None	0.875 in.
9. Loose soil as in 4.	Old foot pads	Old buttons		Pads sank in the soil, base very close to touching
10. Very compact soil.	Old foot pads	Old buttons	None	0.75 in.
11. Loose Soil as in 2. (moderately compacted).	Old foot pads	Long buttons	About 5 lbs	Pads sank all the way. Base very close to the soil

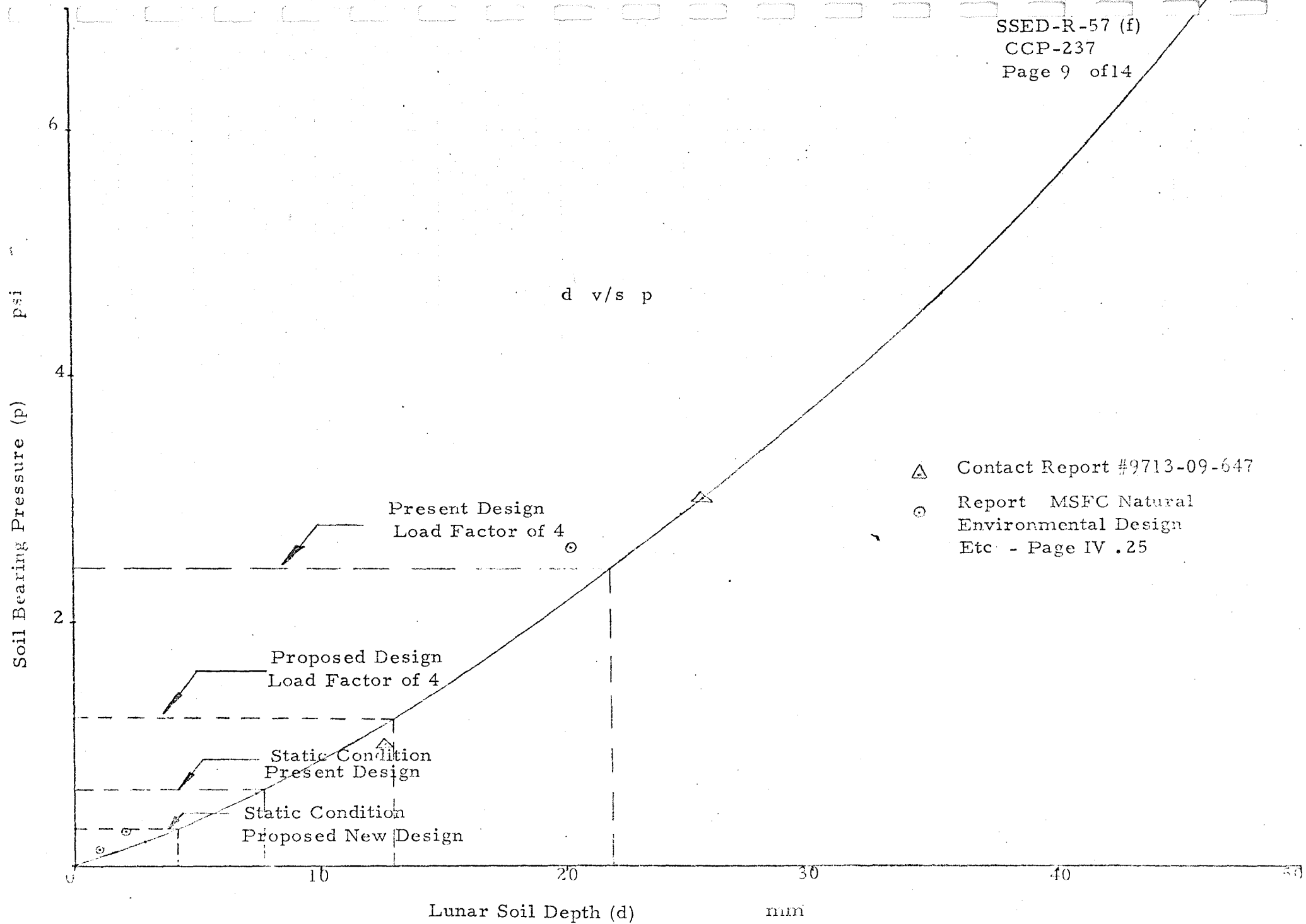


Figure 1 - Lunar Soil Depth vs Soil Bearing Pressure

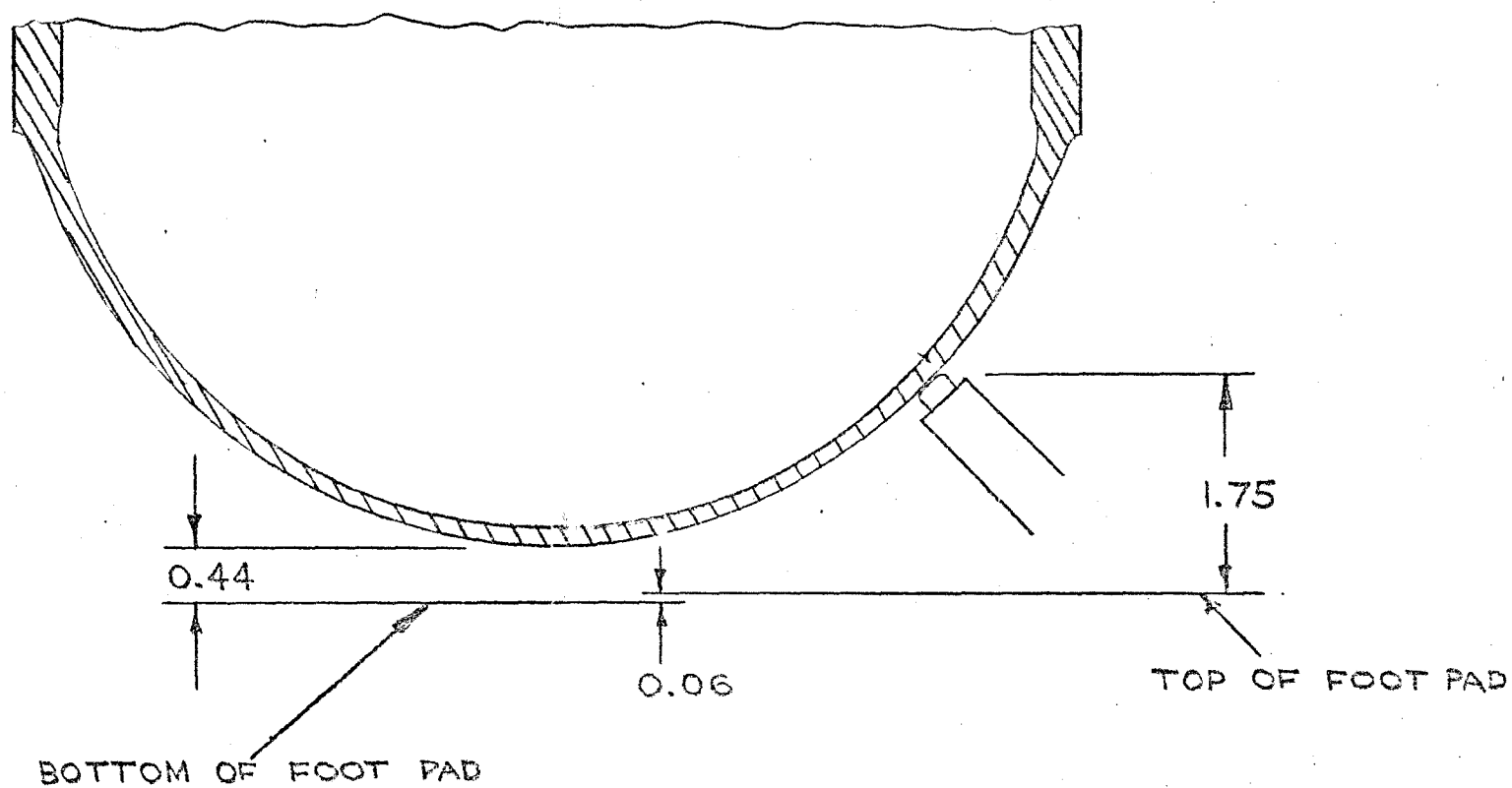


Figure 2

PSS Sensor Base/Leveling Stool Physical Relationship

5

4

3

2

1

RELIABILITY		REVISIONS				
APPO	PREDICTION	ZONE	LTR	DESCRIPTION	DATE	CONFIG MGT APPV'D

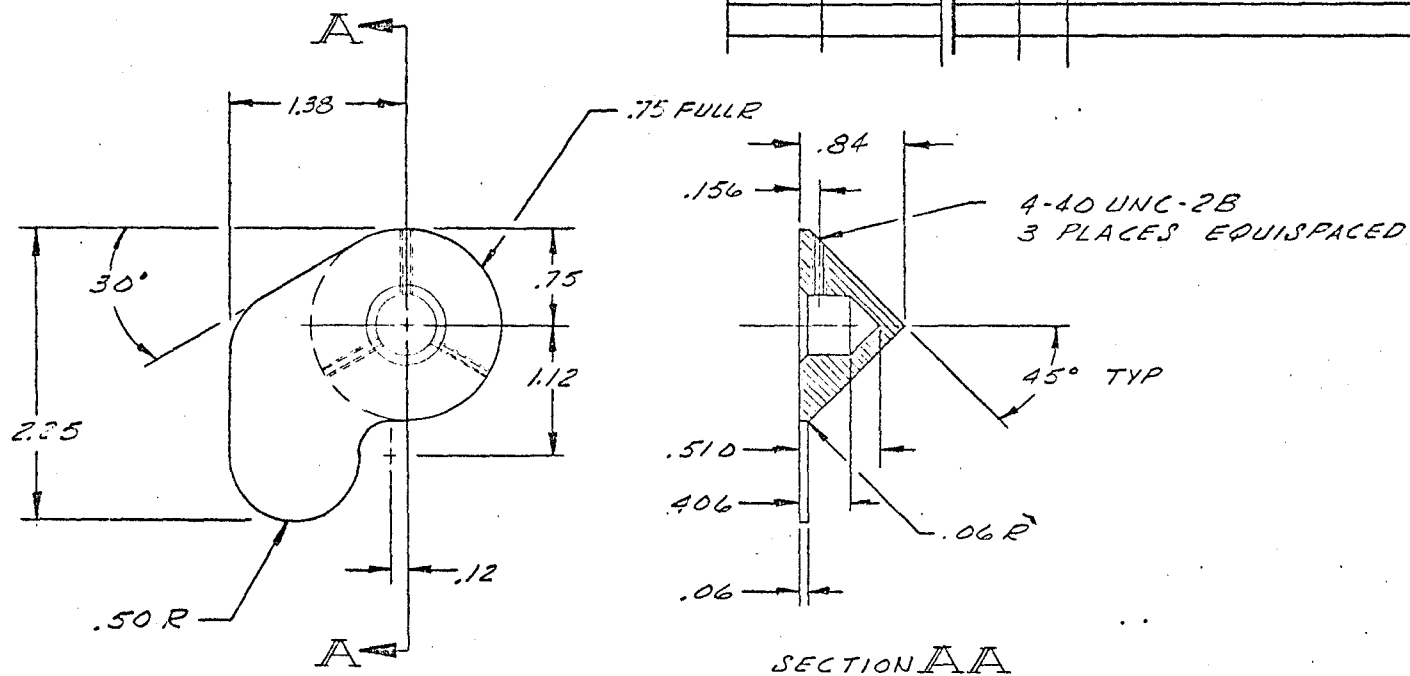


Figure 3 - Foot Pad Configuration -
Astronaut Tool Location

PROPRIETARY NOTICE

THIS DRAWING CONTAINS INFORMATION PROPRIETARY TO THE BENDIX CORPORATION AND OR ITS VENDORS AND SUPPLIERS. THIS DRAWING MAY NOT BE DISCLOSED TO OTHERS FOR ANY PURPOSE NOR USED FOR MANUFACTURING PURPOSES WITHOUT THE WRITTEN PERMISSION OF THE BENDIX CORPORATION.

PART NO.	NEXT ASSY	END ITEM NO.	SERIAL NO.
DRAWING AND PART APPLICATION			
DRAWING CLASS		FINISH	
A <input type="checkbox"/> B <input type="checkbox"/> C <input type="checkbox"/>			

UNLESS OTHERWISE SPECIFIED:
DIMENSIONS ARE IN INCHES
TOLERANCES

DECIMAL ANGLES
.X ±
.XX ±
.XXX ± CHAMFER ± 5°

FINISH MICROINCHES RHR

MATERIAL:

QTY REQ	DESCRIPTION	CODE IDENT	PART OR SPECIFICATION NO.	ITEM
---------	-------------	------------	---------------------------	------

LIST OF MATERIALS

CONTR. NO.

DRAWN

CHECKED

STRESS/WT

DSGN SUPV

PROJ ENGR

QUAL CONT

SYS SPT

DSGN APPL

MFG

CUSTOMER

THE BENDIX CORPORATION

AEROSPACE SYSTEMS DIVISION - ANN ARBOR, MICHIGAN

TITLE

FOOT CONFIGURATION #1

SIZE	CODE IDENT NO.	DRAWING NUMBER	REV.
B	07038		
SCALE	WEIGHT	SHEET	

5

4

3

2

1

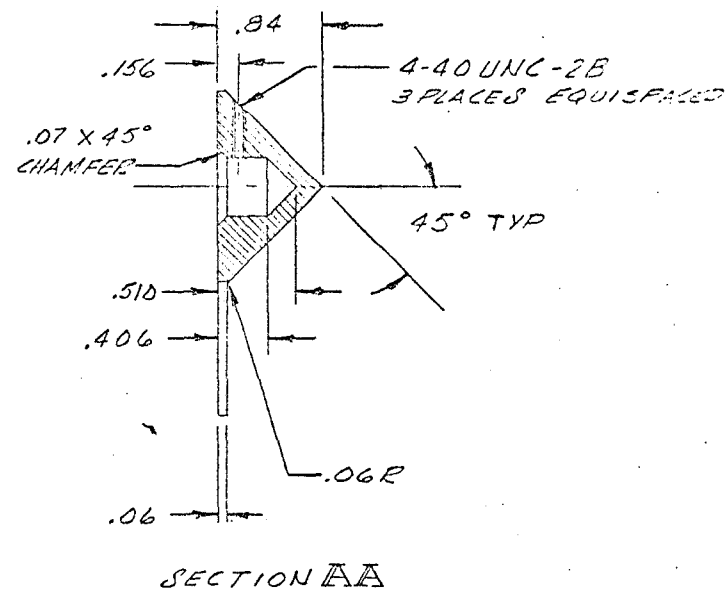
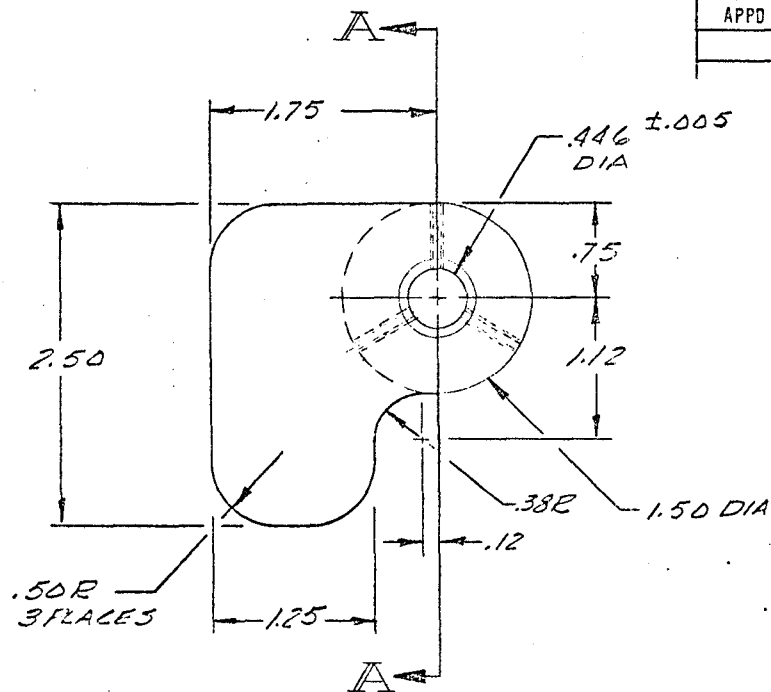


Figure 4 - Foot Pad Configuration
Remaining Two Legs

PROPRIETARY NOTICE

THIS DRAWING CONTAINS INFORMATION PROPRIETARY TO THE BENDIX CORPORATION AND OR ITS VENDORS AND SUPPLIERS. THIS DRAWING MAY NOT BE DISCLOSED TO OTHERS FOR ANY PURPOSE NOR USED FOR MANUFACTURING PURPOSES WITHOUT THE WRITTEN PERMISSION OF THE BENDIX CORPORATION.

PART NO.	NEXT ASSY	END ITEM NO.	SERIAL NO.
DRAWING AND PART APPLICATION			
DRAWING CLASS		FINISH	
A <input type="checkbox"/> B <input type="checkbox"/> C <input type="checkbox"/>			

UNLESS OTHERWISE SPECIFIED:
DIMENSIONS ARE IN INCHES
TOLERANCES
DECIMAL ANGLES
.X ±
.XX ±
.XXX ± CHAMFER ± 5°
FINISH MICROINCHES RHR
MATERIAL:

CONTR NO.
DRAWN
CHECKED
STRESS/HT
DSGN SUPV
PROJ ENGR
QUAL CONT
SYS SPT
DSGN APPL
MFG
CUSTOMER

THE BENDIX CORPORATION			
AEROSPACE SYSTEMS DIVISION - ANN ARBOR, MICHIGAN			
TITLE FOOT CONFIGURATION			
SIZE	CODE IDENT NO.	DRAWING NUMBER	REV.
B	07038		
SCALE	WEIGHT	SHEET	

QTY REQD	DESCRIPTION	CODE IDENT	PART OR SPECIFICATION NO.	ITEM
LIST OF MATERIALS				

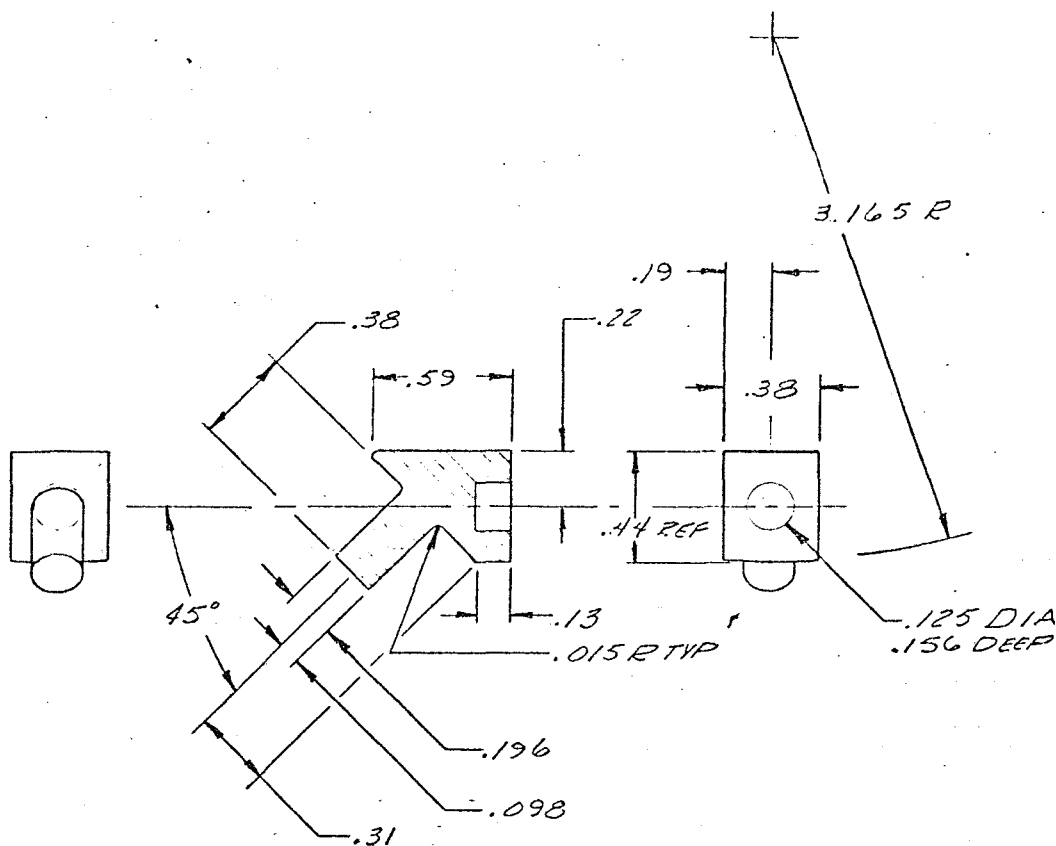


Figure 5-1 Beryllium Insert

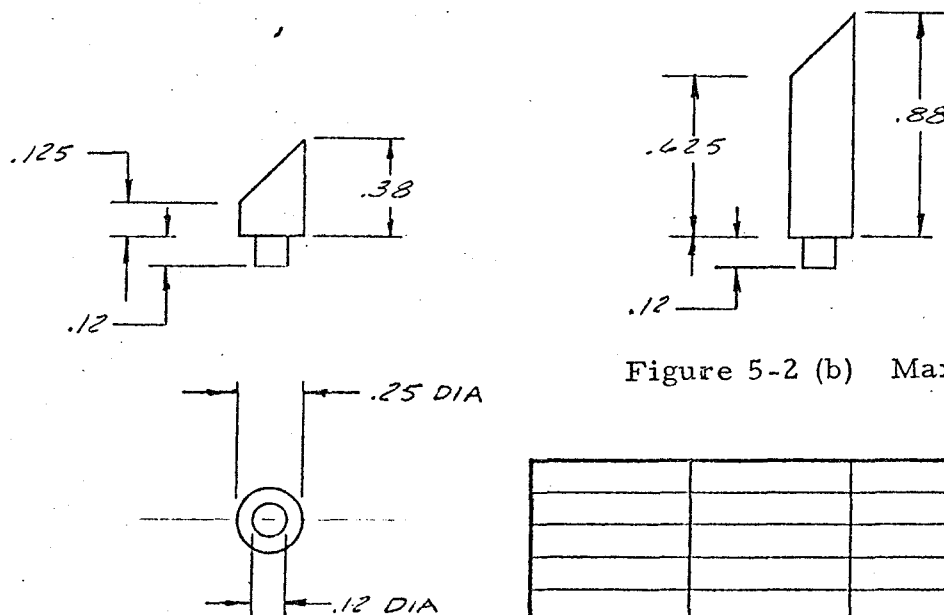


Figure 5-2 (b) Maximum Length Button

Figure 5-2(a) Minimum Length Button

PROPRIETARY NOTICE

THIS DRAWING CONTAINS INFORMATION PROPRIETARY TO THE BENDIX CORPORATION AND/OR ITS VENDORS AND SUPPLIERS. THIS DRAWING MAY NOT BE DISCLOSED TO OTHERS FOR ANY PURPOSE NOR USED FOR MANUFACTURING PURPOSES WITHOUT THE WRITTEN PERMISSION OF THE BENDIX CORPORATION.

DRAWING AND PART APPLICATION				UNLESS OTHERWISE SPEC
PART NO.	NEXT ASSY	END ITEM NO.	SERIAL NO.	DIMENSIONS ARE IN IN
DRAWING CLASS				TOLERANCES
A <input type="checkbox"/> B <input type="checkbox"/> C <input type="checkbox"/>				DECIMAL ANG
FINISH				.X ± ±
				.XX ± ±
				.XXX ± CHAMFE
				SURFACE FINISH
				MICROINCHES RHR
				MATERIAL:

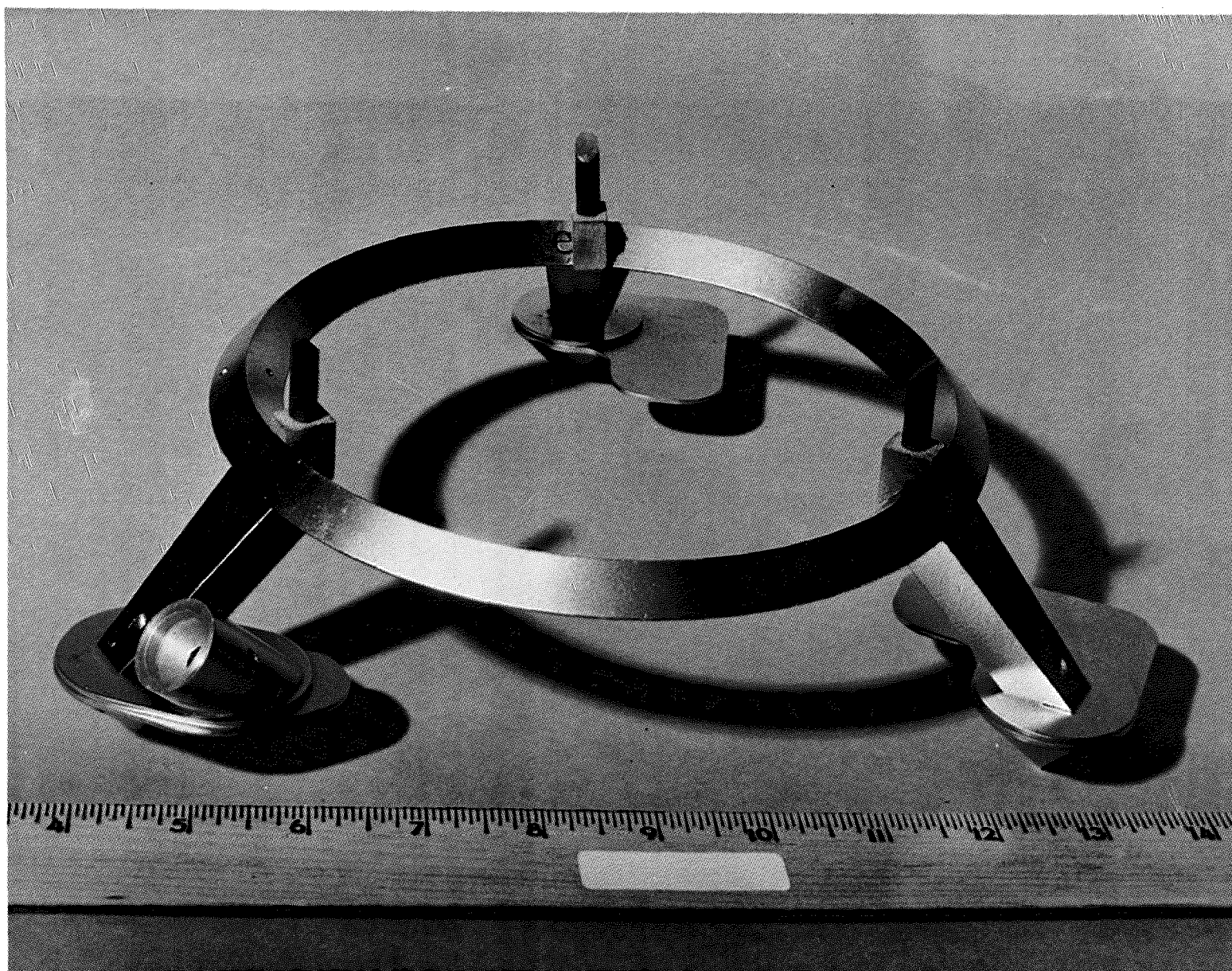


Figure 6 - Completed Stool Assembly